12-11-2015 12:00 AM

Smouldering Remediation: Transient Effects of Front Propagation

Laura L. Kinsman, *The University of Western Ontario*

Supervisor: Dr. Jason Gerhard, *The University of Western Ontario*

A thesis submitted in partial fulfillment of the requirements for the Master of Engineering Science degree in Civil and Environmental Engineering

SMOULDERING REMEDIATION: TRANSIENT EFFECTS OF FRONT PROPAGATION

(Thesis format: Integrated Article)

by

Laura L. Kinsman

Graduate Program in Engineering Science
Department of Civil and Environmental Engineering

A thesis submitted in partial fulfillment
of the requirements for the degree of
Master of Engineering Science

The School of Graduate and Postdoctoral Studies
The University of Western Ontario
London, Ontario, Canada

ABSTRACT

Remediation of sites contaminated with non-aqueous phase liquids (NAPLs) presents a significant challenge, particularly for complex and high molecular weight compounds such as coal tar and creosote. Self-sustaining Treatment for Active Remediation (STAR) is an innovative remediation technology based on the principles of smouldering combustion, which has shown potential for rapid destruction of source zone contaminants. The success of smouldering remediation has been previously demonstrated both at the laboratory and field scale, however, these studies have focused primarily on the overall degree of remediation. Laboratory column experiments were employed to identify key transient processes that have the potential to influence smouldering metrics. It was found that downward liquid fuel mobilization can occur in taller systems operated at low air flow rates, and may result in elevated peak temperatures and a slowing of the propagation velocity of the trailing edge of the smouldering front. Numerical simulations and an analytical model were used to further understand experimental observations and can be used as a simple tool to predict the potential for liquid fuel mobility under different experimental conditions. It was also found that the distribution of heat within a smouldering system influences the transport of condensable products. The processes of fuel volatilization, aerosolization, condensation and deposition are important for gaseous mass transport and impact the rate of mass loss over time. The relative proportion of fuel combustion to gaseous mass transport is expected to be a function of fuel type, and may also be manipulated via operational parameters such as injection air flux.

Keywords: remediation, smouldering, STAR, NAPL, migration, combustion products

CO-AUTHORSHIP

This thesis was written in accordance with regulations and guidelines for integrated-article format by the Faculty of Graduate and Postdoctoral Studies at the University of Western Ontario. The candidate designed, performed and analyzed all data collected from the laboratory experimental program under the supervision and guidance of Dr. Jason I. Gerhard. The candidate wrote the thesis and was the lead author on the manuscript drafts of the following chapters, which are expected to be submitted for publication in the near future:

Chapter 3: Smouldering Combustion and Non-Aqueous Phase Liquid Mobility

By Laura L. Kinsman, Jason I. Gerhard, Jose L. Torero

Chapter 4: Transport of Heat and Condensable Products in Smouldering Column Experiments

By Laura L. Kinsman, Jason I. Gerhard, Jose L. Torero

Laura Kinsman: performed all laboratory experiments, analysis and interpretation of experimental results, conducted numerical model simulations, and wrote all manuscript chapters.

Jason I. Gerhard: initiated research topic, provided the funding and resources for the project, supervised experimental program, modified numerical model, assisted in data interpretation and revised/reviewed draft chapters.

Jose L. Torero: provided guidance on experimental program, assisted in data interpretation and revised/reviewed draft chapters.

ACKNOWLEDGEMENTS

I would like to express my sincere gratitude to my supervisor Dr. Jason Gerhard for your invaluable support and technical guidance. I cannot thank you enough for your optimism, encouragement and patience throughout the past few years. I would also like to thank Prof. Jose Torero for teaching me all of the intricacies of smouldering data, and for hosting me at the University of Queensland. I have learned so much from you.

Thank you to the RESTORE group for making life as a grad student so enjoyable. I was lucky to be surrounded by such wonderful and smart people and cherish the friendships made. Special thanks to Marco and Tarek for always stopping by during my long days in the lab and for sharing your passion for science.

I would like to thank Savron, particularly Dr. Dave, Gavin and Grant, for giving me the opportunity to gain practical experience while finishing my Master's. Thank you for being so accommodating and for making all of my hard work on this thesis seem relevant and important.

I would also like to acknowledge NSERC and OGS for providing much appreciated scholarships to help support my research.

Carlos, thank you for the countless dinners, apartment cleanings and taking care of all other life tasks that I didn't have time for over the final few months. You have been the calm in the middle of all of my stress – te quiero.

Finally, thank you to my parents, Steve and Debbie, and my brother Greg for your continual love and support.

TABLE OF CONTENTS

LIST OF TABLES

LIST OF FIGURES

1 INTRODUCTION

1.1 Problem Overview

Remediation of sites contaminated with non-aqueous phase liquids (NAPLs) remains a challenge despite advances in scientific understanding and technology development. There are an estimated 100,000 contaminated sites in the United States alone where complete remediation will not be possible within a reasonable time frame (NRC, 2013; Kueper et al., 2014). Heavy hydrocarbon NAPLs, such as creosote and coal tar, present a particular challenge for traditional remediation strategies due to their characteristically low aqueous solubility, low volatility and resistance to biodegradation (Birak and Miller, 2009). The costs associated with contaminated sites to the environment, economy and human health are significant. While it is difficult to quantify the costs of soil and groundwater contamination to human and ecosystem health, it is estimated that an excess of $209 billion dollars will be required to mitigate hazards at contaminated sites in the United States over the next 30 years (EPA, 2004; NRC, 2013). Effective remediation of these sites to concentrations below unrestricted exposure levels for soil and groundwater would not only provide environmental and health benefits, but would also provide significant opportunities for redevelopment in areas that have been either restricted or unusable for decades.

Self-sustaining Treatment for Active Remediation (STAR) is an innovative remediation technology based on the principles of smouldering combustion. Smouldering is a flameless exothermic reaction occurring on the surface of a condensed phase fuel (Ohlemiller, 1985). In smouldering remediation, the contaminant (or NAPL) provides

the fuel that supports its own destruction. Following a short duration input of heat, a continuous air supply is used to ignite and propagate a smouldering reaction within the porous soil matrix. This controlled, self-sustaining combustion reaction destroys the NAPL contaminant and thereby renders the soil clean.

STAR has shown significant potential for the treatment of coal tar and petroleum hydrocarbons ex-situ at the laboratory scale (Switzer et al., 2009; Pironi et al., 2009, 2011), intermediate and pilot scale (Switzer et al., 2014), as well as in-situ at a contaminated former industrial site (Scholes et al., 2015). These studies have focused primarily on the degree of remediation via a comparison of the before and after soil conditions, in addition to overall averages of smouldering metrics. There are, however, transient processes occurring during the propagation of a smouldering front that are not captured by considering average conditions. These localized dynamic processes may affect such metrics as peak temperatures and mass loss rates over time, and as such may have important practical implications for the design and optimization of full-scale remediation systems, both in-situ and ex-situ.

1.2 Research Objectives

The objective of this work was to explore transient processes that occur during smouldering remediation of contaminated soils through a detailed assessment of smouldering data as a function of both time and space. This work focuses on two key dynamic processes: liquid fuel (contaminant) mobility and the transport of condensable and non-condensable gaseous compounds formed during the propagation of a smouldering front. To accomplish this objective a series of carefully controlled

laboratory column experiments were conducted. The scale of the column experiments presented in this work was selected to provide a balance between being small enough to permit high controllability, yet large enough to allow the manifestation of transient processes. A detailed investigation of fuel mobility and the transport of gaseous compounds is not only significant for understanding the STAR process but is also fundamental to the relatively unexplored field of liquid smouldering in general.

1.3 Thesis Outline

This thesis is written in an integrated article format in accordance with the guidelines and regulations stipulated by the Faculty of Graduate Studies at the University of Western Ontario. Each chapter in the thesis is described below.

Chapter 2 is a review of relevant literature and presents an overview of the application and limitations of existing remediation strategies at contaminated sites, with an emphasis on thermal remediation technologies. An introduction to smouldering combustion, as well as the use of smouldering for the remediation of contaminated soils is also presented. The influence of heat on the properties of liquid contaminants and resulting processes that may occur in the subsurface are also reviewed.

Chapter 3 presents a lab scale experimental study, as well as an analytical and numerical investigation of liquid fuel mobility during smouldering in a porous matrix. This chapter is written in a manuscript format for future submission to a peer reviewed journal.

Chapter 4 presents a laboratory experimental investigation on the influence of heat on the transport of gaseous compounds within a smouldering column, and the consequent effects

on global mass loss behaviour and emissions in a batch system. This chapter is also written in a manuscript format for future submission to a peer reviewed journal.

Chapter 5 summarizes the research conducted in this work and presents conclusions in addition to recommendations for future work.

Appendices provide supplemental information, referenced throughout the thesis.

1.4 References

Birak, P. S., & Miller, C. T. (2009). Dense non-aqueous phase liquids at former manufactured gas plants: Challenges to modeling and remediation. *Journal of Contaminant Hydrology,* 105(3–4), 81-98.

EPA. (2004). *Cleaning up the nation's wast sites: Markets and technology trends.* EPA 542-R-04-015. U.S. Environmental Proctection Agency.

Kueper, B. H., Stroo, H.F., Vogel, C. M., & Ward, C. H. (2014). *Chlorinated Solvent Source Zone Remediation*. New York: Springer. 713 p.

National Research Council, NRC. (2013). *Alternatives for managing the nation's complex contaminated groundwater sites.* Washington, DC: The National Academies Press.

Ohlemiller, T. J. (1985). Modeling of smoldering combustion propagation. *Progress in Energy and Combustion Science, 11*(4), 277-310.

Pironi, P., Switzer, C., Gerhard, J. I., Rein, G., & Torero, J. L. (2011). Self-sustaining smoldering combustion for NAPL remediation: Laboratory evaluation of process sensitivity to key parameters. *Environmental Science & Technology, 45*(7), 2980-2986.

Pironi, P., Switzer, C., Rein, G., Fuentes, A., Gerhard, J. I., & Torero, J. L. (2009). Small-scale forward smouldering experiments for remediation of coal tar in inert media. *Proceedings of the Combustion Institute, 32*, 1957-1964.

Scholes, G. C., Gerhard, J. I., Grant, G. P., Major, D. W., Vidumsky, J. E., Switzer, C., & Torero, J. L. (2015). Smoldering remediation of coal tar contaminated soil: Pilot field tests of STAR. *Environmental Science & Technology*, Article ASAP.

Switzer, C., Pironi, P., Gerhard, J. I., Rein, G., & Torero, J. L. (2009). Self-sustaining smoldering combustion: A novel remediation process for non-aqueous-phase liquids in porous media. *Environmental Science & Technology, 43*(15), 5871-5877.

Switzer, C., Pironi, P., Gerhard, J. I., Rein, G., & Torero, J. L. (2014). Volumetric scale-up of smouldering remediation of contaminated materials. *Journal of Hazardous Materials, 268*, 51-60.

2 LITERATURE REVIEW

2.1 Non-Aqueous Phase Liquid Contamination

2.1.1 Introduction

Subsurface contamination by non-aqueous phase liquids (NAPLs) presents significant challenges for the development of effective remediation strategies. Due to both accidental spills and inappropriate disposal practices, sites contaminated with these water-immiscible organic compounds have become pervasive throughout the industrialized world. Some common examples of NAPLs include: petroleum hydrocarbon fuels, coal tar formed as waste products from manufactured gas plants, polychlorinated biphenyls contained in transformer oils, chlorinated hydrocarbons used as solvents and degreasers, and creosote used in wood treatment processes (Mercer and Cohen, 1990). As a result of the low threshold concentrations for environmental and drinking water standards, in addition to the low aqueous solubility of these compounds, NAPL contamination of soil and groundwater poses a persistent threat to both human and ecosystem health.

Remediation strategies must overcome the potentially challenging combination of the diverse physicochemical properties of many NAPLs with complex site hydrogeology. Traditionally employed technologies, such as excavation and disposal, physical containment, and pump-and-treat systems, are often costly, energy intensive, or require many years of operation and monitoring. As a result, complete remediation of groundwater to the level of drinking water standards is currently not possible in a timely

and cost-effective manner at many sites, particularly where large source zones are present (Kueper et al., 2014).

2.1.2 Remediation Options

Advancements in remediation science have allowed for a number of technologies to replace standard excavation or pump-and-treat systems. Each technology, however, has its own limitations with respect to contaminant type, concentration and hydrogeological conditions. For example, soil vapor extraction (SVE) is a widely used technology, but is most suitable for soil contaminated with volatile and semi-volatile organic compounds (VOC and SVOCs), and is only applicable for contamination in the unsaturated zone (Khan et al., 2004). Technologies such as in-situ chemical oxidation or enhanced bioremediation have been shown to effectively break down contaminants into less hazardous by-products. These technologies may, however, become less favorable for site conditions such as: large volume and high NAPL saturation source zones, mature contaminants (>10 years) and mixtures that contain oil and grease (ITRC, 2008).

Some oily contaminants, such as coal tar or creosote, resist many forms of remediation due to their complex chemical structure, practical insolubility in water, and low vapor pressure. Furthermore, the mobilization of these contaminants to recovery wells is limited by its high viscosity and consequent low rates of migration. Thermal-based in-situ remediation techniques may, however, be employed to reduce the impacts of some of these properties and permit more effective remediation (Davis, 1997).

2.1.3 Thermal Remediation Options

The delivery of heat to contaminated soil through thermal remediation technologies serves to permit enhanced free product recovery due to changes to the following properties: reduced contaminant density, increased vapor pressure, decreased adsorption to solid phases or absorption to organic matter, increased diffusion into aqueous and gaseous phases, and decreased contaminant viscosity (Davis, 1997). The three most common technologies which employ source zone heating for remediation are: steam-enhanced extraction, electrical resistance heating, and thermal conductive heating (or in-situ thermal desorption) (Triplett Kingston et al., 2014). These technologies operate under the same fundamental mechanisms of contaminant boiling, vaporization, volatilization and enhanced mobility, but differ in terms of the method of delivering heat to the subsurface to permit these processes to occur.

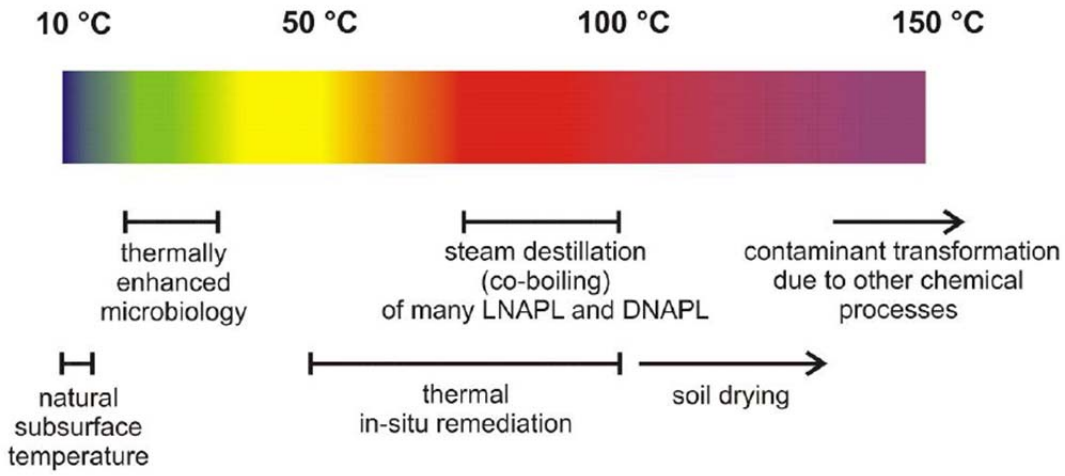

Figure 2.1: Relationship between thermal remediation processes and subsurface temperatures (TASK Leipzig, 2013).

The effects of temperature on subsurface processes are shown in Figure 2.1. As shown in this figure, in-situ thermal remediation strategies typically result in subsurface temperatures between 50 and 100°C. Chemical transformation of the contaminants is unlikely in most applications as these chemical processes typically occur at temperatures in excess of 150°C (TASK Leipzig, 2013).

Steam-enhanced extraction (SEE) was initially developed as an enhanced oil recovery method in the petroleum industry (White and Moss, 1983), and has since been applied to the field of contaminated site remediation. This process involves injecting steam, sometimes with the co-injection of air, under pressure into the subsurface and recovering liquids and vapors through a network of dual-phase extraction wells (Triplett Kingston et al., 2014). The primary mechanisms of contaminant recovery depend largely on the properties of the contaminant. For highly volatile compounds recovery is achieved mainly from vaporization and co-boiling, while for less volatile compounds liquid phase displacement due to reduced viscosity dominates (Heron et al., 2005).

Electrical resistance heating (ERH), which has also been used by the oil industry for enhanced oil recovery, delivers heat to the subsurface through an array of electrodes. The objective is to heat the subsurface to the boiling point of water to create a steam front to strip contaminants. A soil vapor extraction system is used to extract any volatilized contaminants (NRC, 2004).

In-situ thermal desorption (ISTD), involves conductive heating of the subsurface from electrical heating elements in direct contact with the soil. The heating elements used in this application may reach temperatures of approximately 500 to 800°C, which is

significantly higher than the temperatures observed during steam flushing or electrical resistance heating. While high temperatures may be achieved adjacent to heaters, a significant temperature gradient exists between heaters (Triplett Kingston et al., 2014). Similar to ERH, a vacuum extraction system is then used to collect volatilized contaminants from the subsurface (Stegemeier and Vinegar, 2001).

All three of these thermal remediation technologies have shown promise at a number of field sites. There are, however, some limitations in that both steam injection and ERH require the contaminants to be relatively volatile due to the lower peak temperatures attained using these technologies. For heavier contaminant fractions present in coal tar or creosote, for example, higher temperatures used in ISTD are possible and can result in volatilization and potential destruction of some fractions via chemical reactions (Stegemeier and Vinegar, 2001). Due to the endothermic nature of these thermal remediation technologies, there may be significant energy demands depending on site conditions. As the contaminant volatility decreases and heat requirements increase, operation of high temperature systems are required to heat large volumes of the subsurface for extended periods of time. In applications below the water table, the groundwater provides an additional heat sink and greatly increases energy demands. As a result, the energy requirements and economic and life cycle costs associated with operating such systems are substantial (Lemming et al., 2010).

2.2 Self-Sustaining Treatment for Active Remediation (STAR)

2.2.1 Overview of STAR

Self-sustaining Treatment for Active Remediation (STAR) is an innovative remediation technology which has shown potential for rapid and essentially complete destruction of source zone contaminants through the smouldering of NAPLs (Pironi et al., 2009, 2011; Switzer et al., 2009). The viability of STAR can be attributed to the presence of NAPLs with characteristically high heats of combustion contained within a porous soil matrix. The permeable soil matrix contains pathways for oxygen transport to the reaction zone, provides a large surface area per unit volume for reactions to occur, and acts as a thermal insulator to maintain temperatures required for smouldering propagation (Pironi et al., 2009). STAR takes advantage of these properties to produce a self-sustaining controlled burning reaction, destroying the contaminants and thereby rendering soil clean. Contrary to many other remediation technologies, STAR is well suited to sites with high saturations of heavy hydrocarbons or other contaminants of low volatility. Due to the self-sustaining nature of the process, NAPL smouldering requires only a short one-time input of energy to initiate the reaction resulting in energy savings in comparison with other thermal technologies.

2.2.2 Smouldering Combustion

Smouldering is a slow, low temperature, flameless form of combustion sustained by the heat evolved when oxygen directly attacks the surface of a condensed-phase fuel (Ohlemiller, 1985). A smouldering front may propagate through a porous material in either the same direction as the air flow (forward smoulder) or in the opposite direction to

air flow (reverse smoulder) (Ohlemiller and Lucca, 1983). The smouldering front is composed of two different layers: the combustion reaction layer and the heat transfer layer, each theoretically propagating with a constant velocity which may or may not be equal (Schult et al., 1996; Aldushin et al., 1999). The relative velocity of these two layers determines the structure of the smouldering front. In a reaction leading structure (Figure 2.2a), associated with sufficiently high air flux, the combustion layer propagates at a faster velocity than the heat transfer layer.

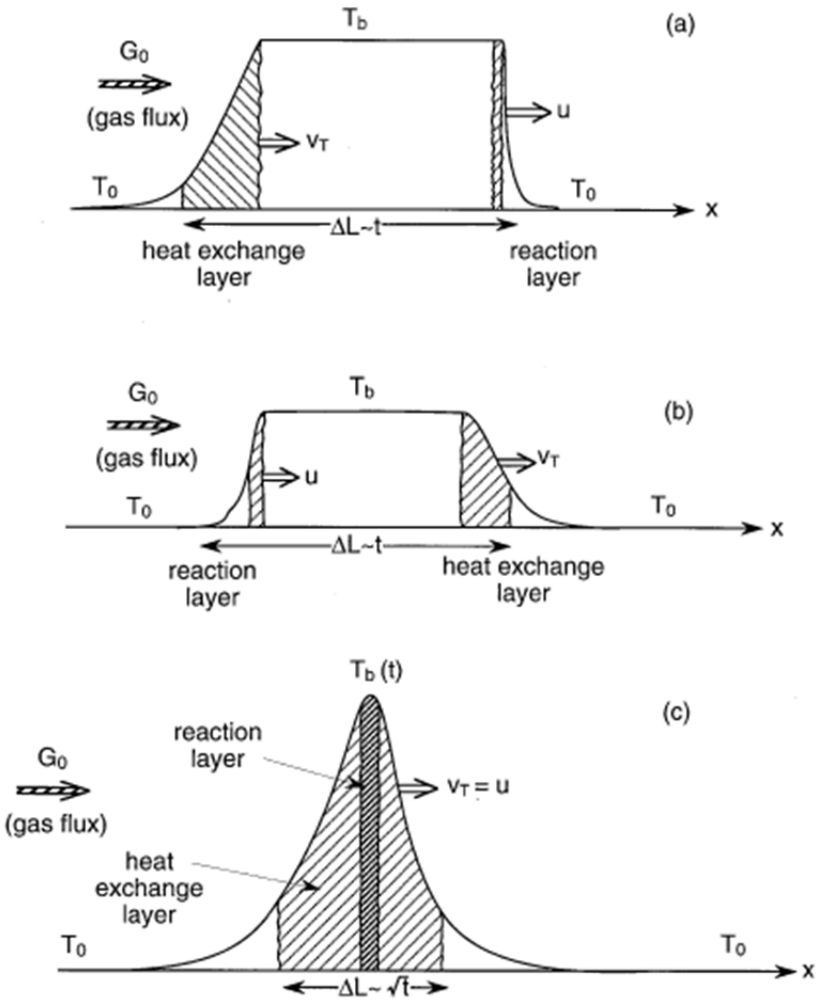

Figure 2.2: Structure of a smouldering front in forward configuration: (a) reaction leading structure, (b) reaction trailing structure, (c) wave with maximal energy accumulation (Aldushin et al., 1999).

The opposite is true for a reaction trailing structure (Figure 2.2b), associated with a sufficiently low air flux, where the velocity of the combustion layer is slower than the heat transfer layer. If the velocity of the combustion and heat transfer layers are equal, a superadiabatic condition may occur (Figure 2.2c), where the combustion temperature, T_b, is highly elevated.

2.2.3 Smouldering Literature and STAR

Traditionally, smouldering has been studied primarily in relation to the development of fires. As such, studies have been conducted on the smouldering of peat or coal which can lead to the development of coal seam and forest fires, as well as dust or polyurethane foam due to the potential hazards for both residential and in-flight aerospace fires. While smouldering literature in itself is relatively limited in comparison to flaming combustion, two key differences exist between the majority of the published smouldering science and STAR experiments.

First, the typical forced air flow velocities employed in STAR, 0.5 to 9.5 cm/s (Pironi et al., 2011), are considerably higher than those typically studied in other smouldering applications. In studying smouldering in the context of the development of fires, the air flow is often either governed by natural convection (e.g., Torero and Fernandez-Pello, 1995; Anderson et al., 2000) or at relatively low forced air velocities (e.g., 0 to 0.8 cm/s) (Ohlemiller and Lucca, 1983; Torero and Fernandez-Pello, 1996). This increased air flow rate used in the application of STAR results in fundamental changes to convective heat transfer and provides significantly more oxygen to sustain the combustion reaction.

Second, in traditional smouldering literature, the fuel is most often a solid (e.g., peat, polyurethane foam, tires, wood fibres or dust) (Rein et al., 2009; Torero and Fernandez-Pello, 1996; Vantelon et al., 2005; Ohlemiller and Lucca, 1983; Palmer, 1957). In the case of STAR, however, the fuel is the NAPL contaminant which is embedded within a soil matrix. While all forms of smouldering require the presence of a porous matrix, in traditional smouldering literature the fuel and the porous matrix are one and the same. In STAR, these are two different materials. Since the fuel is a liquid in the case of STAR, this introduces a new component to the process as the fuel is able to both migrate in its initial liquid state and volatilize into a gaseous phase as the smouldering reaction progresses. Due to the lack of previous studies looking at smouldering in this context (i.e., a liquid fuel and relatively high forced air flow rates), a detailed assessment of the process at a scale large enough to demonstrate potential fuel mobilization phenomena is necessary.

As shown in Figure 2.2, the relative velocity of the heat transfer and combustion layers in a smouldering system is important for determining peak combustion temperatures (T_b). In rare circumstances for immobile fuels, the velocity of the heat transfer and combustion layers become equal and result in increased reaction rates and highly elevated peak temperatures, or superadiabatic combustion (Aldushin et al., 1999). To the author's knowledge, superadiabatic combustion has not been observed experimentally for the smouldering of liquid fuels. An investigation into the potential of superadiabatic combustion and fuel mobilization processes is not only important for understanding STAR, but is significant for the development of a fundamental understanding of smouldering of liquids in general.

2.2.4 Laboratory Scale Experiments

The majority of experiments on NAPL smouldering to date have been conducted in a small laboratory column with dimensions of the contaminated zone ranging from 100 mm in diameter and 50 mm in height to 138 mm in diameter and 150 mm in height. A series of proof-of-concept experiments were conducted at the column scale to demonstrate the remediation of contaminated soils via forward smouldering combustion across a range of contaminant types, contaminant concentrations and soil types, including field-contaminated samples (Switzer et al., 2009). Through these proof-of-concept experiments, it was also demonstrated that STAR is both self-sustaining after an initial energy input and self-terminating when the fuel is completely destroyed or the oxygen supply is eliminated. Additional experiments conducted by Pironi et al. (2009) investigated the effect of air flow rate and contaminant concentrations on average velocities of the smouldering front and peak temperatures. A detailed sensitivity analysis of key parameters, such as contaminant concentration, water saturation, soil type, and air flow rates, on the ability to achieve a self-sustaining reaction was further assessed by Pironi et al. (2011). The lower limits of contaminant concentration and air flow rate, and upper limit of soil grain size, which were defined as the limits where self-sustaining smouldering was still achieved, appeared to be significantly affected by heat losses to the external environment at the small column scale. It was predicted that the effects of heat losses would be reduced with increasing experimental scale.

2.2.5 Larger Scale Demonstrations

While STAR has been proven to be effective through a wide range of conditions at the bench scale, success at industrial scales requires the process to be scaled up significantly.

Investigations into the viability of STAR at larger scales were assessed in intermediate scale (0.3 m^3) and pilot field-scale (3 m^3) vessels for coal tar and petrochemical NAPL contaminants (Switzer et al., 2014). These experiments demonstrated consistent remediation efficiency (97-99.5%) and smouldering propagation velocities with previous bench scale studies. These larger scale experiments conducted by Switzer et al. (2014) also revealed the robust nature of smouldering combustion as both operational challenges and material heterogeneities were able to be overcome to achieve successful remediation. Additionally, as predicted, due to the decrease in surface area of the exterior surfaces of the reaction vessel proportional to the total contaminated material volume at larger scales, lower contaminant concentrations were able to smoulder in a self-sustaining manner than was possible for bench scale experiments (Switzer et al., 2014).

The STAR technology has also been successfully demonstrated in-situ at a former industrial facility (Scholes et al., 2015). Results of in-situ pilot testing demonstrated that field results were consistent with laboratory bench scale testing of site soils. Self-sustaining smouldering remediation of coal tar below the water table was successfully conducted in two different lithological units. Full-scale implementation of STAR is now being applied at this site.

While successful upscaling of the STAR technology has been demonstrated both ex-situ and in-situ, there are numerous questions that remain about the fundamental processes occurring during the smouldering of liquid fuels. Due to the limited size of the previous bench scale experiments, some of these fundamental processes cannot be observed or studied at this small scale. Similarly, the quantity, detail, and systematic analysis of key process parameters conducted at the bench scale may not be practical to replicate at larger

scales where these complex processes are evident. As a result, there is a need for a suite of intermediate scale column experiments large enough to exhibit key heat and mass transfer processes governing at larger scales yet small enough to permit systematic and controlled assessment of such processes.

2.3 Influence of Heat on NAPL Mobility

2.3.1 Overview

As mentioned previously, since the fuel in STAR applications is in a liquid state, it has the potential to mobilize during smouldering. Numerous studies have investigated the migration of NAPLs in the subsurface following a contaminant release, which are critical for contaminated site characterization. Under ambient subsurface conditions, however, NAPL migration may occur over a period of months to years before reaching a stable distribution in the subsurface depending on fluid and aquifer properties (Gerhard et al., 2007). As a result, these rates of migration are relatively inconsequential over the time scales relevant to smouldering remediation. With the influence of heat, however, the fluid properties and the dynamics of NAPL migration change significantly.

The influence of heat on NAPL mobilization has been studied in two key applications in literature which are relevant to STAR: enhanced oil recovery and in-situ thermal remediation.

2.3.2 Enhanced Oil Recovery

A number of different technologies have been proposed and studied to enhance oil recovery below residual saturations from reservoirs. One such technology is in-situ combustion (ISC). In the ISC process, a portion of the oil is ignited and the burn is

sustained through the continuous addition of air (and in some cases a combination of air and water). The heat generated from the combustion reaction along with the force of the injected air and water is used to displace the reduced viscosity oil toward a recovery well (Sarathi, 1999). While ISC differs from STAR in that the objective of ISC is to minimize oil destruction and maximize oil recovery, some of the fundamental processes involved with fuel mobilization in the presence of a combustion front are relevant. As such, it is expected that some mobilization and volatilization of the NAPL contaminant may occur during smouldering remediation, less significant than ISC but at much higher rates than ambient migration processes permit.

2.3.3 NAPL Mobility and Thermal Remediation

As discussed in Section 2.1.3, heat is used in a number of remediation technologies to affect change on fluid properties and permit recovery of NAPL through both volatilization and enhanced hydraulic displacement. These same property changes that permit enhanced NAPL recovery may also lead to undesirable mobilization. Contrary to enhanced oil recovery where residual or remobilized oil that cannot be recovered is merely an economic loss, uncontrolled remobilization of NAPL in the context of contaminated site remediation may be a significant concern.

This type of heat induced mobilization has been observed, for example, during implementation of steam injection for remediation. As steam is injected, the NAPL is volatilized within the high temperature region of the soil, but condenses and accumulates ahead of the steam condensation front. Given sufficient NAPL accumulation in this condensation region, it may form a continuous phase in which gravitational forces will overcome the trapping forces and permit the downward mobilization of NAPL outside of

the target treatment area (Kaslusky and Udell, 2005). While certain techniques are being investigated to minimize the potential for mobilization, such as injecting air with the steam as described by Kaslusky and Udell, the risk is still present.

A detailed investigation on the effect of temperature on the properties of organic fluids was conducted to evaluate the feasibility of thermal remediation techniques (Sleep and Ma, 1997). The correlations between temperature and fluid properties developed were used to assess the potential for negative mobilization consequences with respect to hot water flooding (O'Carroll and Sleep, 2009). Based on numerical simulations conducted on two NAPLs with different densities, it was found that increasing the temperature of the hot water flooding not only enhanced NAPL recovery, but also accelerated downward mobilization for the dense NAPL due to reduced viscosity.

While processes of NAPL volatilization, condensation and mobilization resulting from the presence of heat have been recognized for other thermal remediation technologies, fuel volatilization and mobility in the context of smouldering remediation have not been previously investigated. The extent and effects of volatilization and mobilization both on remediation effectiveness and smouldering metrics are relatively unknown.

2.4 Conclusions

Complete remediation of NAPL contaminated sites continues to be a challenge, particularly for large source zones containing complex contaminants of low volatility, such as coal tar or creosote. STAR presents itself as a promising remediation technology which uses the NAPL contaminant as the fuel to permit its own destruction. This technology has benefits over other thermal remediation technologies in that it is a self-

sustaining process and therefore has significantly reduced energy requirements. The success of this technology has been demonstrated both at the bench and field scales, however these studies have focused primarily on the influence of engineering parameters (e.g., air flux) or site parameters (e.g., permeability) on the overall degree of remediation of the soil.

While there are a number of studies on the smouldering of solids, relatively little is known about the smouldering of liquid fuels. There is currently a knowledge gap on the transient processes that occur ahead of, within and behind the smouldering front as it propagates during contaminant remediation. Two dynamic processes that have not been explored in the context of STAR are NAPL mobility and emission composition. Previous work on in-situ combustion and thermal remediation technologies indicate that NAPL volatilization and mobility may be important to investigate to develop a complete understanding of the STAR process. In order to investigate these processes, it is necessary to not only consider before and after soil conditions, but to analyse smouldering data as a function of both time and space. This is best accomplished through highly controlled laboratory experiments; however, these systems must be of a sufficient length scale to permit the collection of transient data.

This work presents a series of medium and tall column experiments exploring liquid fuel mobility in the context of smouldering remediation and the consequent potential to exhibit superadiabatic conditions (Chapter 3) and presents an assessment of the potential for the volatilization and condensation of combustion products (Chapter 4). While these investigations are fundamental studies of the process, the results may also have significant practical implications on the design of full scale systems.

2.5 References

Aldushin, A. P., Rumanov, I. E., & Matkowsky, B. J. (1999). Maximal energy accumulation in a superadiabatic filtration combustion wave. *Combustion and Flame, 118*(1-2), 76-90.

Anderson, M. K., Sleight, R. T., & Torero, J. L. (2000). Ignition signatures of a downward smolder reaction. *Experimental Thermal and Fluid Science, 21*(1-3), 33-40.

Davis, E. L. (1997). *How heat can enhance in-situ soil and aquifer remediation: Important chemical properties and guidance on choosing the appropriate technique*. EPA 540-S-97-502. Washington, DC: U.S. Environmental Protection Agency.

Gerhard, J. I., Pang, T., & Kueper, B. H. (2007). Time scales of DNAPL migration in sandy aquifers examined via numerical simulation. *Ground Water, 45*(2), 147-157.

Heron, G., Carroll, S., & Nielsen, S. G. (2005). Full-scale removal of DNAPL constituents using steam-enhanced extraction and electrical resistance heating. *Ground Water Monitoring and Remediation*, 25(4), 92-107.

Interstate Technology & Regulatory Council, ITRC. (2008). *In Situ Bioremediation of Chlorinated Ethene: DNAPL Source Zones*. Washington, DC: Interstate Technology & Regulatory Council, Bioremediation of DNAPLs Team.

Kaslusky, S. F., & Udell, K. S. (2005). Co-injection of air and steam for the prevention of the downward migration of DNAPLs during steam enhanced extraction: An experimental evaluation of optimum injection ratio predictions. *Journal of Contaminant Hydrology, 77*(4), 325-347.

Khan, F. I., Husain, T., & Hejazi, R. (2004). An overview and analysis of site remediation technologies. *Journal of Environmental Management, 71*(2), 95-122.

Kueper, B. H., Stroo, H.F., Vogel, C. M., & Ward, C. H. (2014). *Chlorinated Solvent Source Zone Remediation*. New York: Springer. 713 p.

Lemming, G., Hauschild, M. Z., Chambon, J., Binning, P. J., Bulle, C., Margni, M., & Bjerg, P. L. (2010). Environmental Impacts of Remediation of a Trichloroethene-Contaminated Site: Life Cycle Assessment of Remediation Alternatives. *Environmental Science & Technology*, 44(23), 9163-9169.

Mercer, J. W., & Cohen, R. M. (1990). A review of immiscible fluids in the subsurface: Properties, models, characterization and remediation. *Journal of Contaminant Hydrology, 6*(2), 107-163.

National Research Council, NRC. (2004). *Contaminants in the subsurface: Source zone assessment and remediation*. Washington, DC: The National Academies Press.

O'Carroll, D. M., & Sleep, B. E. (2009). Role of NAPL thermal properties in the effectiveness of hot water flooding. *Transport in Porous Media, 79*(3), 393-405.

Ohlemiller, T. J. (1985). Modeling of smoldering combustion propagation. *Progress in Energy and Combustion Science, 11*(4), 277-310.

Ohlemiller, T. J., & Lucca, D. A. (1983). An experimental comparison of forward and reverse smolder propagation in permeable fuel beds. *Combustion and Flame, 54*(1-3), 131-147.

Palmer, K. N. (1957). Smouldering combustion in dusts and fibrous materials. *Combustion and Flame, 1*(2), 129-154.

Pironi, P., Switzer, C., Gerhard, J. I., Rein, G., & Torero, J. L. (2011). Self-sustaining smoldering combustion for NAPL remediation: Laboratory evaluation of process sensitivity to key parameters. *Environmental Science & Technology, 45*(7), 2980-2986.

Pironi, P., Switzer, C., Rein, G., Fuentes, A., Gerhard, J. I., & Torero, J. L. (2009). Small-scale forward smouldering experiments for remediation of coal tar in inert media. *Proceedings of the Combustion Institute, 32*, 1957-1964.

Rein, G., Cohen, S., & Simeoni, A. (2009). Carbon emissions from smouldering peat in shallow and strong fronts. *Proceedings of the Combustion Institute, 32*, 2489-2496.

Sarathi, P. S. (1998). *In-situ combustion handbook: Principles and practices*. DOE-PC-91008-0374. Tulsa, OK: U.S. Department of Energy, National Petroleum Technology Office.

Scholes, G. C., Gerhard, J. I., Grant, G. P., Major, D. W., Vidumsky, J. E., Switzer, C., & Torero, J. L. (2015). Smoldering remediation of coal tar contaminated soil: Pilot field tests of STAR. *Environmental Science & Technology*, Article ASAP.

Schult, D. A., Matkowsky, B. J., Volpert, V. A., & FernandezPello, A. C. (1996). Forced forward smolder combustion. *Combustion and Flame, 104*(1-2), 1-26.

Sleep, B. E., & Ma, Y. (1997). Thermal variation of organic fluid properties and impact on thermal remediation feasibility. *Journal of Soil Contamination, 6*(3), 281-306.

Stegemeier, G. L. & Vinegar, H. J. (2001). Thermal conduction heating for in-situ thermal desorption of soils. In Oh, C. H. (Ed.), *Hazardous & Radioactive Waste Treatment Technologies Handbook* (Ch. 4.6-1). Boca Raton, FL: CRC Press.

Switzer, C., Pironi, P., Gerhard, J. I., Rein, G., & Torero, J. L. (2009). Self-sustaining smoldering combustion: A novel remediation process for non-aqueous-phase liquids in porous media. *Environmental Science & Technology, 43*(15), 5871-5877.

Switzer, C., Pironi, P., Gerhard, J. I., Rein, G., & Torero, J. L. (2014). Volumetric scale-up of smouldering remediation of contaminated materials. *Journal of Hazardous Materials, 268*, 51-60.

TASK Leipzig. (2013). *Guidelines: In situ thermal treatment (ISTT) for source zone remediation of soil and groundwater*. Leipzig: Helmholtz Centre for Environmental Research.

Torero, J. L., & Fernandez-Pello, A. C. (1996). Forward smolder of polyurethane foam in a forced air flow. *Combustion and Flame, 106*(1–2), 89-109.

Torero, J. L., & Fernandez-Pello, A. C. (1995). Natural-convection smolder of polyurethane foam, upward propagation. *Fire Safety Journal, 24*(1), 35-52.

Triplett Kingston, J. L., Johnson, P. C., Kueper, B. H., & Mumford, K. G. (2014). In situ thermal treatment of chlorinated solvent source zones. In Kueper, B. H., Stroo, H.F., Vogel, C. M., & Ward, C. H. (Eds.), *Chlorinated Solvent Source Zone Remediation* (pp. 509-558). New York: Springer.

Vantelon, J. P., Lodeho, B., Pignoux, S., Ellzey, J. L., & Torero, J. L. (2005). Experimental observations on the thermal degradation of a porous bed of tires. *Proceedings of the Combustion Institute, 30*, 2239-2246.

White, P. D. & Moss, J. T. (1983). *Thermal Recovery Methods.* Tulsa, OK: PennWell Books. 384 p.

3 SMOULDERING COMBUSTION AND NON-AQUEOUS PHASE LIQUID MOBILITY

3.1 Introduction

Successful remediation of non-aqueous phase liquid (NAPL) contamination in the subsurface presents a significant challenge. These water-immiscible organic compounds may enter the subsurface as a result of accidental spills or inadequate disposal practices and have the potential to persist and provide a continued source of contamination. Some common sources of NAPL contamination include: petroleum hydrocarbon fuels, coal tar formed as waste products from manufactured gas plants, chlorinated hydrocarbons used as solvents and degreasers, and creosote used in wood treatment processes (Mercer and Cohen, 1990). The complex and high molecular weight structure of some of these compounds, such as coal tar, presents challenges for many existing remediation technologies due to its low aqueous solubility, low volatility and the propensity to resist rapid biodegradation (Birak and Miller, 2009). These same properties, however, also permit coal tar to be a viable fuel for combustion.

The smouldering of NAPL contaminated soil has promise as an effective and energy efficient remediation approach (Switzer et al., 2009). Smouldering combustion is a flameless exothermic reaction occurring on the surface of a condensed phase fuel (Ohlemiller, 1985). As with any combustion reaction, successful combustion requires the presence of fuel, heat, and air. In this case, the fuel is the NAPL contaminant. To initiate controlled combustion of the NAPL, a short duration input of heat is required to preheat the contaminant in the immediate vicinity of the ignition point to required temperatures. Once ignition is achieved the heat source may be removed as the combustion of the

NAPL generates enough heat to sustain the reaction. Continued addition of forced air allows the reaction front to propagate forward, destroying the contaminant in its path and leaving a remediated soil matrix behind. The inorganic porous matrix provided by contaminated soil permits the smouldering reaction to propagate as the soil provides both thermal insulation to minimize heat losses and allows the delivery of oxygen to the fuel via convection and diffusion (Pironi et al., 2009).

Extensive laboratory column studies with an approximate contaminated soil volume of 0.002 m^3 have been conducted to demonstrate the proof-of-concept as well as to define a range of contaminants, soil types and airflow rates amenable to successful remediation (Pironi et al., 2011). Smouldering remediation has also been demonstrated at larger scales, through experiments in both an oil drum (0.3 m^3) and a bin (3 m^3) (Switzer et al., 2014). Additionally, this technology has recently been applied at the pilot scale in an ex-situ prototype reactor (1 m^3) and in-situ at a contaminated former industrial site (Scholes, 2013).

While it is evident from these studies that the overall degree of remediation is consistent across scales, there is a missing link between the small laboratory columns and the larger scale studies which would be useful for understanding differences in smouldering front propagation behaviour. For example, Figure 3.1 shows a comparison of the evolution of temperatures over time within a laboratory column and the ex-situ prototype reactor under the same experimental conditions. For the laboratory experiment in Figure 3.1(a), a 78 minute preheating period permitted the NAPL immediately above the ignition coil in the base of the column to reach ignition temperatures at which point the forced air supply was turned on. The distinct inflection of temperatures indicates the presence of

exothermic reactions and the start of smouldering combustion. Once the smouldering reaction has been initiated, the ignition coil can be turned off as the energy from the combustion reaction is sufficient to sustain the process. Typical of small-scale laboratory column experiments, the temperature history displays regularly spaced and overlapping temperature curves with relatively constant peak temperatures and is representative of a self-sustaining smouldering reaction (Walther et al., 2000).

For the larger scale conditions in Figure 3.1(b), similar rapid increases in temperature are observed when smouldering commences in the vicinity of each thermocouple location and similar peak temperatures are reached. The temperature history, however, also displays some distinct differences to the column despite the identical experimental conditions. Some of these differences include: (1) a low temperature plateau below 100°C before ignition is observed at each thermocouple location (shown in TC5 to TC17), (2) brief periods of decreasing temperatures within ignition curves (e.g. TC5), and (3) elevated peak temperatures at select thermocouples (e.g. TC 11). While the significance of the differences in these temperature plots will be explained in more detail for the experiments in this study, it is evident from looking at these figures that more complex behaviour occurs at larger scales. It is important to study the cause of these behaviours as conditions such as highly elevated peak temperatures can result in operational issues and the potential to transition to flaming in large scale ex-situ systems.

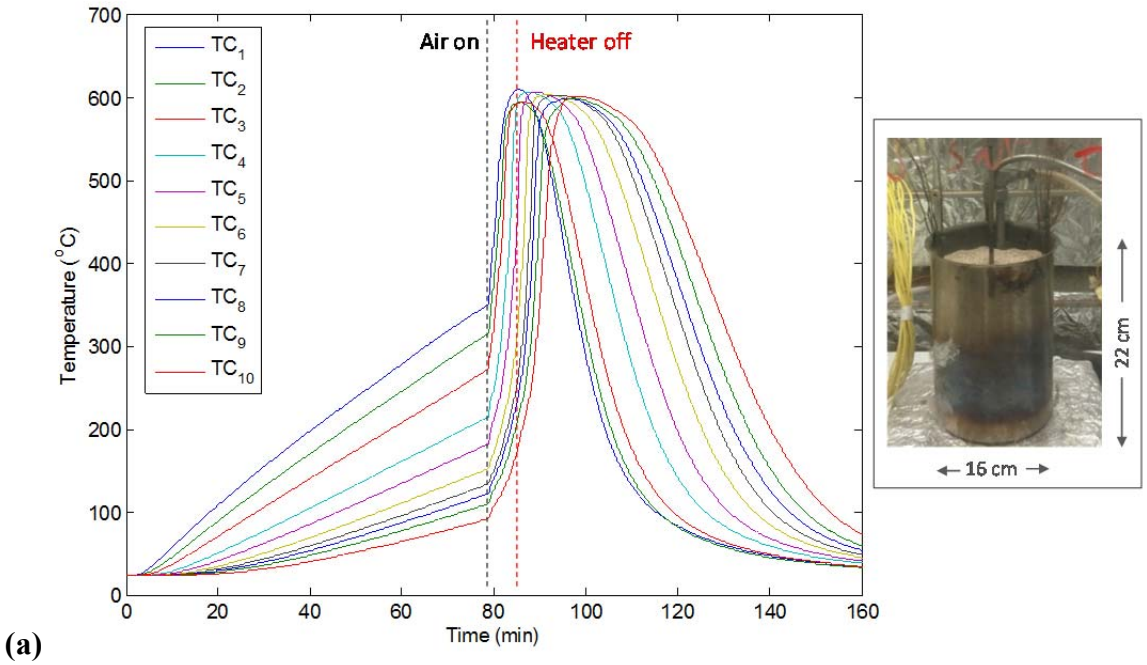

(a)

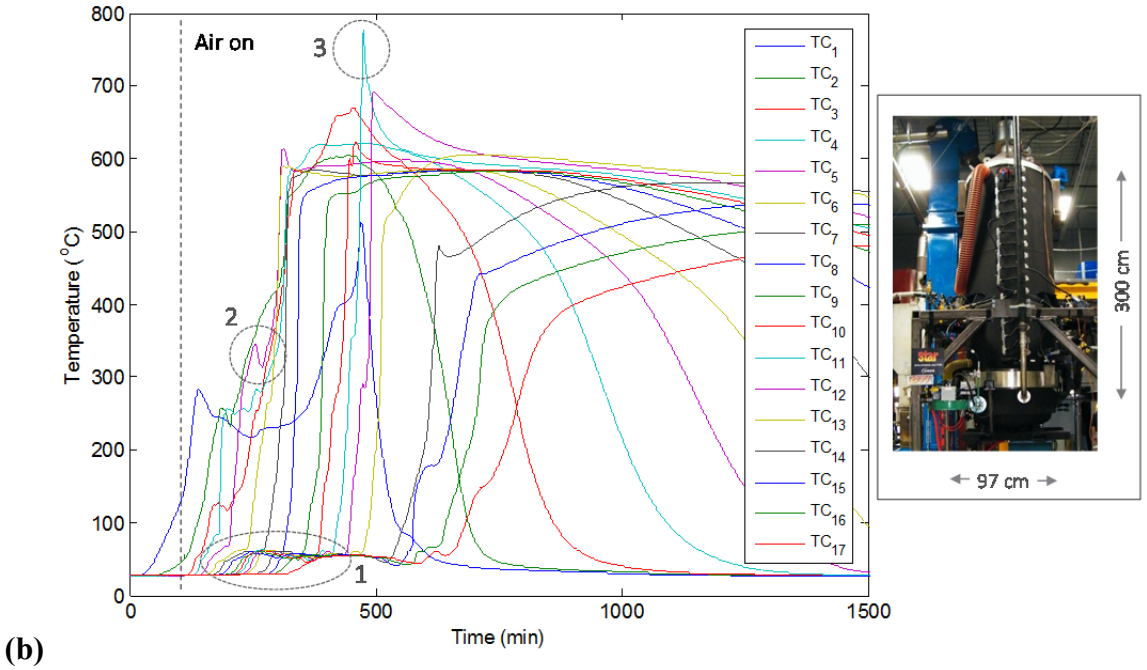

(b)

Figure 3.1: Evolution of temperature versus time for (a) a small laboratory column (0.002 m^3) in comparison to (b) the ex-situ prototype reactor (1 m^3) under the exact same experimental conditions, including: contaminant type and concentration, sand type and air flux. Thermocouples (TCs) are located at equal distances along the apparatus centreline, and are numbered sequentially from the heater at the base.

3.1.1 Conceptual Model of Smouldering Front

Figure 3.2 represents a conceptual model of the vertical spatial distribution of temperature and oxygen concentrations for an upward forward smouldering combustion reaction, depicted at a particular moment in time. In the uppermost region, sand and NAPL are unaffected by the smouldering reaction. The NAPL is present in the porous matrix at ambient temperatures (T_∞) and is therefore unchanged physically or chemically.

In the preheating zone, due to closer proximity to the exothermic oxidation zone, the NAPL is exposed to elevated temperatures. These elevated temperatures are a result of heat transfer from the pyrolysis and oxidation zones below via conduction, convection and radiation to the unreacted sand and fuel. A significant portion of the NAPL in this preheating zone remains as a liquid at elevated temperatures. Therefore, there is the potential for the NAPL embedded within the porous matrix in the preheating zone to move at a certain velocity (V_{NAPL}) due to the relative influence of the forces of air and gravity.

The air flowing through the both the preheating and pyrolysis zones is oxygen deficient due to consumption in the oxidation zone. In the presence of highly elevated temperatures closest to the oxidation zone, some of the NAPL may begin to undergo endothermic pyrolysis reactions, which involves nonoxidative decomposition of the fuel (Torero and Fernandez-Pello, 1996). These pyrolysis reactions may result in the formation of a solid char.

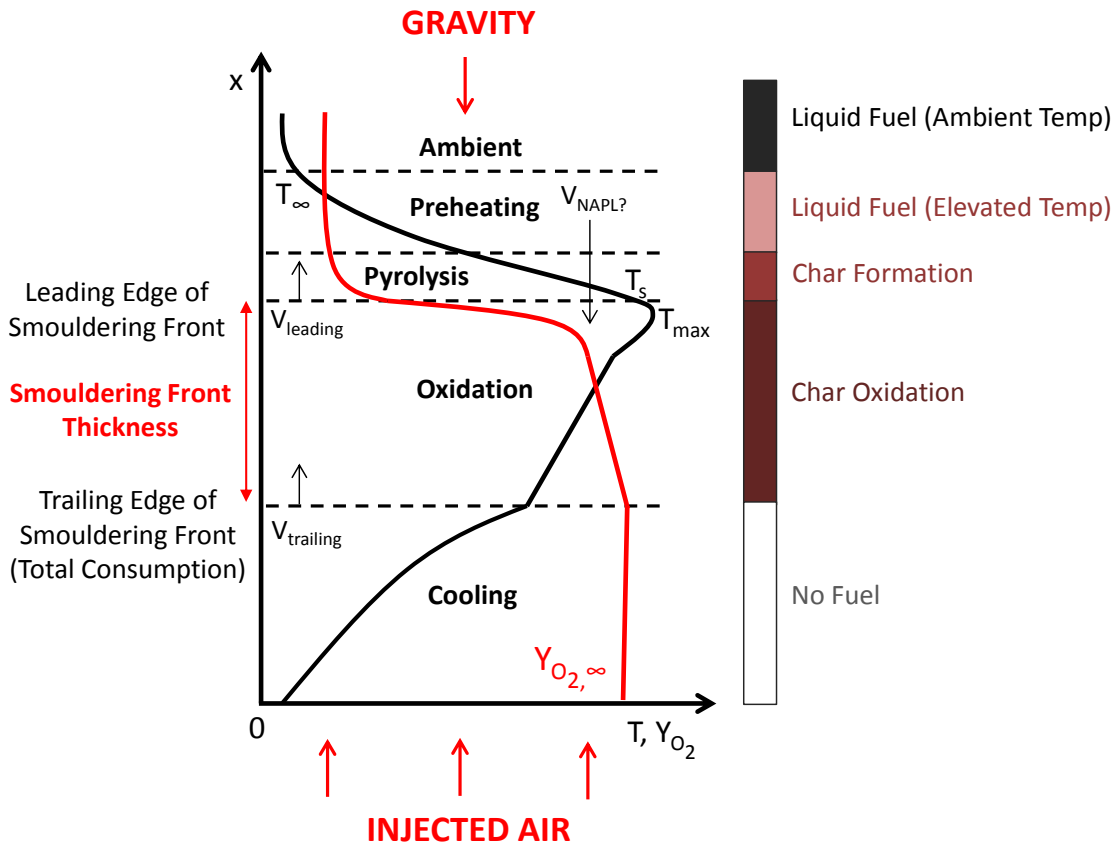

Figure 3.2: Conceptual model of the distribution of temperature and oxygen concentrations in a column experiencing upward, forward propagation of a smouldering reaction (Torero, personal communication, March 2013). The key force vectors (red arrows) are labelled. The key regions in the system are named and the associated form of the NAPL (fuel) is identified on the right hand side.

As the temperatures in the pyrolysis zone approach the smouldering ignition temperature for the given contaminant (T_s) and oxygen concentrations are sufficient to sustain smouldering, exothermic oxidations reactions will occur. These conditions mark the leading edge of the smouldering front. The zone between the boundaries of the leading and trailing edge of the smouldering front defines the oxidation zone and the smouldering front thickness. In this oxidation zone, as oxygen diffuses to the surface of the NAPL, exothermic reactions occur between the NAPL and oxygen, resulting in a decrease in oxygen concentrations and an increase in temperature to the characteristic peak

temperature for the given contaminant (T_{max}). The NAPL in this reaction region has previously been converted through pyrolysis reactions to a char and is therefore considered to be immobile.

The trailing edge of the smouldering front is most often synonymous with total fuel consumption. Below this point, no NAPL remains and therefore this marks the end of the oxidation zone. Since the trailing edge of the smouldering front is defined by the completion of smouldering whereas the leading edge of the smouldering front is defined by the onset of smouldering, the velocity of these two fronts ($V_{leading}$ and $V_{trailing}$) are often not equal. The leading edge will generally be controlled by heat transfer from the front towards the hot zone, while the trailing edge is determined purely by the rate of destruction, more often controlled by combustion chemistry. Typically, the time required to destroy all fuel at the trailing edge results in $V_{trailing} < V_{leading}$, and consequently an expansion in the smouldering front thickness over time.

Above the trailing edge temperatures are originally low, so chemistry is slow and oxygen is only partially consumed. Oxygen consumption will result from a complex function of the relative speed of the chemistry with respect to residence times, i.e. Damköhler number. Closer to the leading edge the temperatures will be higher, the chemistry faster and therefore oxygen consumption will be more significant. Complete depletion of oxygen is expected at the leading edge.

Below the trailing edge of the smouldering front, all NAPL has been consumed by the passing smouldering front and the remaining porous matrix undergoes cooling. As air enters from the bottom of the column ($x = 0$), the oxygen concentration is initially at

ambient air conditions ($Y_{O_2,\infty}$). In this cooling zone, no reactions are occurring and therefore the oxygen remains constant at ambient concentrations. The temperatures in the cooling region are decreasing mainly due to convection from the forced air flow below and since there is no fuel source in this region, no additional heat is being produced.

3.1.2 Potential for NAPL Mobility

Contrary to traditional smouldering literature where the fuel is often a solid, such as dust or polyurethane foam, the fuel in the context of soil remediation is a liquid. The fuel (NAPL) therefore has the ability to move as the smouldering reaction progresses. The potential for fuel mobilization is utilized during in situ combustion through the generation of a combustion front to reduce oil viscosity ahead of the front (Thomas, 2008). This allows the previously trapped residual oil to become mobile and permits oil recovery from a subsequent well. Similar to in situ combustion, in the preheating zone located ahead of the leading edge of the smouldering front, the liquid contaminant is exposed to highly elevated temperatures prior to pyrolysis and oxidation reactions occurring. While the oil mobilization and recovery during in situ combustion often occurs in a horizontal configuration in the subsurface, NAPL mobilization has the potential to occur vertically within a smouldering column. The main difference between these two applications is that in situ combustion is designed to minimize oil destruction and enhance oil recovery, whereas smouldering combustion for remediation is designed to destroy the contaminant.

Fluid viscosity has a dominant effect on the rate of NAPL migration (Gerhard et al., 2007). At ambient temperatures, the viscosity of long chain hydrocarbons and coal tars are relatively high, meaning migration is very slow even in the presence of significant

hydraulic gradients. However, liquid viscosity decreases exponentially with increasing temperatures (Potter and Wiggert, 2002) and therefore the migration process may be accelerated in the presence of the elevated temperatures observed in exothermic smouldering reactions. Figure 3.3 shows the decrease in viscosity that occurs with increasing temperatures (from 20 to 140°C) for a range of NAPLs used in smouldering remediation columns. Even over this limited range of temperatures, viscosity may decrease by a factor of 10 to up to 1,000,000. Within the preheating zone, NAPLs may be exposed to elevated temperatures up to 300 to 400°C above ambient and therefore the potential for decreased viscosity and subsequent NAPL migration is significant.

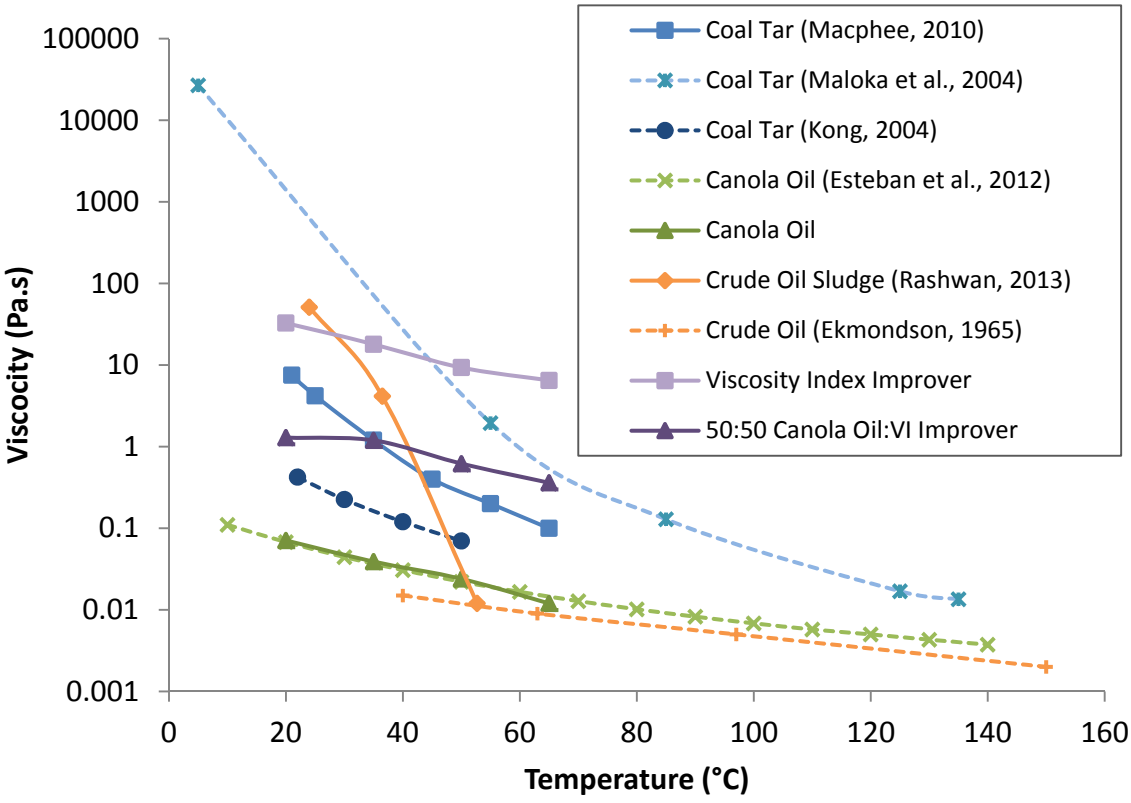

Figure 3.3: Relationship between viscosity and temperature for a range of NAPLs (adapted from Rashwan, 2013).

This migration is dependent on a combination of both reduced viscosity in the preheating zone (Figure 3.3) and the force balance between gravity and forced air in the preheating region (Figure 3.2). The resultant force will determine the direction of migration, while the influence of temperature on viscosity will affect the rate of NAPL migration.

While temperature also results in small changes in NAPL density, these small density changes have insignificant effects on the relative density between the NAPL and air and therefore the influence of gravity is similar in all cases. Therefore, the force balance and potential for migration is primarily affected by forced air flux and NAPL viscosity. This migration process may affect the spatial distribution of NAPL and therefore can influence smouldering metrics.

The objective of this work was to explore, for the first time, whether NAPL mobility is an important issue in smouldering remediation; in other words, whether it occurs and, if it does, whether it influences smouldering behaviour. If NAPL mobility was observed, it was necessary to determine under what conditions mobility is expected, as well as the influence on smouldering metrics. Additionally, a further objective was to develop predictive tools to help analyze and understand the conditions under which NAPL mobility is expected to be important. These objectives were investigated through carefully controlled laboratory column experiments of contaminant smouldering using varying contaminated zone heights. Experimental results were combined with analytical and numerical modelling to explore the interplay of forces and timescales acting on the NAPL within a smouldering column. The improved understanding of NAPL mobility in the context of smouldering remediation will aid in the design and implementation of commercial applications of this technology.

3.2 Materials and Methodology

The investigation of NAPL mobility was divided into three parts. The first was a laboratory investigation of smouldering metrics under a range of experimental conditions where mobility varied in significance. The second part involved the development of an analytical model that accounts for a simple vertical force balance between the air and NAPL to determine the potential for NAPL mobility. In the third part, the experimental and analytical model results were compared to a numerical model to better understand the factors promoting or inhibiting NAPL mobility in a smouldering column.

3.2.1 Experimental Setup

A series of forward smouldering column experiments were conducted in two reaction vessels with different heights to explore the relationship between NAPL mobility and injection airflow rate and the resulting effect on smouldering metrics at increasing length scales. The two stainless steel columns were 16 cm in diameter, with the shorter column measuring 63 cm in height and containing a 30 cm contaminated zone, and the taller column measuring 127 cm in height and containing a 90 cm contaminated zone. These two columns will herein be termed “30 cm” and “90 cm” columns, respectively, due to the importance of the total contaminated zone height.

The experimental setup was based upon the standard configuration developed by Switzer et al. (2009). A schematic diagram of the 30 cm column experimental apparatus in an upward smoulder configuration is shown in Figure 3.4. The 90 cm column was identical except for the height of the contaminated zone and the presence of 26 thermocouples

instead of 9. The removable base connection allowed for columns of various heights to be accommodated using the same equipment.

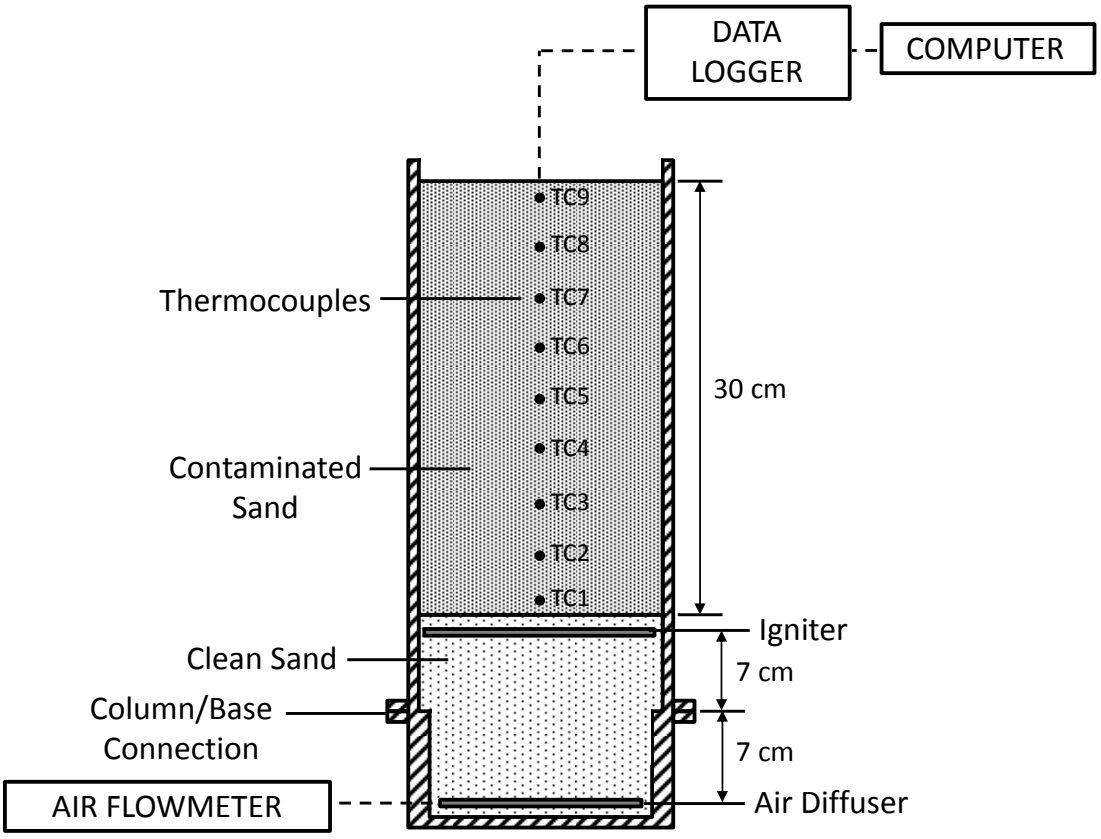

Figure 3.4: Schematic diagram of 30 cm column experimental apparatus. The 90 cm column setup consists of the same configuration, with the respective column height connected to the removable base.

An air diffuser, consisting of eight perforated radial extensions from a centralized support, was placed in the bottom of the column and connected to the compressed house air supply. A 762 mm long Inconel-sheathed electrical cable heater with a 3.25 mm square cross section (Watlow, USA, 450 W) was coiled into a flat spiral and placed above the air diffuser. Clean sand filled the bottom of the column until a height that covered the heater by a few millimetres. Quartz sand (#12ST, Bell and Mackenzie Co. Ltd., Canada) with a bulk density of 1600 kg/m^3, mean grain size of 0.88 mm, and an

average porosity of 0.38 was used in all experiments. The contaminated material was prepared by mechanically mixing (KitchenAid, Pro Line) the desired mass ratio of sand to NAPL until visually homogeneous. A 30 cm (or 90 cm) layer of the contaminated material was packed in 10 cm lifts above the diffuser and heater. Care was taken in packing to prevent a preferential air flow path between the contaminated material and the wall. Inconel-sheathed type K thermocouples spaced at 3.5 cm intervals were placed along the centreline of the contaminated zone, with the first thermocouple located 1.0 cm above the heater. The thermocouples were connected to a data acquisition system (Multifunction Switch/Measure Unit 34980A, Agilent Technologies) and a personal computer to record data at two second intervals. Insulation (McMaster-Carr, 2" rigid very-high-temperature mineral wool) also encircled the columns to minimize heat losses.

A standardized preheating procedure was developed for the NAPLs investigated based on the ignition protocol described by Switzer et al. (2009), where the conductive heating coil was used to preheat the base of the contaminated zone until the adjacent thermocouple (TC1) reached 360˚C, typically requiring approximately 90 minutes. The air supply was then initiated and maintained until completion of the experiment. For all column tests, the heater was turned off after TC1 reached its peak temperature, approximately five minutes after the start of air flow; thus, from this time onwards, the reaction propagated in a self-sustaining manner. The air flow through the column was regulated using a mass flow controller (FMA5544, Omega Engineering Inc.) to ensure that the oxidizer flow remained constant throughout the duration of the experiment, despite decreases in pressure drop through the porous material as the smouldering front progressed (Torero and Fernandez-Pello, 1996). The inlet (Darcy) air flux reported for all experiments was

calculated by dividing the volumetric flow at standard temperature and pressure by the horizontal cross-sectional area of the reaction vessel.

Table 3.1 outlines the set of experiments conducted. In order to better understand NAPL migration, six column experiments were performed at three different forced air flow rates (1.25, 2.50 and 6.25 cm/s) and two different contaminated zone heights (30 and 90 cm). Sand type, contaminant type, contaminant concentration and air mass flux were kept constant between the two column scales. By varying air flow rate and contaminated zone height, the relative significance of forces acting on the NAPL within the column also varied. The increase in injected air flow increased the upward force of air acting on the NAPL, and the increase in contaminated zone height increased the total NAPL head over which gravity could act upon. Evidence of NAPL migration can be assessed through temperature data with more significant migration changing both the typical temperature distribution and peak temperatures observed within a smouldering column. In order to assess the smouldering temperature behaviour over time and space in the column, temperature histories (temperature vs. time) and temperature profiles (temperature vs. distance) can be utilized.

Table 3.1 Summary of Smouldering Column Experiments

Test Number	Canola Oil:VI Improver (% by mass)	NAPL Concentration (g/kg)	Air Flux (cm/s)	Height of Contaminated Zone (cm)
1			1.25	
2	50:50	60	2.50	30
3			6.25	
4			1.25	
5	50:50	60	2.50	90
6			6.25	

The NAPL used was an equal part mixture of canola oil and viscosity index improver (V-158, Tempo Canada ULC). This fuel was developed as a non-toxic, chemically homogeneous surrogate for hazardous liquid contaminants. These properties permit easier laboratory handling and provide more predictable behaviour to better understand trends in data analysis. Viscosity index improver was added to the canola oil in an attempt to minimize mobilization within the column during initial preheating and isolate migration occurring during the combustion process. As shown in Figure 3.3, the viscosity of pure canola oil is very low and decreases further with the presence of elevated temperatures. With the addition of viscosity index improver, both the initial viscosity of canola oil and the viscosity at elevated temperatures are increased to the same order of magnitude as more viscous NAPLs, such as coal tar.

3.2.2 Nondimensionalization

In order to compare smouldering behaviour in different sized columns, time was nondimensionalized according to:

$$Nondimensionalized\ Time = Time\ (min) * \frac{Average\ Smouldering\ Velocity\ \left(\frac{cm}{min}\right)}{Length\ of\ Contaminated\ Zone\ (cm)} \quad (\mathbf{1})$$

Temperature histories were used to calculate the local propagation velocity of the smoulder front based on the time lapse of the front arrival at two consecutive thermocouples and the known distance between them (Torero and Fernandez-Pello, 1996). The front arrival time at a particular thermocouple was defined as the average of the times at which three predetermined temperatures were reached, which varied depending on the characteristic peak temperatures of the fuel (Pironi et al., 2009). The

average smouldering velocity is defined as the average of all the local smouldering propagation velocities calculated between consecutive thermocouples. Using Equation (1), a nondimensionalized time of one is the time at which the leading edge of the smouldering front reaches the end of the contaminated zone, regardless of the height of the column. As a result of incorporating both the smouldering front velocity and contaminated zone length, this nondimensionalized time can also be used to compare experiments at different airflow rates across various length scales. To maintain consistency and comparability between experiments with different contaminated zone heights, this nondimensionalized time approach will be used for all graphs to follow.

3.2.3 Analytical Model

The objective of the analytical model was to develop a simple method for predicting whether a given scenario exhibited the potential for NAPL mobilization. Towards this end, a simple equation would be useful that could approximate the magnitude and direction of the NAPL hydraulic gradient across the contaminated zone. The total NAPL head at the top and bottom of a vertical column is:

$$\frac{\Delta h}{\Delta L} = \frac{h_{NAPL}^{top} - h_{NAPL}^{base}}{L} \quad \textbf{(2)}$$

where h is the total hydraulic head of the NAPL at the top and bottom of the NAPL saturated zone, respectively, and $\Delta L = L$ is the length of the contaminated zone given that the datum is considered to be the base of the column. Since liquids will flow from a region of high hydraulic head to low hydraulic head, if $h_{NAPL}^{top} > h_{NAPL}^{base}$ there is the potential for downward migration of NAPL. This corresponds with a positive hydraulic

gradient. Similarly, if $\Delta h/\Delta L$ is negative ($h_{NAPL}^{top} < h_{NAPL}^{base}$) then there is the potential for upward mobilization of NAPL.

The hydraulic head consists of the sum of the pressure and elevation head, such that:

$$h_{NAPL}^{top} = \frac{P_{NAPL}^{top}}{\rho_{NAPL} \cdot g} + z_1 \quad \text{and} \quad h_{NAPL}^{base} = \frac{P_{NAPL}^{base}}{\rho_{NAPL} \cdot g} + z_2 \tag{3}$$

where P is the pressure, ρ is density, g is gravitational acceleration and z is the elevation above the datum (in this case the base of the column).

Therefore, substituting (3) into (2), where $z_1 = L$ and $z_2 = 0$:

$$\frac{\Delta h}{\Delta L} = \frac{\frac{P_{NAPL}^{top}}{\rho_{NAPL} \cdot g} + L - \frac{P_{NAPL}^{base}}{\rho_{NAPL} \cdot g}}{L} \tag{4}$$

For two-phase flow in porous media, the wetting phase pressure (P_{NAPL}) is equal to the non-wetting phase pressure (P_{air}) minus the capillary pressure (P_c):

$$P_{NAPL} = P_{air} - P_c \tag{5}$$

For the relatively high forced air flow conditions typically employed in liquid smouldering, it can be assumed that P_c is negligible and therefore:

$$P_{NAPL} \cong P_{air} \tag{6}$$

Note that this is an assumption that will be tested in the Results. For an open column, the air pressure at the top of the column is equal to atmospheric and therefore, based on (6), it can be assumed that the NAPL pressure at the top of the column is approximately equal

to zero. Substituting this assumption for NAPL pressure at the top and bottom of the column into (4):

$$\frac{\Delta h}{\Delta L} = \frac{L - \frac{P_{air}^{base}}{\rho_{NAPL} \cdot g}}{L} \quad \textbf{(7)}$$

or

$$\frac{\Delta h}{\Delta L} = 1 - \frac{P_{air}^{base}}{\rho_{NAPL} \cdot g \cdot L} \quad \textbf{(8)}$$

The air pressure at the base of the column can be approximated using the Kozeny-Carman equation (McCabe et al., 1993):

$$\frac{\Delta P}{L} = \left[\frac{180 V \mu_{air}}{\varphi_s^2 D_p^2}\right]\left[\frac{(1-\varepsilon)^2}{\varepsilon^3}\right] \quad \textbf{(9)}$$

where, ΔP is the pressure drop across the length of the packed column, L is the length of the column, V is the forced air flux (volumetric flow rate divided by cross-sectional area of the column), μ_{air} is the dynamic viscosity of air, φ_s is the sphericity of the particles in the column, D_p is the mean diameter of the particles, and ε is the effective air porosity (total porosity minus the percent volume occupied by NAPL).

Since for an open column $P_{air}^{top} = 0$, P_{air}^{base} can be approximated as:

$$P_{air}^{base} = L\left[\frac{180 V \mu_{air}}{\varphi_s^2 D_p^2}\right]\left[\frac{(1-\varepsilon)^2}{\varepsilon^3}\right] \quad \textbf{(10)}$$

Substituting (10) into (8) and simplifying:

$$\frac{\Delta h}{\Delta L} = 1 - \frac{\left[\frac{180 V \mu_{air}}{\varphi_s^2 D_p^2}\right]\left[\frac{(1-\varepsilon)^2}{\varepsilon^3}\right]}{\rho_{NAPL} \cdot g} \quad \textbf{(11)}$$

Therefore, if the hydraulic gradient calculated using (11) is positive then there will be a downward NAPL hydraulic gradient in the column and the potential for downward NAPL mobilization will exist. Equation (11) indicates that the contaminant hydraulic gradient depends primarily on the forced air flux and is independent of the height of the column.

For the NAPL and soil type investigated in this study, the applicable analytical model parameters for (11) are provided in Table 3.2.

Table 3.2 Fluid and Porous Medium Analytical Model Parameters

Fluid and soil properties	**Value**
NAPL density (ρ_{NAPL})	920 (kg/m^3)[a]
Air viscosity (μ_{air})	0.000025 (Pa·s)[b]
Sphericity (φ_s)	0.8[c]
Mean particle diameter (D_p)	0.88 (mm)[d]
Porosity (ε)	0.27[e]

[a] For canola oil at temperature of 20°C (Przybylski and Mag, 2002)
[b] At temperature of 200°C
[c] Approximate sphericity for silica sand (Solimene et al., 2003; Grewal, 1980)
[d] Technical data sheet (Bell&Mackenzie Co. Ltd)
[e] Laboratory measured total porosity of 0.38 with a NAPL saturation of 30%

3.2.4 Numerical Model

The purpose of numerical modeling in this work was two-fold. First, the numerical model was used to confirm assumptions built into the analytical model (e.g., capillary pressure can be considered negligible). This allowed for increased confidence in the utility of the analytical model as a simple predictive tool for the potential for NAPL mobilization. Second, the numerical model was used to assess the time-dependent flow of air and NAPL for key scenarios within a smouldering experiment. This time-dependent behaviour cannot be studied using the analytical model, and therefore the numerical model is critical for understanding the rates and cumulative volumes of NAPL migration under varying experimental conditions. For this purpose, this work employed a one-dimensional version of the three-dimensional, finite difference, two phase flow numerical model DNAPL3D (Gerhard and Kueper, 2003a, 2003b, 2003c; Gerhard et al., 1998; Grant et al., 2007). The model solves the wetting and non-wetting phase mass conservation equations, which include Darcy's Law, fluid incompressibility assumptions, the capillary pressure definition $P_C = P_N - P_W$, and the fluid saturation relationship $S_W + S_N = 1.0$:

$$\frac{\partial}{\partial z}\left[\frac{k_i k_{r,W}}{\mu_W}\left(\frac{\partial P_W}{\partial z} + \rho_W g\right)\right] - \emptyset\frac{\partial S_W}{\partial t} = 0 \qquad \textbf{(12)}$$

$$\frac{\partial}{\partial z}\left[\frac{k_i k_{r,N}}{\mu_N}\left(\frac{\partial (P_C + P_W)}{\partial z} + \rho_N g\right)\right] - \emptyset\frac{\partial (1 - S_W)}{\partial t} = 0 \qquad \textbf{(13)}$$

where z is the vertical coordinate, k_i is the intrinsic permeability, $k_{r,W}$ and $k_{r,N}$ represent the relative permeability of the wetting and nonwetting phase, respectively, μ_W and μ_N represent the viscosity of the wetting and nonwetting phase, respectively, P_W is the

wetting phase pressure, P_C is the capillary pressure, ρ_W and ρ_N represent the wetting and nonwetting phase densities, respectively, g is gravitational acceleration, $\emptyset$ is the porosity, S_W is the wetting phase saturation, and t is time.

Constitutive relationships to close these equations, capillary pressure-saturation-relative permeability relations, were developed and validated for the flow of two immiscible fluids in heterogeneous porous media (Gerhard and Kueper, 2003a, 2003b, 2003c; Grant et al., 2007). The equations are solved using a fully implicit finite difference scheme with second-order accurate spatial operators and a first-order accurate temporal derivative (Rosenburg, 1969) to determine phase pressures and saturations. The internode absolute permeabilities are calculated using harmonic means and the internode relative permeabilities are calculated based on fluid saturations of the upstream nodes (Aziz and Settari, 1979). Full Newton-Raphson iteration accounts for the nonlinearities of the governing equation and the preconditioned system is solved with a modified Orthomin routine (Behie and Forsyth, 1984). The model has been successfully applied to a wide range of problems in which two immiscible fluids are flowing through a porous medium (Gerhard and Kueper, 2003a, 2003b, 2003c; Grant et al., 2007; West et al., 2008; Pang, 2010; MacPhee et al., 2012; Power et al., 2014).

The objective in this work was to use modelling to evaluate the time-dependent migration of NAPL under different conditions resulting from smouldering. In this work, the NAPL is the wetting phase and air is the non-wetting phase in the soil matrix. These equations simulate the evolving NAPL and air saturations over time within the porous media subject to pressure, gravity, and capillary forces and subject to the influences of soil permeability, multi-phase relative permeability, and fluid viscosities. It is noted that

Equations (12) and (13) do not incorporate temperature, energy or smouldering reactions. Thus, the purpose of each simulation was neither to simulate smouldering nor to simulate the movement of the front in time. Rather, the purpose was to model the fluid forces and movement for a single 'scenario'; scenario in this context means the location of the front, the length of the preheated zone ahead of the front, the length of clean sand behind the front, and the total contaminated height for a short period of time in a single experiment. The model provides a prediction of whether downward NAPL migration is expected for a single scenario, like the analytical model, and – in addition – the relative amount of NAPL migration expected in a timeframe relevant to smouldering. For the purpose of this modelling, the distinction between the pyrolysis and oxidation zones discussed above are ignored and the smouldering front is considered a thin line. In this work, the pressure and saturation distributions are solved only in the vertical direction, representing the distribution as a function of height within the column. By exploring a range of scenarios (e.g., preheating zone lengths, front heights, air flow rates) it is possible to examine the conditions under which NAPL migration is possible and, when possible, the extent to which it is expected to be significant (here 'significant' is taken to mean 'to the extent that it is expected to impact smouldering behaviour').

A key modification was made to the model for this work. All published simulations with DNAPL3D assumed a single fluid viscosity for the wetting phase. In this work, in order to simulate temperature effects on the NAPL, the viscosity of the wetting phase was assigned one of two values depending on location: one for the Ambient region and a lower value for the Preheated region (see Figure 3.2). While the extent of viscosity reduction at column temperatures above 100ºC cannot easily be measured, it can be

estimated from literature (Figure 3.3) and also can be considered a parameter to be explored in sensitivity simulations.

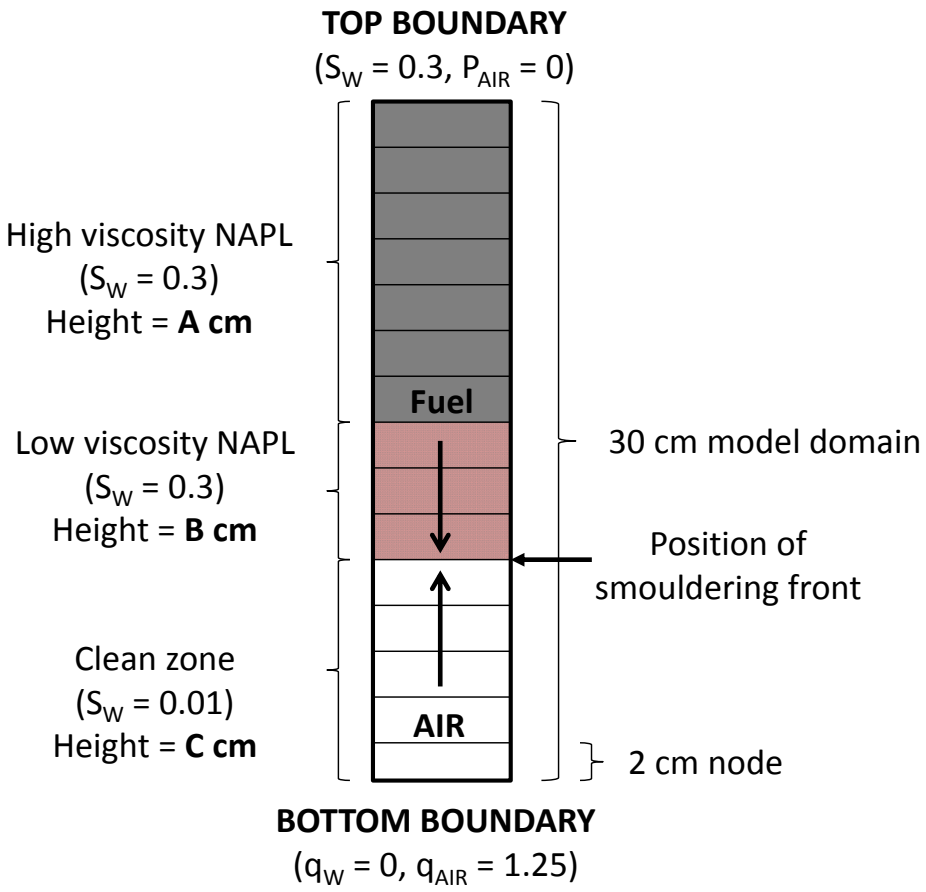

Figure 3.5: Sample model domain, boundary conditions and initial conditions for a 30 cm column with an initial contaminant saturation of 0.3 and a forced air flux of 1.25 cm/s. The scenario modelled is defined by: the distance C that the smouldering front has propagated from the base of the column, the height B of the elevated temperature preheating zone with reduced NAPL viscosity, and the height A of the remaining ambient temperature (ambient viscosity) NAPL zone.

The one-dimensional model domain height was varied to match the height of the experiments' contaminated zone. The domain height was then discretized into 2 cm nodes. The top boundary condition was set to a fixed NAPL saturation (Sw = 0.3), which corresponds with the experimental initial saturation. It was also assigned a fixed air

pressure of zero, corresponding to an open-top column. The bottom boundary condition consisted of a NAPL flux of zero, so that any NAPL entering the clean sand below the front would accumulate, and a specified air flux, chosen to match the forced air flow rate for each simulated experimental condition. The model domain and boundary conditions, shown for one example scenario, are summarized in Figure 3.5.

The model input parameters with the expected highest sensitivity were measured in the laboratory including: NAPL viscosity and saturation, and soil porosity and permeability. The remainder of the parameters for porous media and fluid properties were selected based on literature values. While air properties as a function of temperature are not accounted for in this model, the zone of primary interest for all model simulations is the Preheating region located immediately above the smouldering front. Based on experimental measurement of air temperatures at the top of the column as the smouldering front approached the end of the contaminated zone, an air temperature of 200°C was considered to be a reasonable assumption. A summary of these properties is listed in Table 3.3.

Each scenario (i.e., each simulation) was run for 1200 seconds, or 20 minutes. This simulation time was considered long enough to evaluate whether a significant amount of NAPL migration was expected to occur, but short relative to the speed of the smouldering front. The typical velocity of the trailing edge of the front, which defines when smouldering is complete at a given location, is 0.2-0.3 cm/min. This means that a maximum of 4 to 6 cm movement of the front is expected in 20 minutes. Thus, over this period, applying the model to simulate forces and fluid migration assuming a single

location of the front and single thickness of the Preheating region is considered reasonable.

Table 3.3 Fluid and Porous Medium Numerical Simulation Parameters

Fluid and soil properties	**Value**
Wetting phase (NAPL) density (ρ_w)	920 (kg/m^3)[a]
Wetting phase viscosity – high temperature (μ_w)	0.01 (Pa·s)[b]
Wetting phase viscosity – ambient temperature (μ_w)	0.5 (Pa·s)[b]
Air density (ρ_{air})	0.75 (kg/m^3)[c]
Air viscosity (μ_{air})	0.000025 (Pa·s)[c]
Interfacial tension (σ)	0.04 (N/m)
Porosity (ϕ)	0.38[b]
Residual wetting phase saturation (S_{rw})	0.10
Emergence wetting phase saturation (S_{w_emerg})	0.90
Pore size distribution index (λ)	2.50
Mean grain size (d)	0.88 (mm)[d]
Uniformity index (C_u)	1.6[d]
Mean permeability (k)	5.0 x10^{-10} (m^2)[b]

[a] For canola oil at temperature of 20°C (Przybylski and Mag, 2002)
[b] Laboratory measured parameters
[c] At temperature of 200°C
[d] Technical data sheet (Bell&Mackenzie Co. Ltd)

Using this model, the influence of varying four parameters were investigated: forced air flux (0.1 to 8.3 cm/s), height of the contaminated zone (16 to 120 cm), height of the preheating zone (0 and 10 cm), and the viscosity of the NAPL within the preheating zone (0.001 to 0.1 Pa·s). The base case simulation consisted of a 90 cm contaminated zone with a forced air flux of 1.25 cm/s, and a 10 cm preheating zone. Where normalized values of the volume of NAPL migration are presented, other simulation results are normalized by the results of this base case condition.

3.3 Results and Discussion

3.3.1 Experimental Observations of NAPL Mobility as a Function of Length Scale and Airflow Rate

Based on the configuration of the STAR laboratory column experiments, the liquid fuel (or NAPL contaminant) is subjected to two main forces: the downward force of gravity and the upward force of the injected air; capillary forces are expected to be relatively minor in the presence of forced air gradients. The net balance of these two forces will therefore determine whether the net gradient on the NAPL is significantly upwards, downwards, or negligible. However, regardless of the liquid hydraulic gradient, a highly viscous liquid will migrate at such a slow rate that its mobility is effectively negligible. Indeed, numerous liquid contaminants/fuels exhibit high viscosities (i.e., greater than 0.1 Pa·s) at ambient conditions, including the fuel used here (see Figure 3.3).

A background experiment was conducted in which a column was packed to a height of 50 cm with the same NAPL and sand mixture as used for the combustion tests and left at ambient conditions for 20 hours, after which it was incrementally excavated and analyzed for NAPL concentration. A comparison of before and after concentrations showed that there was no significant migration occurring at ambient conditions (details in Appendix A).

A temperature history as a function of nondimensionalized time (NDT) for Test 2 is shown in Figure 3.6, exemplifying typical smouldering behaviour in the absence of significant NAPL mobility. A nondimensionalized time of "zero" is assigned to the time at which the air supply, and therefore smouldering, was initiated. Conductive preheating

caused TC1, located 1 cm above the heater, to reach approximately 360°C when the initiated air flux of 2.5 cm/s caused a distinct slope change at NDT 0 representing the onset of combustion. Once TC1 reached its peak temperature and began to decline, the ignition coil was turned off and only the air remained on. These declining temperatures are indicative of convective cooling following the completion of smouldering at this location. The consistent temperature-time slopes, crossing curves, and consistent peak temperatures, are indicative of a self-sustaining smouldering process (Walther et al., 2000). Typical of a case with no NAPL migration, the velocity of the leading edge of the smouldering front is steady in time (here equal to 0.41 ± 0.04 cm/min).

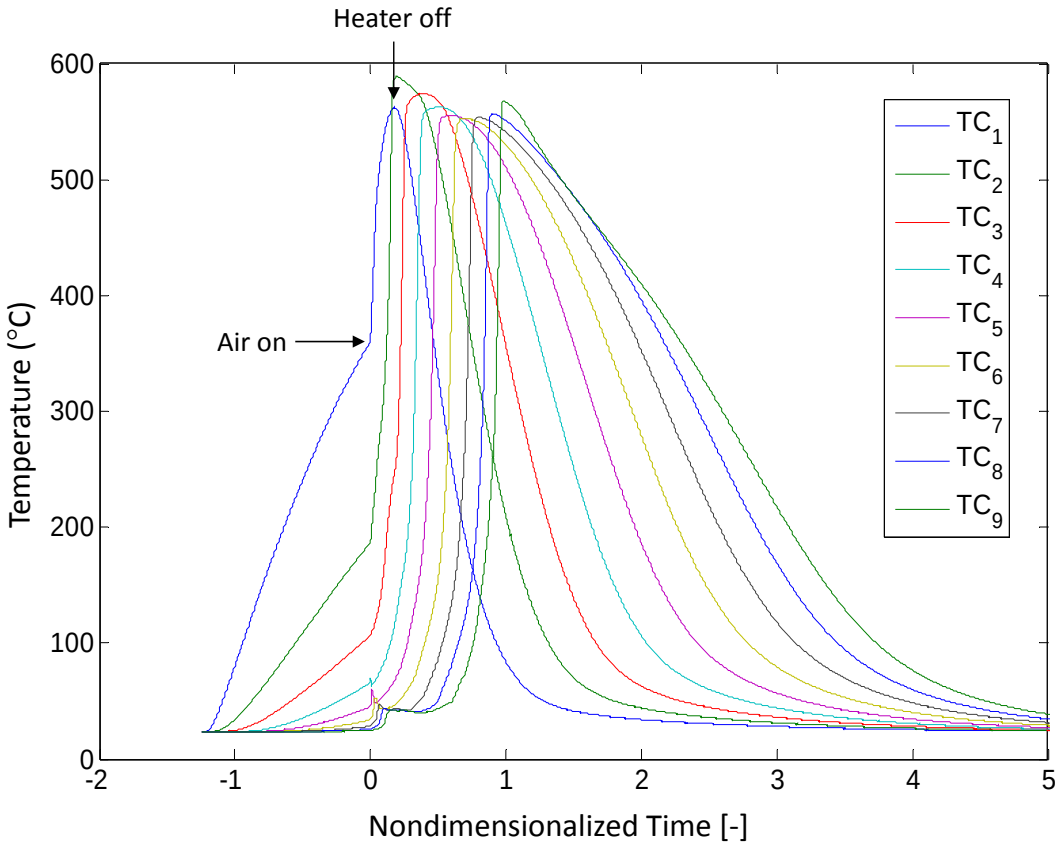

Figure 3.6: Temperature history for 30 cm contaminated zone with forced air flux of 2.5 cm/s, displaying typical self-sustaining smouldering behaviour in the absence of significant NAPL migration.

The evolving temperature profiles for the same experiment are shown in Figure 3.7. Each curve represents the distribution of temperatures as measured by all thermocouples in the smouldering column at a single nondimensionalized time. The nondimensionalized time of "0.8" is represented in red to show the typical shape of the temperature profile at a single moment in time. This can be compared to the theoretical temperature profile of the front in Figure 3.2. The regions of the front articulated in Figure 3.2 are identified with labels relating to the measured data in Figure 3.7 at NDT 0.8. For the purpose of analyzing experimental data, the pyrolysis and preheating regions in Figure 3.2 are collapsed into a single 'preheating' zone which is considered to be the region ahead of the leading edge of the smouldering front where T>100°C. This definition of the preheating zone was made consistently throughout analysis of the experimental results due to the inability to precisely define the boundary between the pyrolysis and preheating zones solely based on experimental temperature data. The proportion of the NAPL in the preheating zone that has been converted through pyrolysis to a char is considered to be small relative to the total height of the preheating zone and therefore this is considered to be a reasonable assumption. As indicated previously, in the case of negligible NAPL mobilization, the peak temperatures remain relatively constant (564 ± 12 °C).

An estimation of the instantaneous smouldering front thickness, as indicated in Figure 3.7, can be determined based on slope changes of the temperature profile. The leading and trailing edge of the smouldering front define the front and back of the reaction (oxidation) zone, respectively. The temperature increase at the leading edge of the smouldering front occurs over a very short distance and is therefore a sharp front. The slope change at the trailing edge of the front, indicating NAPL consumption versus

convective cooling of clean sand, (Figure 3.2) was selected consistently in this work at the inflection point as is indicated in Figure 3.7. The velocity of the leading (0.41 ± 0.04 cm/min) and trailing edge (0.30 ± 0.06 cm/min) of the smouldering front were not equal in the base case experiment, resulting in an increase in the thickness of the smouldering front over time (from 1 to 10.5 cm over the course of approximately 80 minutes of smouldering). No evidence of NAPL migration was observed in the base case.

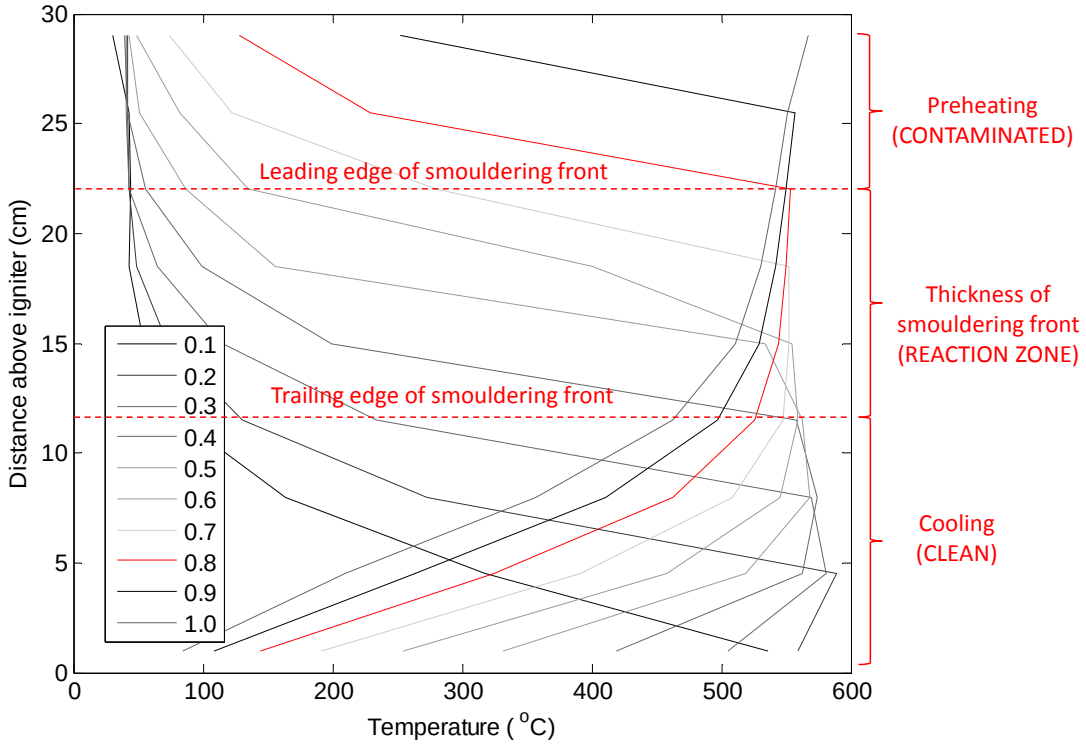

Figure 3.7: Temperature profile for 30 cm contaminated zone with forced air flux of 2.5 cm/s, displaying typical self-sustaining smouldering behaviour in the absence of significant NAPL migration. The legend provides the non-dimensionalized time for each profile. The labels refer to the smouldering regions in relation to the profile at NDT = 0.8 (red plot).

Self-sustained smouldering with no evidence of NAPL migration was similarly observed in the 30 cm columns at the other two air fluxes (1.25 and 6.25 cm/s). The temperature profiles for these two cases are shown in Figure 3.8(a) and (b). The same typical features are displayed with relatively steady progression of the leading edge of the smouldering

front (0.34 ± 0.06 cm/min and 0.50 ± 0.03 cm/min, respectively), slightly reduced velocities of the trailing edge of the front (0.24 ± 0.06 cm/min and 0.35 ± 0.05 cm/min, respectively) and consistent peak temperatures (560 ± 15 °C and 573 ± 14°C, respectively). A linear dependence of smouldering front velocity on injected air flux is expected (Pironi et al., 2011) since smouldering is an oxygen limited reaction.

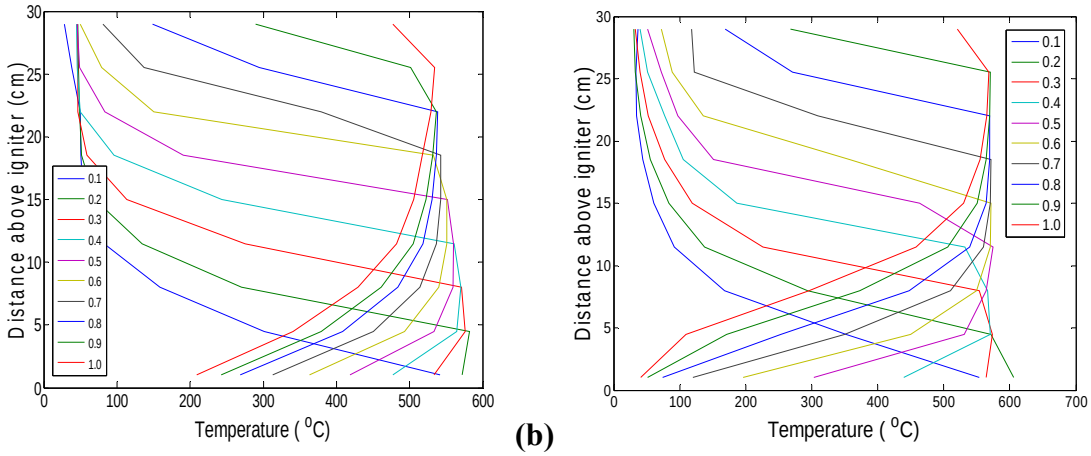

Figure 3.8: Temperature profiles for 30 cm columns showing evolution of the smouldering front structure for forced air fluxes of (a) 1.25 cm/s and (b) 6.25 cm/s. Each curve displays a snapshot in time and the legend provides the nondimensionalized time for each curve.

It was not until the height of the contaminated zone was increased that migration effects were observed in the temperature data. Figure 3.9(a) shows the temperature history for the 90 cm column with a forced air flux of 2.5 cm/s, which is the same experimental conditions as the temperature history in Figure 3.6 except with an increased contaminated zone height. This temperature history displays typical smouldering behaviour from approximately TC1 to TC12, including relatively constant propagation of the leading edge of the smouldering front (0.41 ± 0.07 cm/min), trailing edge of the front (0.32 ± 0.07 cm/min), and consistent peak temperatures (564 ± 17 °C). These smouldering front velocities and peak temperatures correspond with the observations in the 30 cm column.

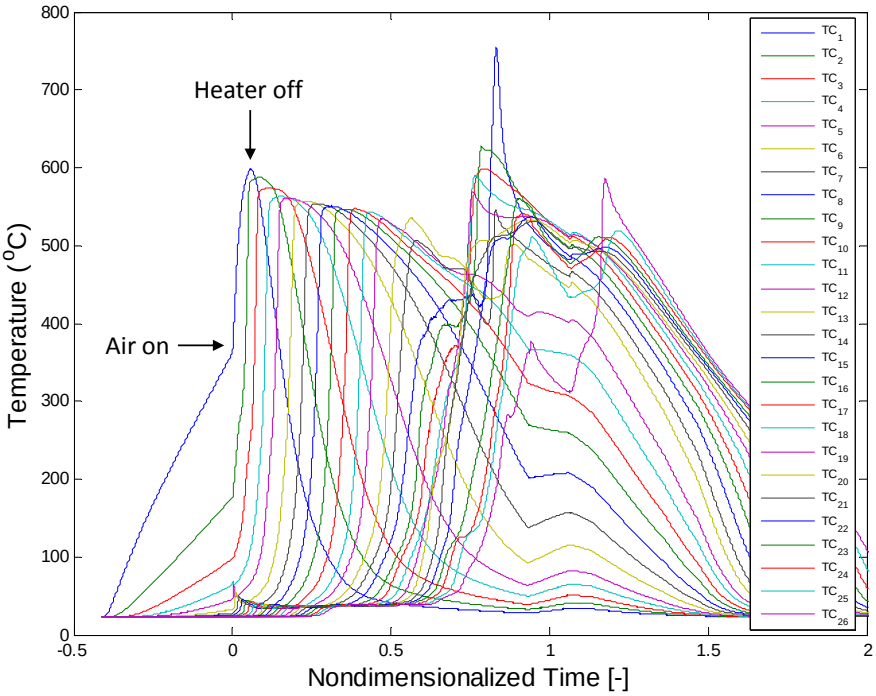

(a)

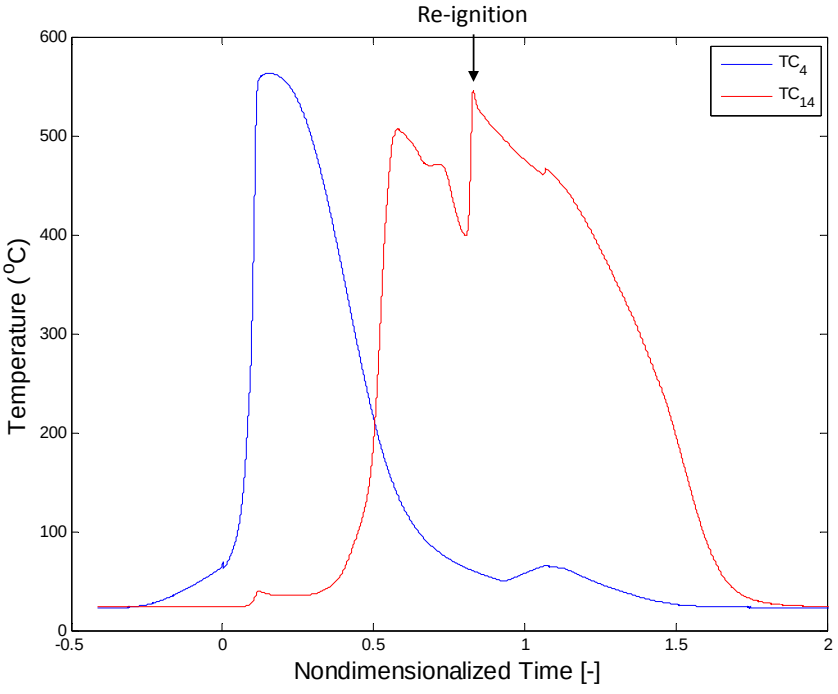

(b)

Figure 3.9: (a) Temperature history for 90 cm column with forced air flux of 2.5 cm/s, and (b) isolated temperature history for TC4 and TC14 located 12 cm and 46.5 cm above the heater, respectively.

For this intermediate air flux (2.5 cm/s) migration effects are only observed beginning at a nondimensionalized time of 0.6 when the leading edge of the smouldering front is approximately 50 cm above the heater (shown in the temperature profile in Figure 3.10). Between a nondimensionalized time of 0.6 and 0.7 the trailing edge of the smouldering front stalls (i.e., velocity of 0 cm/min) while the leading edge of the front continues to advance. This corresponds to a regime change in smouldering behaviour characterized by an accelerated growth of smouldering front thickness and elevated peak temperatures. In order to confirm that this regime change was not an isolated incident, a repeat column test was conducted (Appendix B), yielding similar results.

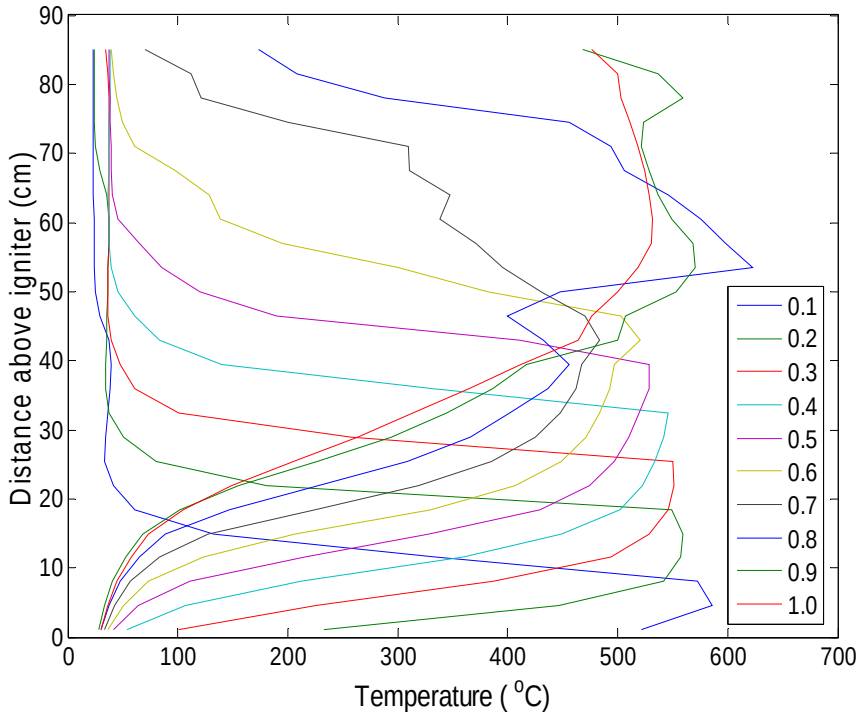

Figure 3.10: Temperature profile for 90 cm column with forced air flux of 2.5 cm/s, showing evolution of the smouldering front structure. Each curve displays a snapshot in time with the legend providing the associated nondimensionalized time.

In all cases, with or without migration, all NAPL was consumed and the entire column was remediated. While the end outcome was the same in all cases, there are key differences in the thermocouple data when migration is present, including: higher than normal peak temperatures and stalling of the trailing edge of the smouldering front. These characteristic differences are likely to be caused by NAPL mobility and can be explained by looking in more detail at individual thermocouples within the temperature history (Figure 3.9(b)). Figure 3.9(b) highlights TC4 and TC14, located 12 and 46.5 cm above the ignition coil, respectively. As described previously, TC4 displays typical ignition behaviour with a distinct temperature increase to a given characteristic peak temperature followed by completion of smouldering at that location and a continuous cooling curve. At TC14, there is the same characteristic sharp increase in temperature indicating ignition, however it reaches a peak at a lower temperature. As cooler (relative to combustion temperatures) low viscosity NAPL from above migrates downward to this location, some of the heat released from smouldering is consumed in preheating and pyrolysis of this new fuel. This previously mobilized NAPL then causes clear reignition behaviour at a much later time than the initial ignition. While TC14 is one of the first thermocouples to show signs of migration, latter thermocouples peak at much higher temperatures as migration becomes more dominant. The average peak temperature in the upper half of the column from TC13 to TC26 is 572 ± 60 °C. The average peak temperature is both higher and shows significantly more variability than the lower half of the column (564 ± 17 °C).

Higher than average peak temperatures due to downward NAPL migration can result from the concentration of NAPL and energy at a particular location within the column.

In other words, the smouldering reaction may approach quasi-superadiabatic conditions. Superadiabatic conditions have been documented in smouldering of solid porous fuels (e.g., coal, foam) when the rate of heat transfer away from the oxidation region is less than the rate of heat generation in the oxidation region; this imbalance results in the concentration of energy at the smouldering front (Aldushin et al., 1999). Since temperature and oxidation rate are coupled, this leads to a strong feedback effect between the two that can result in overheating such that the peak temperatures exceed typical thermodynamic smouldering temperatures (Aldushin et al., 1999). Here it is hypothesized that NAPL migration within the smouldering column is also leading to overheating via continued addition of fuel to the reaction zone. A smouldering reaction remains self-sustaining because heat is recovered from the oxidation region via preheating and pyrolysis of the virgin fuel ahead of the front. However, when the fuel is migrating downwards, similar to the superadiabatic conditions described by Aldushin et al. (1999), this recovered heat is concentrated at the front. This results in lower heat losses and consequently elevated peak temperatures at the front.

The fuel mobilization can similarly explain the stalling of the trailing edge of the smouldering front evident in Figure 3.10 as the mobilized NAPL continues to provide a fuel source to sustain combustion at these lower regions of the column not allowing the trailing edge of the smouldering front (which is associated with the contaminated/clean sand divide, Figure 3.2) to move upwards in the column.

The presence or absence of these NAPL mobility effects is dependent on the forced air flux, which is the only variable between the three 90 cm columns. At the lowest air flux in Figure 3.11(a), evidence of migration is observed through the presence of elevated

peak temperatures from the onset of combustion. In the bottom third of the column, average peak temperatures were 630 ± 22 °C, which was noticeably higher than the comparable 30 cm column experiment. These elevated peak temperatures are expected to be a result of higher fuel concentrations caused by downward NAPL mobilization. Similarly, in the top third of the column, average peak temperatures are reduced (538 ± 38 °C) since NAPL has mobilized from this upper region to lower regions within the column. At this low air flux (1.25 cm/s), the trailing edge of the smouldering front remains within the first 15 cm of the column. Since the upward force of air on the NAPL is reduced in this low flow case, downward NAPL migration is able to occur causing sustained combustion throughout the lower regions of the column as the leading edge of the smouldering front continues to move upwards at a velocity of 0.38 ± 0.07 cm/min.

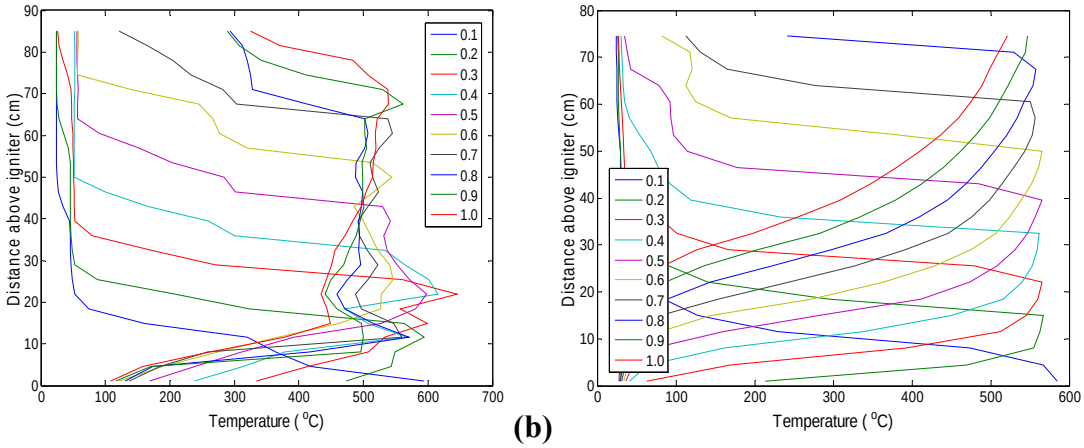

Figure 3.11: Temperature profiles for 90 cm columns showing evolution of the smouldering front structure, with each curve displaying a snapshot in time represented as nondimensionalized time for forced air fluxes of (a) 1.25 cm/s, and (b) 6.25 cm/s.

At the highest airflow rate tested in the 90 cm column, 6.25 cm/s (Figure 3.11b), there is no evidence of downward NAPL migration at any time during the experiment. Similar to the 30 cm column experiments, there was steady upward progression of both the leading (0.53 ± 0.04 cm/min) and trailing edge (0.45 ± 0.08 cm/min) of the smouldering front and peak temperatures remained constant (563 ± 5 °C).

It was evident from these temperature results that the upward force of injected air was not the only factor controlling NAPL mobilization behaviour as no NAPL mobilization was observed in the 30 cm columns at any of the three tested air flow rates, while mobilization was present in the 90 cm columns at two of the three air flow rates. As mentioned previously, NAPL mobilization is greatly enhanced at lower viscosities. Therefore, it is important to consider the height of the elevated temperature preheating zone which represents the amount of NAPL available to migrate at time scales relevant to the experiment and impact smouldering metrics. As mentioned previously, the height of the preheating zone is defined as the distance between the leading edge of the smouldering front and the location ahead of the smouldering front that is at a temperature of 100°C. 100°C was selected as the threshold at which the viscosity of the NAPL is significantly reduced from ambient conditions (Figure 3.3) to provide a zone of NAPL with high mobility potential.

Figure 3.12 shows the position and height of the various fuel states within the smouldering column as a function of nondimensionalized time, including: the clean sand where all NAPL has previously been consumed (no mobility potential), the combustion zone where NAPL has been converted to a char (low mobility potential), the elevated

temperature preheating zone where low viscosity NAPL is present (high mobility potential), and the contaminated sand where ambient temperature high viscosity NAPL is present (low mobility potential). These four regions in relation to the conceptual model of the smouldering front were previously introduced in Figure 3.2. Similar to Figure 3.7, the pyrolysis and preheating zone have been combined into a single 'preheating' zone.

In all 30 cm columns, no downward migration effects were observed even at low airflow rates. As shown in Figure 3.12, in the 30 cm experiments the position and thickness of the combustion zone over nondimensionalized time is relatively consistent across all airflow rates. The thickness of the smouldering front expands from approximately 1 cm to 10.5 cm, shrinking again at late time when the leading edge of the front reaches the end of the contaminated zone. Both the leading and trailing edges of the front propagate in a steady manner upwards. In no case and at no time does the thickness of the preheating zone exceed 10.5 cm. These all point to the absence of NAPL mobilization in the 30 cm cases.

For the 90 cm columns, mobility effects are observed when two conditions are met. First the forced air flux must be low (i.e. no mobility effects are observed for the 6.25 cm/s case). Second, clear evidence of NAPL mobilization are observed only when the preheating zone height reaches a critical thickness greater than or equal to 10.5 cm. As shown in Figure 3.12, for the lowest linear air flux, 1.25 cm/s, the height of the preheating zone reaches 10.5 cm from the onset of combustion (NDT = 0.1). The height of this preheating zone continues to expand as the reaction progresses. At a NDT of 0.4, the trailing edge of the smouldering front stalls, indicating that a significant quantity of NAPL is continuing to be added to that zone to sustain combustion. These observations

match the temperature data presented in Figure 3.11(a), where it was similarly determined that NAPL mobility effects were present from the beginning of smouldering.

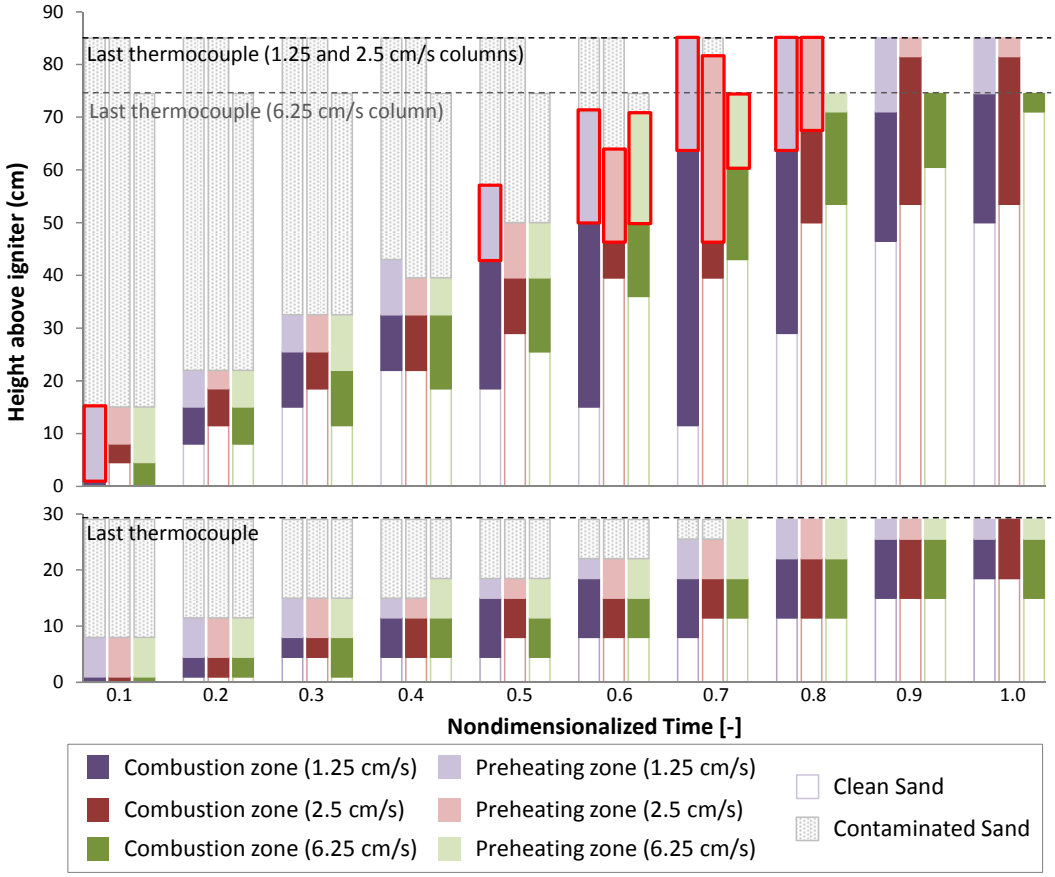

Figure 3.12: Height and position of the combustion and preheating (defined as the region ahead of the combustion zone where T>100°C) zones for 30 and 90 cm columns at forced air fluxes of 1.25, 2.5 and 6.25 cm/s. The red outline identifies preheating zone heights of 10.5 cm or greater.

For the intermediate air flux, 2.5 cm/s, the increase in preheating zone height and stall of the trailing edge of the smouldering front occurs slightly later at a NDT of 0.6 to 0.7. This time corresponds directly with the time that elevated temperatures are observed in the temperature profile (Figure 3.10), confirming that an increase in preheating zone height and a stall in the progression of the trailing edge of the smouldering front is

indicative of downward NAPL migration consequently resulting in elevated smouldering temperatures.

What is special about a critical preheating zone height greater than or equal to 10.5 cm? It is hypothesized that this height of low viscosity NAPL represents a critical volume of NAPL that can migrate towards the front and that can therefore manifest quasi-superadiabatic effects in the temperature data. While the value of 10.5 cm is specific to the fuel and soil type (i.e., canola oil/VI improver and coarse sand) used here, it is expected that analogous critical heights will exist and can be determined for other experimental systems.

For the highest airflow rate, 6.25 cm/s, while the height of the preheating zone does reach a maximum of 21 cm at a NDT of 0.6 (Figure 3.12), there is no corresponding stall in the smouldering front or presence of elevated temperatures in the temperature profile (Figure 3.11b). Therefore, for this high airflow rate, the upward force of the injected air appears to be sufficient to prevent the downward mobilization of NAPL into the smouldering front even with a significant low viscosity zone. Indeed, experimental observations of NAPL droplets being ejected from the smouldering column at this highest forced air flux indicate that the upward force of air is sufficient to cause upwards NAPL migration in this case.

Therefore, exceeding a critical preheating zone height appears to be a necessary, but not sufficient, condition of downward NAPL migration. Downward migration also requires a downward NAPL gradient across the low viscosity preheating zone, which appears to be dependent on the relative upward force applied by the injected air.

In summary, based on the experimental results, it is hypothesized that for smouldering to be influenced by downward NAPL migration, the simultaneous presence of three conditions is required:

1. A downward NAPL hydraulic gradient,
2. A height of preheating region large enough to provide a sufficient volume of NAPL to the front,
3. The viscosity of the NAPL in the preheating zone must be sufficiently low such that the rate of NAPL migration is significant relative to the time scale of smouldering.

The goal of the analytical and numerical modelling is to further investigate this hypothesis by examining these three conditions.

3.3.2 Analytical Modelling of NAPL Gradient

Using the parameter values identified in Table 3.2, Equation (11) can estimate the magnitude and direction of the NAPL gradient, as a function of injected air flux. These calculations are summarized and compared to the experimental results in Table 3.4 below. The numerical modeling results shown in the table will be discussed in Section 3.3.3.

Table 3.4 Comparison of Analytical Model to Experimental and Numerical Model Results for 90 cm Columns

V (cm/s)	Δh/ΔL Analytical Model (m/m)	Δh/ΔL Numerical Model (m/m)	Experimental Evidence of Downward NAPL Migration?
1.25	0.66	0.59	Yes
2.50	0.32	0.17	Yes
6.25	-0.70	-1.09	No

Table 3.4 reveals that for the conditions where evidence of downward NAPL migration was experimentally observed (forced air flux of 1.25 and 2.50 cm/s in the 90 cm columns), the analytical model predicted a positive (i.e., downwards) NAPL hydraulic gradient. It also reveals that, as expected, as the injected (upwards) air flux is increased, the downward NAPL gradient decreases; eventually it is reversed and becomes a negative (i.e., upwards) NAPL gradient as in the 6.25 cm/s air flux case. This helps confirm the hypothesis as to why no NAPL migration was experimentally observed in this case.

It is anticipated that this analytical model can be used as a simple predictive tool to determine whether downward NAPL mobilization is possible for any combination of soil and contaminant types and forced air flow rates. Using this model, a larger magnitude of the hydraulic gradient (either positive or negative) corresponds with a greater potential for NAPL mobilization (either downward or upward, respectively). Moreover, if it was desired to ensure that NAPL mobilization effects on smouldering were prevented, then it would provide the minimum air flux required for the operator. As indicated in the derivation of Equation (11), the NAPL gradient is independent from the height of the column.

In order to examine dynamic (i.e., time-dependent) aspects of the problem, including the migration of a sufficient NAPL volume in the preheating zone and the influence of NAPL viscosity in the preheating zone on migration rates, a numerical model is required.

3.3.3 Numerical Modelling of NAPL Migration in Comparison with Experimental Results

The numerical modelling described in Section 3.2.4 was employed to better understand the time-dependent relationship between the upward flowing air and downward migrating NAPL for selected scenarios in the conducted experiments. Several sensitivity studies were also conducted (e.g., to NAPL viscosity in the preheating zone). It is expected that this model can further be used as a predictive tool to investigate the extent to which NAPL mobility is likely to be present in other scenarios (e.g., other contaminant types, saturations, soil types, airflow rates).

First the numerical model was employed to examine the NAPL gradient condition considered in the analytical modelling. Figure 3.13 presents the simulated pressure distributions for the NAPL and air phases and NAPL hydraulic head for the largest and smallest experimental injected air fluxes in the 90 cm columns. In these simulations, the height of the three zones defined in Figure 3.5 were set to A = 70 cm, B = 10 cm and C = 10 cm (i.e., the smouldering front has advanced 10 cm from the base of the column). The results are presented for time = 20 min into the 20 min simulation period; it is noted that pressures and heads change very little during the simulations. The pressure plots illustrate that at all heights the NAPL (wetting phase) pressure is, as expected, equal to the air (non-wetting phase) pressure minus the capillary pressure. They further reveal that the capillary pressures are small (i.e., < 1000 Pa) relative to the total fluid pressures, providing support for the assumption of negligible capillary pressure in the analytical modelling. The figure further reveals that for the 1.25 cm/s air flux the NAPL head is higher at the top of the NAPL contaminated zone than at the bottom, while the opposite is

true for the 6.25 cm/s case. This matches expectations from the experiments and analytical modelling.

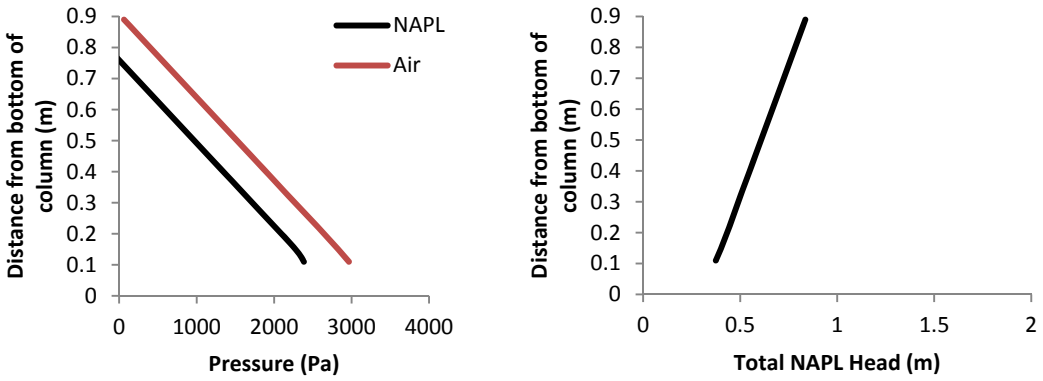

(a)

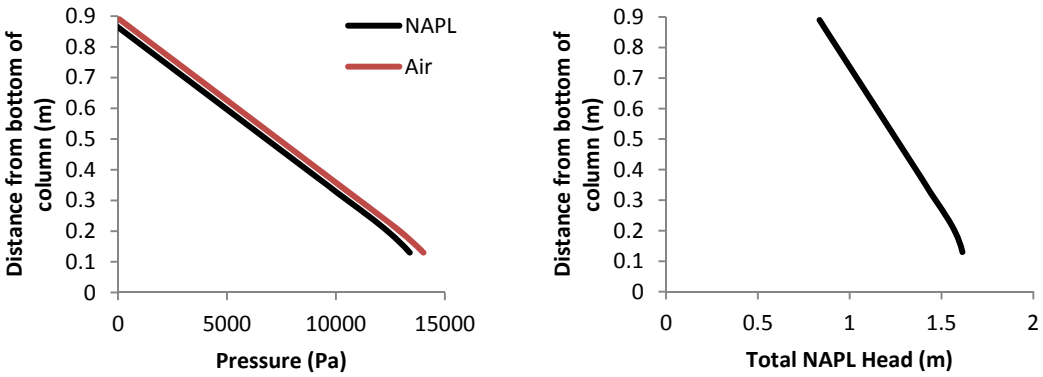

(b)

Figure 3.13: (a) Air and NAPL pressure distributions and total NAPL head for a column with a forced air flux of 1.25 cm/s. Total NAPL head is greater at the top of the column and therefore NAPL has the potential to migrate downwards, and (b) Air and NAPL pressure distributions and total NAPL head for a column with a forced air flux of 6.25 cm/s. For both cases, A=70, B=10 and C=10.

Figure 3.14 plots the NAPL hydraulic gradient ($\frac{\Delta h}{\Delta L}$) calculated from the numerically simulated heads over the 80 cm length of the NAPL-contaminated zone; it does so for both the simulations shown above as well as for a range of air fluxes (0.1 to 8.3 cm/s) greater than and less than that used in the smouldering experiments. As with the

analytical model, a positive hydraulic gradient represents potential downward NAPL migration. As expected, larger positive gradients were found for lower air flow rates, due to the dependence of NAPL head on air pressure. An air flux of approximately 3.0 cm/s is predicted to result in zero NAPL gradient, and as air flux is further increased, the simulated NAPL gradient becomes more negative (i.e., potential for upwards NAPL migration).

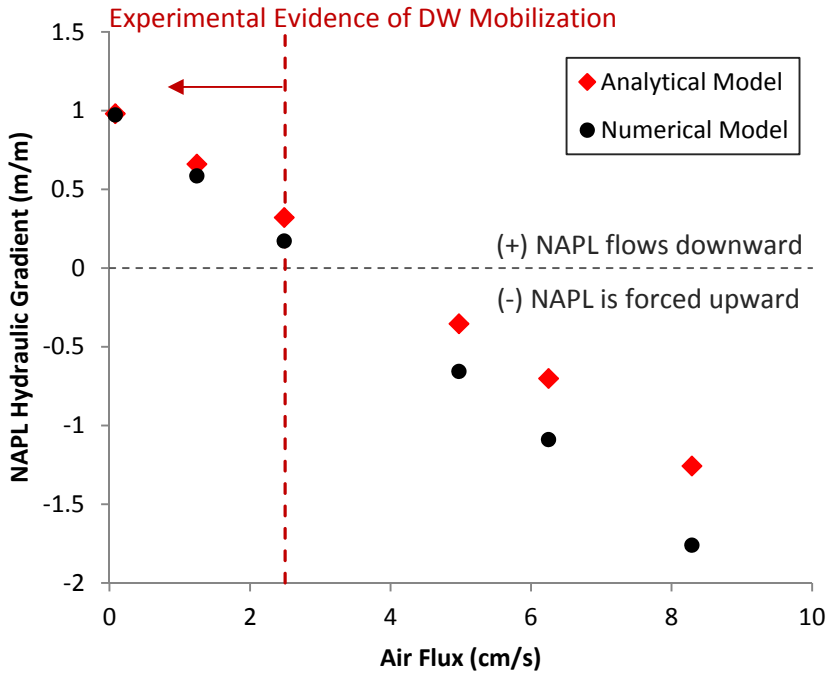

Figure 3.14: NAPL hydraulic gradient as a function of forced air flux represented as black circles for the numerical simulations of a 90 cm contaminated zone with a 10 cm preheating zone immediately above the front (A = 80, B = 10, C = 0). NAPL hydraulic gradients calculated using the analytical model are shown in red.

Figure 3.14 compares the NAPL gradients predicted from the numerical model and analytical model, illustrating they are of similar sign and magnitude in all cases. The figure underscores that the cases for which NAPL migration was observed to impact smouldering were indeed those cases with a downward NAPL gradient. Table 3.4

provides a comparison of the analytically and numerically predicted NAPL gradient values for the three 90 cm experiments with varying air fluxes. In all three cases, the values match well and correspond to the experimental results. In the lowest (1.25 cm/s) air flux experiment, there was clear evidence of downward NAPL migration from early time (Figure 3.11a), which is supported by the high downward gradient of ~ 0.6. For the highest (6.25 cm/s) air flux experiment, no evidence of any downward NAPL migration occurred (Figure 3.11b) in agreement with the large negative hydraulic gradient of ~ -1.0. In the case of the intermediate (2.5 cm/s) air flux, experimental evidence of downward NAPL migration occurred only later as the leading edge of the smouldering front approached the midpoint of the contaminated zone (Figure 3.10). This also agrees with the analytical and numerical simulations which predict a small positive NAPL hydraulic gradient of ~0.2. It is possible that at low, positive NAPL gradients it takes more time to deliver sufficient NAPL to the front to produce an effect on smouldering metrics. Also, complex experimental conditions not accounted for in the model, such as the changing length of the contaminated and preheating zones, may contribute to the regime transition – from no migration to downward migration – observed in the experimental data at intermediate time.

The similar magnitude and sign of the hydraulic gradient between those calculated using the numerical and analytical models suggests that the assumptions made in forming the analytical model are reasonable. The analytical model tends to predict a slightly larger (or less negative) NAPL gradient than the numerical model predicts, with the difference between them increasing with increasing air flux (Figure 3.14). The discrepancies between the two may be the result of including several additional physical forces in the

numerical model that were not incorporated into the analytical model, including gravity, capillary pressure, and relative permeability. While the constitutive relationships are valuable for simulating flowing phases with the numerical model, they do not play an important role in predicting the (relatively static over 20 min) hydraulic gradient. This supports the conclusion that the analytical model is sufficient for its purpose as an initial predictive tool with respect to the NAPL gradient precondition for downward migration.

Recall that, in addition to the NAPL gradient, experimental evidence indicated that column height also influenced whether downward NAPL migration was significant. To test the hypothesis that it is the height of the preheating zone that controls migration as opposed to the overall contaminated zone height, numerical simulations were first conducted with varying column heights but with no preheating zone (B=0). These results indicate that while the air pressure at the base of the column increases with a larger contaminated zone height (Figure 3.15), the change in air pressure is proportional to the change in contaminated zone height and therefore there is no effect on NAPL hydraulic gradient (Figure 3.16). Since downward NAPL mobilization effects were observed experimentally in 90 cm columns but not in 30 cm columns, this confirms that total initial NAPL height is not in itself the key factor in determining when NAPL migration will be significant.

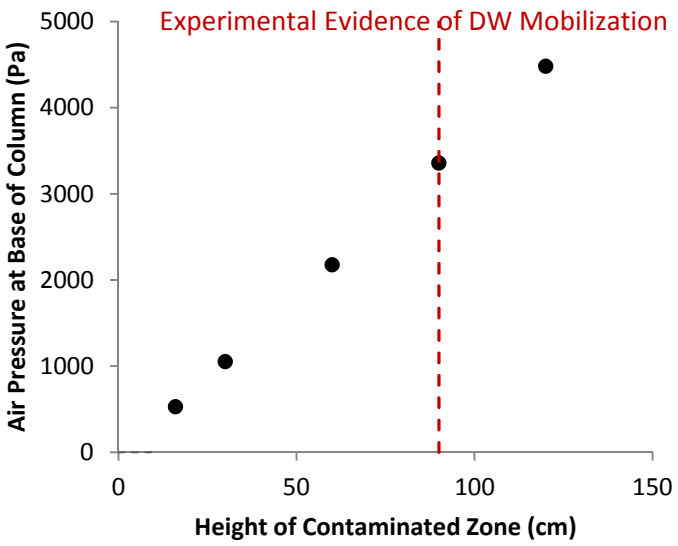

Figure 3.15: Air pressure at the base of the column as a function of NAPL height for a forced air flux of 1.25 cm/s (A=16 to A=120, B=0, C=0).

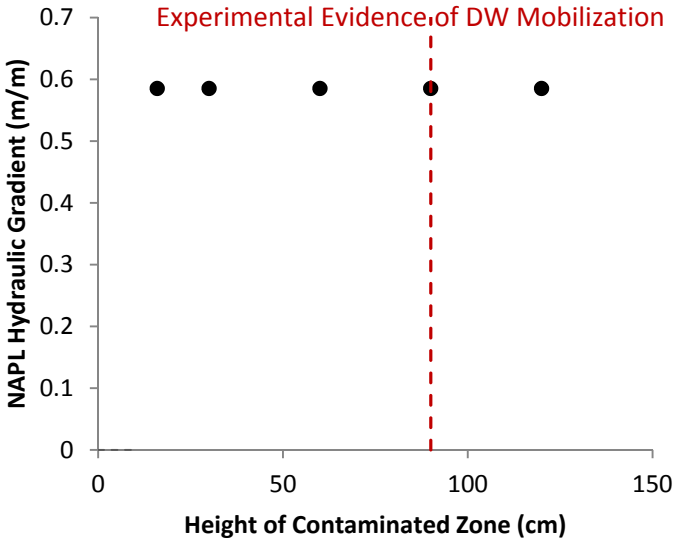

Figure 3.16: NAPL hydraulic gradient as a function of contaminated zone height for a forced air flux of 1.25 cm/s (A=16 to A=120, B=0, C=0).

Rather, the experimental results show that the preheating zone height increases with time and has the potential to increase to substantially larger values in taller columns. Furthermore, as the height of the preheating zone increases, the volume of potentially mobile low viscosity NAPL increases proportionally. As such, when the preheating zone height increases from 10 cm to 20 cm – as it does at later times in the tall column experiments - the volume of NAPL that has the potential to migrate downwards at a rate that is significant for smouldering also increases by a factor of two.

This hypothesis about the rate and total amount of NAPL migrating to the smouldering front depends on the reduced NAPL viscosity in the preheating region. Note that when considering smouldering remediation, we are considering almost exclusively NAPLs (heavy hydrocarbons, coal tar) that are very viscous at ambient temperatures (i.e., > 1 Pa·s) and whose viscosity is likely to reduce by a factor of at least 50 at 100ºC (Figure 3.3). This is important because the rate of downward NAPL migration is expected to be governed not only by the gradient but also, via relative NAPL permeability in the presence of air, by the NAPL viscosity immediately above the smouldering front. This was explored with a series of numerical simulations using the base case configuration of 90 cm column, 1.25 cm/s air flux, 0 cm advance of the smouldering front, and 10 cm high preheating zone (A=80, B=10, C=0). The key metric was the NAPL volume that migrated in 20 minutes downwards into (+) or upwards out of (-) the preheating zone. Migrated NAPL volumes were determined by integrating the difference in NAPL saturation distributed over the 10 cm height between time = 0 and 20 min. In all cases the NAPL viscosity in the ambient zone was 0.5 Pa·s (matching that of the NAPL used in the experiments) while the NAPL viscosity in the preheating zone was varied between

0.1, 0.01, and 0.001 Pa·s. All three NAPL viscosities were evaluated for air flux values from 0.1 to 8.3 cm/s.

As shown in Figure 3.17, high NAPL viscosities (0.1 Pa·s) in the preheating zone results in relatively minimal NAPL migration over a time scale relevant to combustion. This corresponds with the experimental result of the 20 hour ambient temperature mobility test (Appendix A). Even at low air flow rates (<3.0 cm/s), minimal downward NAPL migration into the smouldering front is predicted despite there being a substantial downward NAPL gradient (Figure 3.14). As shown by viscosity measurements as a function of temperature (Figure 3.3), this may be expected for NAPLs such as coal tar; however, the oil/VI improver NAPL used in this study is expected to exhibit a viscosity in the preheating zone at least an order of magnitude less than this. Based on model simulations, Figure 3.17 reveals that as NAPL viscosity decreases by a factor of 10 the predicted volume of NAPL migrating into the front increases by a factor of 1.7, and as viscosity decreases by a factor of 100 the relative NAPL volume increases by a factor of 13.7. These simulations lend support to the hypothesis that the presence of low viscosity NAPL in the preheating zone is essential for significant migration effects in smouldering. Further investigation is required to determine the variables controlling the height of the preheating zone and is outside of the scope of this study; however it appears that larger preheating zone heights are formed at later times in taller columns and this is expected to contribute to more substantial NAPL migration effects on smouldering.

It is noted that Figure 3.17 also reveals that substantial upwards migration of NAPL may be expected ahead of the front when using very large air fluxes. This could cause NAPL

saturation decreases ahead of the front, which might inhibit self-sustained smouldering. It could also cause NAPL to be ejected from the column as the front approaches the top of the contaminated zone. Since the goal of smouldering is in situ NAPL destruction, this may be undesirable. Clearly the ability to control the air flux is an important tool for smouldering remediation operators.

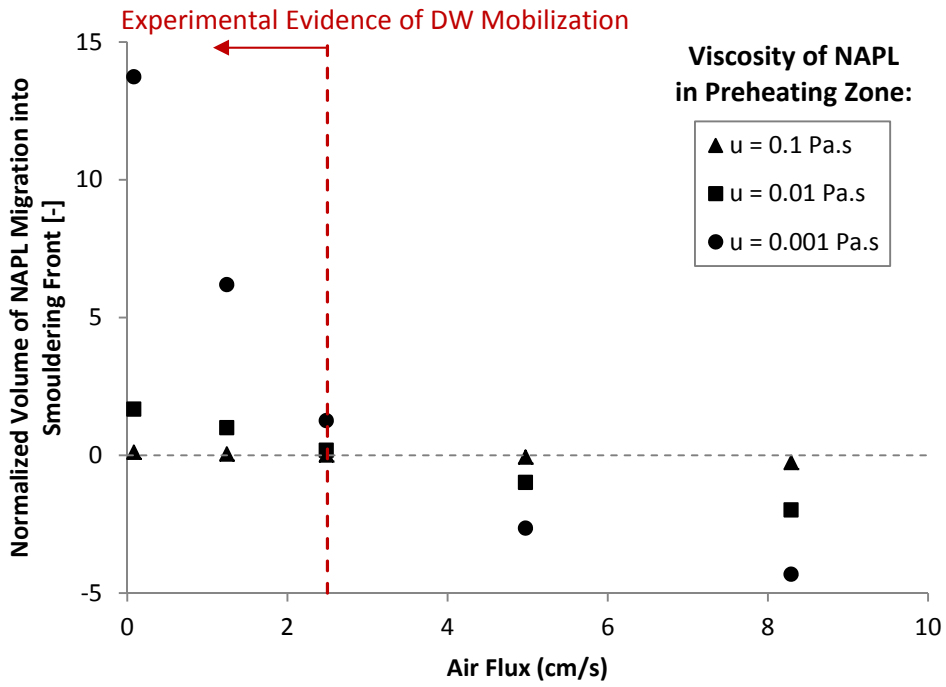

Figure 3.17: Volume of NAPL entering (+) or leaving (-) the bottom 10 cm of a 90 cm column over 20 minutes as a function of (i) forced air flux and (ii) viscosity of the NAPL in the preheating zone. Simulation results are for a 10 cm high preheating zone located at the base of an 80 cm ambient, NAPL-contaminated zone (μ = 0.5 Pa·s), where A = 80, B = 10 and C = 0. Volumes are normalized relative to the base case (1.25 cm/s flux, μ = 0.01 Pa·s).

3.4 Summary

A new conceptual model of the key regions that comprise a NAPL smouldering treatment system was presented, providing a basis for understanding important processes that occur both ahead and behind the propagating smouldering front. A detailed investigation of laboratory smouldering columns with two different contaminated zone heights and three different injected forced air flow rates indicated – for the first time – that NAPL mobility can influence NAPL smouldering behaviour. Experimental evidence of downward NAPL migration occurred in the 90 cm columns at low air flow rates. Downward NAPL migration caused three key effects on smouldering metrics: a stall in the trailing edge of the smouldering front, quasi-superadiabatic conditions leading to elevated peak temperatures, and a rapid increase in thickness of the smouldering front. While in all cases, the NAPL was still all eliminated and the excavated sand afterwards was completely clean, it is important to understand the conditions under which these phenomena are expected to occur.

Experimental results suggested the hypothesis that it is necessary for three conditions to exist simultaneously for significant downward NAPL migration in smouldering to occur. First, the forced air flux must be sufficiently low to permit a downward NAPL hydraulic gradient within the column. Second, the viscosity of the NAPL in the preheating zone must be sufficiently low to enable migration to occur at a rate relevant to smouldering. And third, the preheating zone height must be large enough to provide a sufficient volume of low viscosity liquid NAPL such that the migration will influence smouldering metrics. The length of the preheating zone generally grows in time for forward

smouldering, therefore, as larger columns or reactors are used, the likelihood of achieving the third condition is increased. The critical preheating zone height of approximately 10.5 cm observed in these experiments is likely system dependent and probably varies with NAPL type, sand type, and other factors that affect the heat transfer and NAPL characteristics ahead of the smouldering front.

An analytical model was developed that provides an easy method for approximating the first condition: the magnitude and direction of the NAPL gradient for a chosen injected air flux value. The predicted values were confirmed with one-dimensional numerical modelling. Moreover, the numerical model was able to provide evidence supporting the second and third conditions by predicting the volume of NAPL mobilized given a specified air flux, viscosity contrast between the preheated and ambient temperature NAPL, as well as contaminant and soil properties. Both models agreed well with the experimental results, predicting significant NAPL migration into the smouldering front in only those cases where it was observed. Modelling results suggest that NAPL mobility is expected to be minor, regardless of NAPL gradient, for NAPLs whose viscosity in the preheating zone is above 0.1 Pa·s (e.g., high viscosity coal tars). However, for other NAPLs, NAPL mobilization can be prevented by judiciously adjusting the air flux rate to minimize the NAPL gradient. This model will be used in the future to further explore the potential for NAPL mobility for other scenarios including NAPL types, initial saturations, and soil types.

While more significant NAPL migration effects were observed at lower airflow rates and at later times in larger columns, it is noted that this does not impact the overall degree of remediation of NAPL-contaminated soils due to the robust nature of the smouldering

process. Indeed, it was demonstrated that the length of the smouldering front adjusts to accommodate the influx of NAPL and the trailing edge does not advance until all the NAPL is oxidized, leaving clean sand throughout every time. However, the processes discussed here are still important. Due to the potential for NAPL migration to lead to elevated temperatures (super-adiabatic conditions), this phenomenon needs to be considered in the design of large, ex situ smouldering remediation treatment systems, including consideration of both construction materials and operating conditions.

3.5 References

Aldushin, A. P., Rumanov, I. E., & Matkowsky, B. J. (1999). Maximal energy accumulation in a superadiabatic filtration combustion wave. *Combustion and Flame*, 118(1-2), 76-90.

Aziz, K. & Settari, A. (1979). *Petroleum Reservior Simulation*: Applied Science, London.

Behie, G. A., & Forsyth, P. A. (1984). Incomplete factorization methods for fully implicit simulation of enhanced oil-recovery. *Siam Journal on Scientific and Statistical Computing*, 5(3), 543-561.

Bell & Mackenzie Co. Ltd. (n.d.). *#12ST silica sand*. Hamilton, ON: Bell & Mackenzie Co. Ltd.

Birak, P. S., & Miller, C. T. (2009). Dense non-aqueous phase liquids at former manufactured gas plants: Challenges to modeling and remediation. *Journal of Contaminant Hydrology*, 105(3–4), 81-98.

Gerhard, J. I., & Kueper, B. H. (2003a). Capillary pressure characteristics necessary for simulating DNAPL infiltration, redistribution, and immobilization in saturated porous media. *Water Resources Research*, 39(8).

Gerhard, J. I., & Kueper, B. H. (2003b). Relative permeability characteristics necessary for simulating DNAPL infiltration, redistribution, and immobilization in saturated porous media. *Water Resources Research*, 39(8).

Gerhard, J. I., & Kueper, B. H. (2003c). Influence of constitutive model parameters on the predicted migration of DNAPL in heterogeneous porous media. *Water Resources Research,* 39(10).

Gerhard, J. I., Kueper, B. H., & Hecox, G. R. (1998). The influence of waterflood design on the recovery of mobile DNAPLs. *Ground Water*, 36(2), 283-292.

Gerhard, J. I., Pang, T., & Kueper, B. H. (2007). Time scales of DNAPL migration in sandy aquifers examined via numerical simulation. *Ground Water*, 45(2), 147-157.

Grant, G. P., Gerhard, J. I., & Kueper, B. H. (2007). Multidimensional validation of a numerical model for simulating a DNAPL release in heterogeneous porous media. *Journal of Contaminant Hydrology*, 92(1–2), 109-128.

Grewal, N. S., & Saxena, S. C. (1980). Comparison of commonly used correlations for minimum fluidization velocity of small solid particles. *Powder Technology*, 26(2), 229-234.

MacPhee, S. L., Gerhard, J. I., & Rein, G. (2012). A novel method for simulating smoldering propagation and its application to STAR (Self-sustaining Treatment for Active Remediation). *Environmental Modelling & Software*, 31, 84-98.

McCabe, W. L., Smith, J. C., & Harriott, P. (1993). *Unit Operations of Chemical Engineering*: McGraw-Hill, Inc.

Mercer, J. W., & Cohen, R. M. (1990). A review of immiscible fluids in the subsurface: Properties, models, characterization and remediation. *Journal of Contaminant Hydrology*, 6(2), 107-163.

Ohlemiller, T. J. (1985). Modeling of smoldering combustion propagation. *Progress in Energy and Combustion Science*, 11(4), 277-310.

Pang, T. (2010). DNAPL *Remediation of Fractured Rock Evaluated by Numerical Simulation*. (Ph.D.), The University of Edinburgh, Edinburgh, Scotland.

Pironi, P., Switzer, C., Gerhard, J. I., Rein, G., & Torero, J. L. (2011). Self-Sustaining Smoldering Combustion for NAPL Remediation: Laboratory Evaluation of Process Sensitivity to Key Parameters. *Environmental Science & Technology*, 45(7), 2980-2986.

Pironi, P., Switzer, C., Rein, G., Fuentes, A., Gerhard, J. I., & Torero, J. L. (2009). Small-scale forward smouldering experiments for remediation of coal tar in inert media. *Proceedings of the Combustion Institute*, 32, 1957-1964.

Potter, M. C., & Wiggert, D. C. (2002). *Mechanics of Fluids*: Brooks Cole /Thompson Learning.

Power, C., Gerhard, J. I., Karaoulis, M., Tsourlos, P., & Giannopoulos, A. (2014). Evaluating four-dimensional time-lapse electrical resistivity tomography for monitoring DNAPL source zone remediation. *Journal of Contaminant Hydrology*, 162, 27-46.

Przybylski, R. & Mag, T. (2002). Canola/rapeseed oil. In: *Vegetable Oils in Food Technology: Composition, Properties and Uses* (ed. F.D. Gunstone): Blackwell Publishing, CRC Press.

Rashwan, T. (2013). *Exploration of Fuel Mobility during Self-sustaining Treatment for Active Remediation*. (Undergraduate Thesis), The University of Western Ontario, London, ON.

Rosenburg, D. U. (1969). *Methods for the Numerical Solution of Partial Differential Equations*: Elsevier Science, New York.

Scholes, G.C. (2013). *Ignition Method Development and First Field Demonstration of In Situ Smouldering Remediation*. (M.E.Sc), The University of Western Ontario, London, ON.

Solimene, R., Marzocchella, A., & Salatino, P. (2003). Hydrodynamic interaction between a coarse gas-emitting particle and a gas fluidized bed of finer solids. *Powder Technology*, 133(1-3), 79-90.

Switzer, C., Pironi, P., Gerhard, J. I., Rein, G., & Torero, J. L. (2009). Self-Sustaining Smoldering Combustion: A Novel Remediation Process for Non-Aqueous-Phase Liquids in Porous Media. *Environmental Science & Technology*, 43(15), 5871-5877.

Switzer, C., Pironi, P., Gerhard, J. I., Rein, G., & Torero, J. L. (2014). Volumetric scale-up of smouldering remediation of contaminated materials. *Journal of Hazardous Materials*, 268, 51-60.

Thomas, S. (2008). Enhanced Oil Recovery - An Overview. *Oil & Gas Science and Technology* - Rev. IFP, 63(1), 9-19.

Torero, J. L., & Fernandez-Pello, A. C. (1996). Forward smolder of polyurethane foam in a forced air flow. *Combustion and Flame*, 106(1–2), 89-109.

Walther, D. C., Anthenien, R. A., & Fernandez-Pello, A. C. (2000). Smolder ignition of polyurethane foam: effect of oxygen concentration. *Fire Safety Journal*, 34(4), 343-359.

West, M. R., Grant, G. P., Gerhard, J. I., & Kueper, B. H. (2008). The influence of precipitate formation on the chemical oxidation of TCE DNAPL with potassium permanganate. *Advances in Water Resources*, 31(2), 324-338.

4 TRANSPORT OF HEAT AND CONDENSABLE PRODUCTS IN SMOULDERING COLUMN EXPERIMENTS

4.1 Introduction

Smouldering is a flameless, oxygen-limited combustion reaction that has the ability to propagate through a porous organic fuel bed (e.g., coal, peat, polyurethane foam) or an inert matrix embedded with fuel (e.g., oil-soaked insulation) (Drysdale, 2011). The smouldering combustion front is quite complex, involving a travelling heat wave, endothermic pyrolysis reactions, and heterogeneous (i.e., gas phase oxygen and solid phase fuel) exothermic oxidation reactions (Torero and Fernandez-Pello, 1995). The heat wave preheats the fuel, the pyrolysis reactions convert the fuel to char, and the oxidation reactions convert the char to (primarily) heat, carbon dioxide, and water. In each of these steps, both condensable and non-condensable gaseous compounds can be formed. The heat wave can volatilize lighter compounds, pyrolysis can generate thermal degradation products with the potential for more volatilization, and oxidation – in addition to producing water vapour – typically generates carbon monoxide and other byproducts of incomplete combustion (Ohlemiller and Shaub, 1988). As a result, the emissions associated with smouldering is a complex problem.

The smouldering of non-aqueous phase liquid (NAPL) contaminated soil is one of the first engineering applications of smouldering (i.e., intentional smouldering under controlled conditions). Considerable work has started to illuminate the similarities and differences between smouldering of solid fuels and liquid fuels (Switzer et al., 2009; Pironi et al., 2009, 2011). Initial work with column experiments identified that smouldering coal tar produces an emissions stream dominated by non-condensable

combustion gases (e.g., CO_2 and CO) but also containing lower concentrations of other organic compounds (e.g., naphthalene) (Switzer et al., 2009). Column experiments smouldering vegetable oil and the chlorinated solvent trichloroethylene (TCE) identified that approximately 75% of the TCE was routinely volatilized ahead of the front (Salman et al., 2015). Recent work on in situ smouldering of coal tar at the pilot field scale has identified that approximately 98% of the coal tar is converted to CO and CO_2 while only about 2% is emitted as a variety of volatile organic compounds (Scholes et al., 2015). This field system utilizes a vapour extraction system connected to (i) a large knock-out tank for the water vapour (both due to steam production below the water table and combustion), and (ii) a thermal oxidizer for treatment of VOCs.

Ongoing work on applying smouldering as an ex situ treatment process for sludges and contaminated soils is looking at smouldering large batches in above ground piles and reactors (not yet published). For these in situ and ex situ engineering applications of smouldering, the rate and total amount of water vapour, volatiles and other condensable gaseous products as well as non-condensable gases generated is important to understand. These rates and amounts are essential to designing appropriate gas management and treatment systems. Moreover, optimizing the process – i.e., maximizing the mass destroyed by combustion and minimizing the mass emitted and requiring treatment – depends on understanding these two distinct types of emissions and the factors that affect the ratio between them.

While significant emphasis has been placed on investigating the smouldering reaction and degree of soil remediation from the application of STAR (Switzer et al., 2009, 2014; Pironi et al., 2009, 2011), there has yet to be a detailed investigation into the quantities, rates, and the dynamic nature of the gaseous combustion products. In this study, the use of medium and tall columns, as well as a surrogate contaminant and real contaminants, in a controlled laboratory environment allows for the study of the transport of heat and condensable and non-condensable gaseous compounds ahead of the smouldering front. The paper does not investigate the detailed chemistry of the emissions. Rather, it takes a practical, engineering perspective to consider the factors that affect the mass loss behaviour and the ratio between mass destroyed via combustion and the mass transported as gaseous compounds through the column and emitted and thereby requiring external treatment.

4.1.1 Contaminant Volatilization, Aerosol Formation and Condensation

Enhanced volatilization of contaminants through the addition of heat to a system is a key component of other remediation technologies, such as steam or hot air injection. When an organic chemical is heated, the vapor pressure will increase with temperature. For common organic contaminants, the vapor pressure may increase by a factor of 5 to 50 by increasing the temperature from 10°C to 100°C. This increase in vapor pressure also results in an increase of Henry's constant (H_c), which governs the relative proportions between the aqueous and gaseous states at equilibrium. As H_c increases with exposure to elevated temperatures, the extent to which a contaminant will partition to the air phase similarly increases (Davis, 1997).

In addition to increased potential for volatilization in the presence of elevated temperatures, there is also increased potential for the formation of aerosols. Aerosol formation as a function of temperature has been studied for cooking oils due to possible health effects of exposure to polycyclic aromatic hydrocarbons (PAHs) by inhalation of oil aerosols. It was found that both the number and size of oil droplets increase with increasing temperatures up to 260°C (Siegmann and Sattler, 1996).

While the contaminant may both volatilize and form aerosols through exposure to elevated temperatures, subsequent exposure to lower temperatures will result in condensation or deposition. This phenomena is observed in remediation via steam enhanced extraction where the NAPL that is evaporated in the heating phase condenses and accumulates in the cooler soils at the edge of the heated zone, leading to increased NAPL phase saturations ahead of the temperature front (Kaslusky and Udell, 2005). It is also observed in in situ thermal desorption (ISTD) systems where the entire source zone must be heated above the boiling temperature of the target chlorinated solvent in order to ensure the volatilized compound does not condense before being extracted at the surface for treatment (Triplett Kingston et al., 2014).

4.1.2 Conceptual Model of Temperature Distribution in One-Dimensional Smouldering

While contaminant volatilization is not the primary aim of smouldering remediation, the same mechanisms of contaminant volatilization and subsequent condensation may occur due to the presence of elevated temperatures and injection of air. Figure 4.1 presents a conceptual model of the vertical spatial distribution of temperatures for an upward forward smouldering combustion reaction, depicted at a single time. It also presents a

hypothesis, to be tested in this paper, of how the various temperature regions correspond to key processes that generate gaseous emissions.

In the cooling region behind the travelling front, all of the fuel (i.e., contaminant) has been consumed by the smouldering reaction and therefore is losing heat steadily due mainly to convection from the injected air below. In the oxidation zone, exothermic reactions are resulting in the transformation of the fuel into a range of complete and incomplete combustion products. These reactions yield primarily carbon dioxide, carbon monoxide, water vapor and heat (Switzer et al., 2009). Also a range of organic compounds could result, either directly from incomplete combustion or indirectly via secondary reactions between gaseous compounds. The fuel in this region, prior to ignition, was altered from its initial composition due to exposure to a progression of temperatures from ambient to the ignition temperature of the fuel. The altered fuel is devoid of any fractions lost to processes in the preheating zone, and has been transformed via pyrolysis to a char, the primary material that is oxidized (described below).

Ahead of the reaction zone is the endothermic pyrolysis zone. It is in this zone that the high temperatures transform the fuel via pyrolysis into char. Pyrolysis can also produce gaseous products both directly and indirectly (Demirbas, 2010). Ahead of the pyrolysis zone is the preheating zone, where heat is transferred from the oxidation and pyrolysis zones below via conduction, convection and radiation to the unreacted sand and fuel. In this region, there is the potential for low and intermediate molecular weight hydrocarbons and other compounds to volatilize and also for a fraction of the liquid fuel to become suspended in the gas stream as an aerosol. Both of these processes occur to a greater extent at higher temperatures, but still require the presence of a liquid fuel. Also

occurring in this zone is the boiling of any water present in the fuel or adjacent to the fuel in the pore space. The exact temperatures at which these volatilization, aerosolization, pyrolysis, and oxidation processes occur, and thus the boundaries between these regions, are fuel dependent (Guillen et al., 1996).

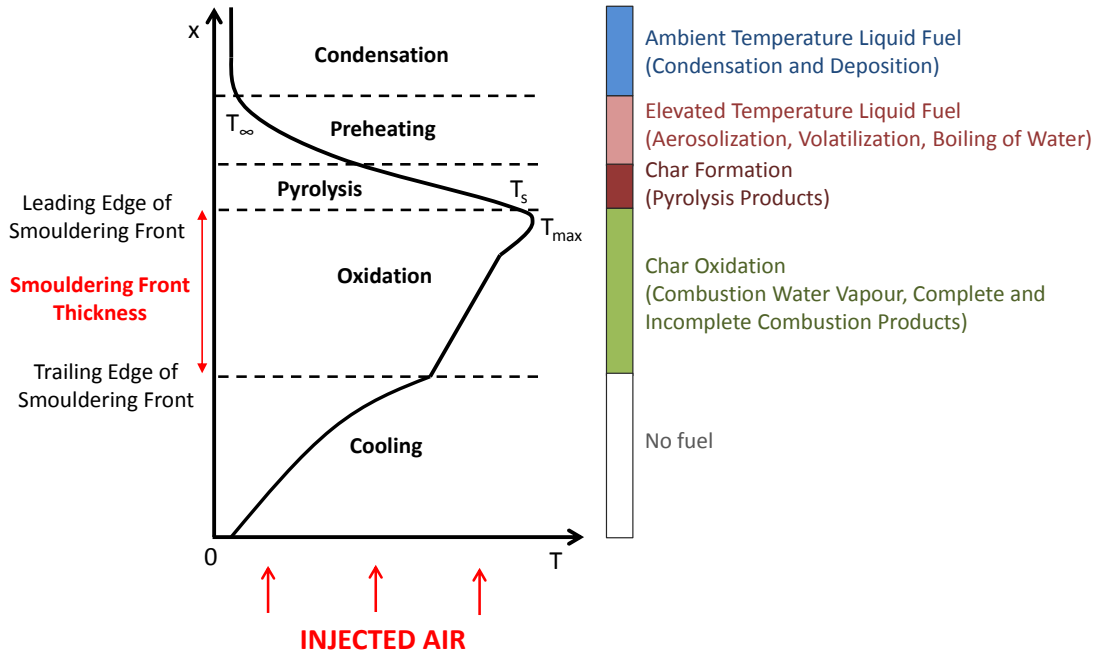

Figure 4.1: Conceptual model of temperature distributions within a vertical smouldering column for the upward propagation of a smouldering reaction in forward configuration (Torero, personal communication, March 2013). The relevant form of the fuel for each temperature region, as well as the expected emissions, are indicated on the right hand side of the plot.

Due to the relatively high heat capacity of sand, temperatures decline fairly rapidly through the preheating zone. As a result, for the majority of an experiment, there is a cool upper region in the column. In Figure 4.1 this is labeled the 'Condensation' zone since this is where any condensable compounds - water vapor, volatilized compounds, aerosols, pyrolysis products and condensable incomplete combustion products - may be deposited. The amount of deposition is expected to depend on the chemical properties of

the compounds, the sorptive and intercepting properties of the contaminated or clean material above (e.g., organic fraction, surface area), the rate of temperature drop, and the residence time of the gas, which in turn depends primarily on the air injection rate and the length of the condensation zone, that latter which is changing with time. For any given location, it is expected that these condensed and deposited products remain in this region until the heat front progresses upwards causing temperatures to increase. Due to the dynamic, propagating nature of the smouldering front, certain fractions of the contaminant may undergo a continuous cycle of volatilization/aerosol formation followed by condensation/deposition until reaching the top of the column.

While the influence of heat on the processes of volatilization, aerosolization and condensation have been investigated independently in various applications, including for example, steam enhanced remediation of NAPLs (Kaslusky and Udell, 2005) or health impacts of cooking oils (Siegmann and Sattler, 1996), these processes have not been studied in the context of smouldering of liquid fuels. It is hypothesized that these processes may be important for understanding emissions relationships and mass loss behaviour for remediating NAPL contaminated soils via smouldering combustion.

The objective of this work was to assess the relative significance of liquid fuel volatilization, aerosolization and subsequent condensation during smouldering. This was investigated through a series of controlled laboratory column experiments with varying contaminated zone heights, forced air flow rates and contaminant types. A more detailed understanding of the dynamic nature and global effect of these processes on a batch smouldering column is relevant for the design of large scale remediation applications and emissions treatment systems.

4.2 Materials and Methodology

4.2.1 Experimental Setup

A series of medium and tall forward, upwards smouldering column experiments with contaminated zone heights of 30 cm and 90 cm, respectively, were conducted to assess the transport of heat and condensable products. The experimental setup was identical to that reported in Chapter 3, with three key differences: combustion gas (CO and CO_2) and oxygen (O_2) concentrations in the gaseous emissions stream at the top of the column were measured continuously using a non-dispersive infrared absorption method (MGA3000 Multi-gas Analyser, ADC Gas Analytics Ltd), the column was placed on a mass balance (KCC150, Metler Toledo) and continuous mass loss data was collected throughout the duration of the experiment, and the contaminated zone was covered with a clean sand cap of variable height for a select few experiments.

The complete experimental setup, including additional data streams not reported in Chapter 3, is shown in Figure 4.2. The same ignition procedure was used as reported in Chapter 3, with the ignition temperature varying slightly depending on the properties of the fuels investigated.

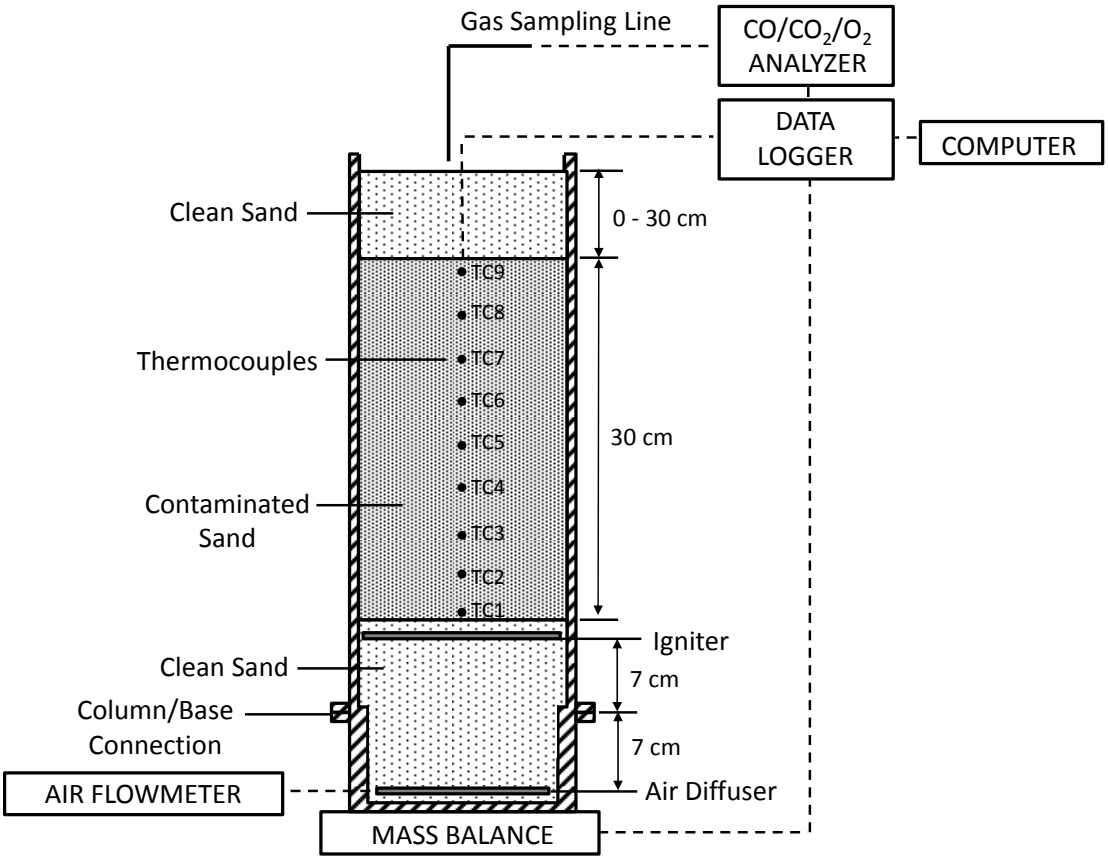

Figure 4.2: Schematic diagram of 30 cm column apparatus (modified from Figure 3.4). The 90 cm column setup consists of the same configuration, with the respective column height connected to the removable base.

A series of key experimental parameters were investigated to understand the transport of condensable combustion products. First was the contaminated zone height. An increase in contaminated zone height provides a larger condensation zone ahead of the combustion front. The second was air flux, represented as the air flow rate divided by the cross-sectional area of the column. The air flux can influence the propagation rate of the reaction, the peak temperature of the reaction, and numerous features related to heat transfer such as the thickness of the various regions shown in Figure 4.1. The third was the presence of a clean sand cap above the contaminated layer. While the clean sand cap serves a similar purpose to contaminated zone height in that it provides additional height

for condensable combustion products to condense, with the absence of fuel in this region, condensation behaviour can be studied independently from combustion. The fourth variable investigated was fuel type. While the majority of experiments were conducted with canola oil and viscosity index improver surrogate fuel, additional experiments with common NAPL contaminants under a select limited range of air flow rates was conducted to verify that the phenomenon investigated was not observed exclusively for the surrogate fuel. The final variable studied was moisture content, which has the potential to affect the distribution of heat within the column.

Three key metrics were used to investigate the transport of condensable combustion products: mass loss rate which combines mass destroyed via combustion reactions and mass emitted from the top of the column in the form of aerosols or other combustion products. It is, however, not possible to separate the different forms of mass loss, and therefore other key metrics must also be used to understand this behaviour. Temperature histories show the evolution of temperatures at a given location within the column over time and indicate the location of the smouldering front. The measurement of carbon monoxide and carbon dioxide concentrations in the gaseous emissions stream also provides an indication of the extent of combustion reactions occurring at a given time. The detection and relative magnitude of these combustion products provide a clear distinction between times when exothermic smouldering reactions are occurring and solely heat transfer scenarios after combustion is complete.

Table 4.1 outlines the experiments used to assess the transport of condensable combustion products through a smouldering column.

Table 4.1 Summary of Smouldering Column Experiments

Test Number[1]	Fuel Type	[Fuel] (g/kg)	[Water] (g/kg)	Air Flux (cm/s)	Height of Contaminated Zone (cm)	Height of Clean Sand Cap (cm)
1	50:50 Canola:VI	60	0	1.25	30	0
2				2.50		
3				6.25		
4	50:50 Canola:VI	60	0	1.25	90	0
5				2.50		
6				6.25		
7	50:50 Canola:VI	60	0	2.50	30	30
8[2]	50:50 Canola:VI	60	0	2.50	20	0
9	Crude Oil Sludge	60	0	3.65	30	20
10			45[3]	3.65		20
11			0	6.25		0
12	Coal Tar	60	0	6.25	30	0

[1] Experimental data from Tests 1 to 6 were also used in Chapter 3
[2] Column test was conducted in a closed system
[3] Equivalent to 18% saturation of pore volume

Tests 1 to 6 were conducted using a fuel composed of canola oil and viscosity index (VI) improver and consisted of a systematic change of contaminated zone height and air flow rate. Note that Tests 1-6 were also described in Chapter 3, however, there is no overlap in data or analyses between the two chapters. For these tests, the canola oil and VI improver mixture was selected as a non-toxic surrogate fuel for viscous NAPL contaminants. Test 7 was conducted using the same fuel, but was designed to further assess the transport of condensable combustion products through having an additional 30 cm clean sand cap above the contaminated zone.

Test 8 was conducted in a closed system, where all emissions were passed through a water bubbler to attempt to collect condensable compounds present in the emissions. The collected condensable compounds were then separated using a separatory funnel into

water and oil fractions. The relative mass of water and oil provided an indication of the origin of the condensable products; note that since the original fuel contained no moisture, all water collected would have been a combustion product. The oil fraction was further analyzed using elemental analysis to compare the elemental composition (carbon, hydrogen, nitrogen, oxygen and sulfur) of the condensate in comparison with the original fuel.

Four additional experiments (Tests 9 to 12) were conducted with a field mixture of crude oil sludge (Sarnia, Canada) and a commercial coal tar (Alpha Aesar, USA) to compare the behaviour of the surrogate fuel with real contaminants, with and without a clean sand cap. Test 10 also assessed the impact of the addition of initial water saturation on the transport of condensable combustion products.

As described in Chapter 3, all experimental data will be expressed as a function of non-dimensionalized time, unless otherwise noted. This permits a direct comparison between column experiments with different contaminated zone heights and forced air flow rates. Using this metric, a nondimensionalized time equal to one represents the time at which the leading edge of the smouldering front reaches the end of the contaminated zone.

4.3 Results and Discussion

4.3.1 Experimental Mass Loss Behaviour

In order to understand the experimental mass loss behaviour, it is necessary to consider the structure of a smouldering front and the different temperature regions present within a column over time. For the majority of a smouldering column experiment, there are four temperature zones in the column that are important for emissions and mass loss behaviour. These are described conceptually in Figure 4.1, and corresponding experimental data is provided in Figure 4.3. Figure 4.3 shows the distribution of temperatures within the column as a function of height for Experiment No. 6, which employed a 90 cm column and 6.25 cm/s air flux. Each curve represents a snapshot of the temperature profile at a particular moment in time, presented as nondimensionalized time (NDT). This case is used as an example to demonstrate the processes governing mass loss behaviour; the same temperature regions and their evolution is observed for all other experiments.

In Figure 4.3(a), the temperature profile at a NDT of 0.2 is shown as a red line. At this time, the reaction zone where exothermic oxidation reactions are converting the fuel into primarily carbon dioxide, carbon monoxide, water vapor and heat is located between 8 and 15 cm above the base of the contaminated soil pack (green shading). The preheating zone, which is defined as between the leading edge of the smouldering front and a temperature of 50°C (the pyrolysis zone defined in Figure 4.1 is considered to be thin and therefore the pyrolysis and preheating zones are collapsed into a single 'preheating zone' in Figure 4.3), is located from 15 to 32 cm above the base of the column (red shading).

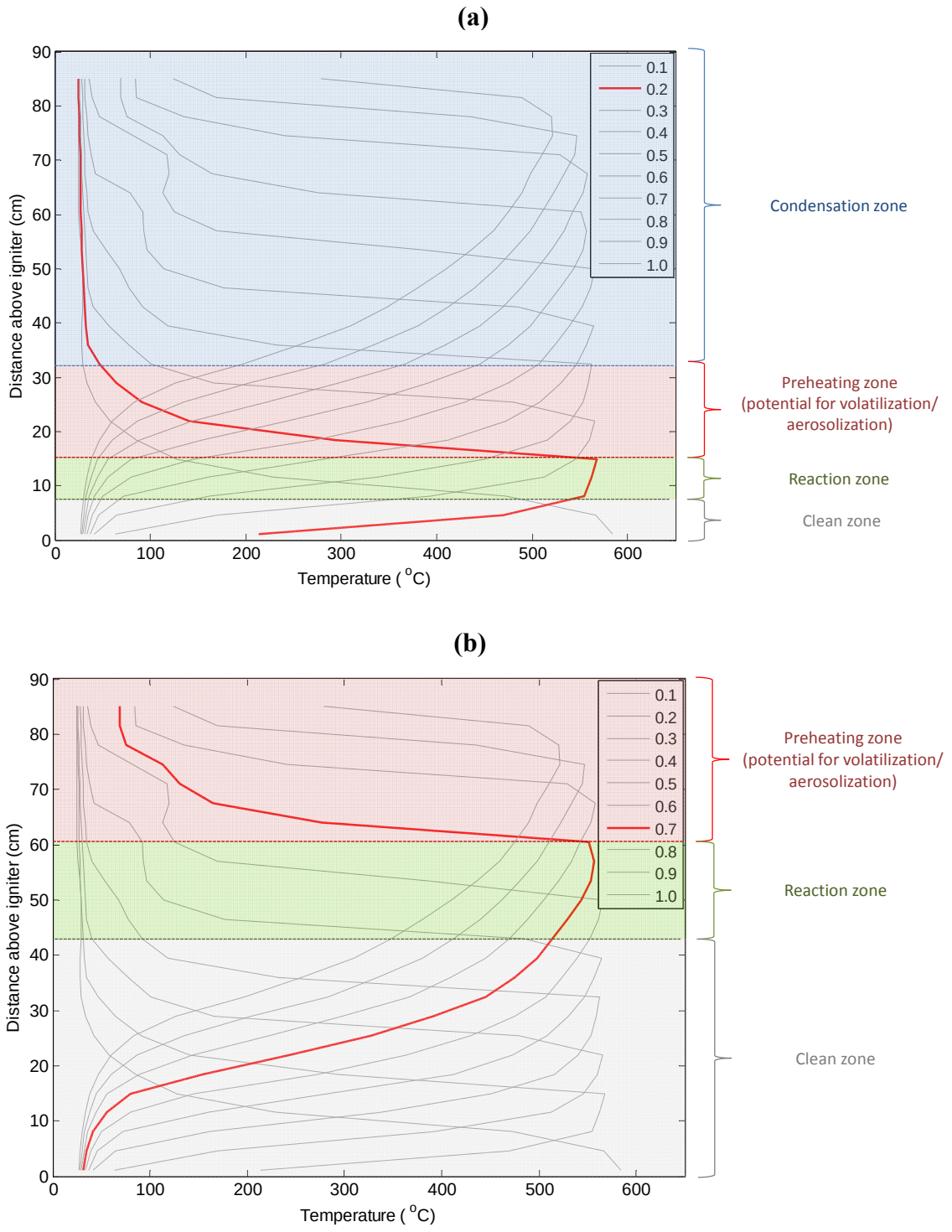

Figure 4.3: Temperature profile for 90 cm contaminated zone with a forced air flux of 6.25 cm/s. The legend provides the non-dimensionalized time associated with each profile. The labels on the right refer to the temperature zones present in a smouldering column that are relevant to the processes of volatilization, aerosolization and condensation for (a) NDT 0.2 and (b) NDT 0.7 (red curves).

In this preheating region, due to the exposure of the liquid fuel to elevated temperatures, there is the potential for volatilization of light fractions and aerosolization processes to occur. The condensation zone, located from 32 to 90 cm is at ambient temperatures (blue shading). The substantial thickness of this cool zone means that there is ample opportunity (i.e., residence time) for volatile compounds and aerosols in the gas stream to condense ahead of the front.

Figure 4.3(b) is identical to 4.3(a) except that the temperature profile at a NDT of 0.7 is now shown as the red line. All of the aforementioned processes are still occurring, with the exception that there is no longer a condensation zone present; this is because the top of the column has exceeded 50°C. Therefore, compounds with the potential to condense are expected to be released from the column system.

This expectation is confirmed by examining the rate of mass loss of contaminant as a function of nondimensionalized time (NDT). The rate mass loss plots are shown in Figure 4.4 for 30 cm and 90 cm contaminated zone heights (Tests 1 to 6) with an air flux ranging from 1.25 to 6.25 cm/s; these are typical of all the experiments conducted in which there was no clean sand cap overlying the contaminated zone. In these experiments, the leading edge of the smouldering front travelled at a velocity of 0.34 to 0.53 cm/min, depending on air flux. Not shown, because of the non-dimensionalized axis, is that the front reached the top of the contaminated zone in times ranging from 60 to 250 minutes from ignition, depending on column length and air flux.

Figure 4.4 reveals that there is a consistent, baseline average rate of mass loss of 2.3 to 3.9 g/min that occurs until a NDT of approximately 0.7. After this time, there is a

significant increase in the rate of mass loss to a maximum of between 17.5 g/min (30 cm column, 1.25 cm/s air flux) and 47.5 g/min (90 cm column, 2.50 cm/s) as the leading edge of the smouldering front approaches the end of the contaminated zone. While the peak mass loss rate was similar for a forced air flux of 2.50 and 6.25 cm/s (>30 g/min), there was a lower peak mass loss rate (17.5 g/min) for the 1.25 cm/min (lowest) forced air flux case. This suggests that manipulating air flow rates may minimize the mass loss peak associated with end effects. Note that any data missing between a NDT of 0.8 and 1 in Figure 4.4 is a result of stopping the experiment slightly before the smouldering front reached the free surface at the top of the contaminated zone as a safety precaution.

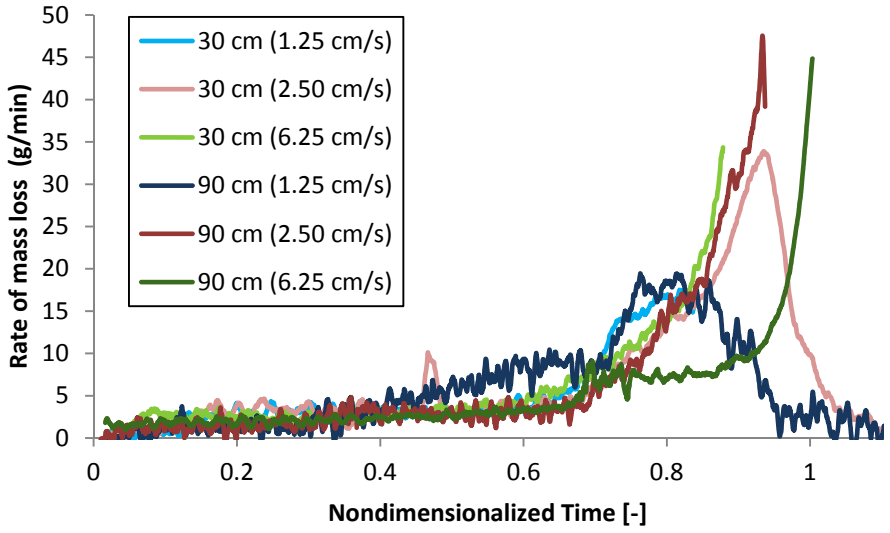

Figure 4.4: Mass loss rate behaviour for 30 cm and 90 cm contaminated zone heights (no clean sand cap) with a forced air flux ranging from 1.25 to 6.25 cm/s.

It was hypothesized that this mass loss rate behaviour – i.e., a baseline, pseudo-steady mass loss rate followed by a sharp acceleration and peak in mass loss as the smouldering front approached the end of the contaminated zone – was due to the recondensation of gaseous compounds (e.g., moisture, volatiles, aerosols and combustion products). While

there was still a region at the top of the column at ambient temperatures – a condensation region of appreciable thickness – these products are able to condense and are retained within the column system. This corresponds with a NDT from 0 to 0.7 in Figure 4.3. During this period the baseline rate of mass loss is observed. As the temperature at the top of the column increases, however, it is hypothesized that these products are released as emissions and represent an additional source of mass loss. An NDT of 0.7 corresponds with the time at which the condensation zone is eliminated (Figure 4.3b).

This hypothesis was further evaluated by plotting the rate of mass loss against the temperature at the top of the contaminated zone in Figure 4.5. This temperature was measured by the last thermocouple located in the contaminated zone, which was approximately 1 to 2 cm below the free surface (depending on precise packing configuration). The critical temperature associated with the start of the condensation zone, 50°C, is denoted as well as the average pseudo-steady mass loss rate of 3.0 g/min. Note that approximately 65% of the data shown in the figure is in the bottom left corner of the plot as temperatures do not rise above 50°C at the top of the column until the front is, on average, within 12 cm and 27 cm from the top of the column for the 30 cm and 90 cm columns, respectively. The figure reveals that, indeed, the rate of mass loss is approximately linearly dependent on the temperature at the top of the column. This is strong evidence that the rate of mass destruction by combustion is relatively steady while the rate of mass loss due to condensable compounds being emitted is a linear function of temperature at the top of the column. The slope of the average plot in Figure 4.5 may represent the increasing fraction of compounds that cannot be condensed below a certain temperature or, in other words, the distribution of boiling points of the large number of

compounds in the emissions. The exact temperature at the top of the column that corresponds with an increase in mass loss rate is dependent on the properties of the fuel and may vary from the 50°C threshold identified in Figure 4.5. This critical temperature will occur at the top of the column as the smouldering front approaches the end of the contaminated zone.

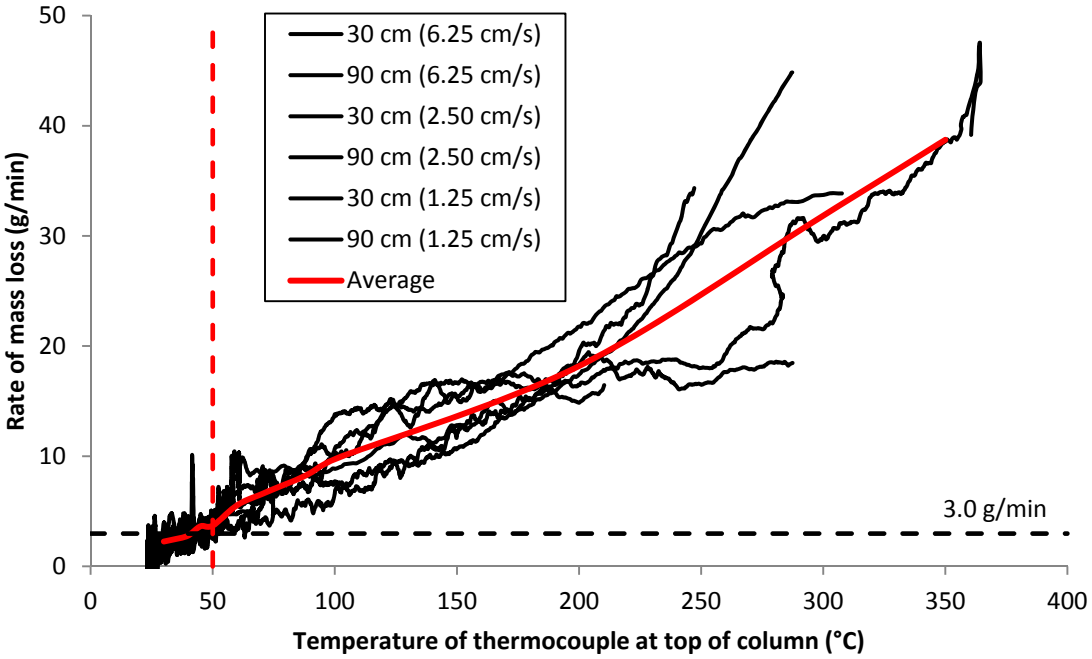

Figure 4.5: Mass loss rate as a function of the temperature just below the interface between the contaminated sand pack and the air within the column. The black dotted line represents the mean mass loss rate prior to any significant increases associated with end effects, and the red dotted line represents the critical temperature where the mean mass loss rate begins to increase approximately linearly with temperature at the top of the sand pack.

A similar change in the rate of mass loss was described, although not shown, in a recent publication by Baud et al. (2015). That work conducted smouldering of aluminum particles coated with solid carbon and reported a steady rate of mass loss until the last thermocouple reached 58°C, followed by a sharp rise in the mass loss rate over time.

Their explanation was that water vapour – generated from combustion – and volatiles were released only after the top of the column reached 58°C. This study demonstrated corroborating evidence for the presence of a condensation front inside the column in the thermocouple histories. They argue that the presence of temperature plateaus at 58°C ahead of the smouldering front are the result of heat released from condensation (i.e., the latent heat of condensation) (Baud et al., 2015). Indeed, such plateaus are observed in the condensation zone in these experiments. For example, Figure 4.6 illustrates the temperatures histories for all thermocouples in Test 5.

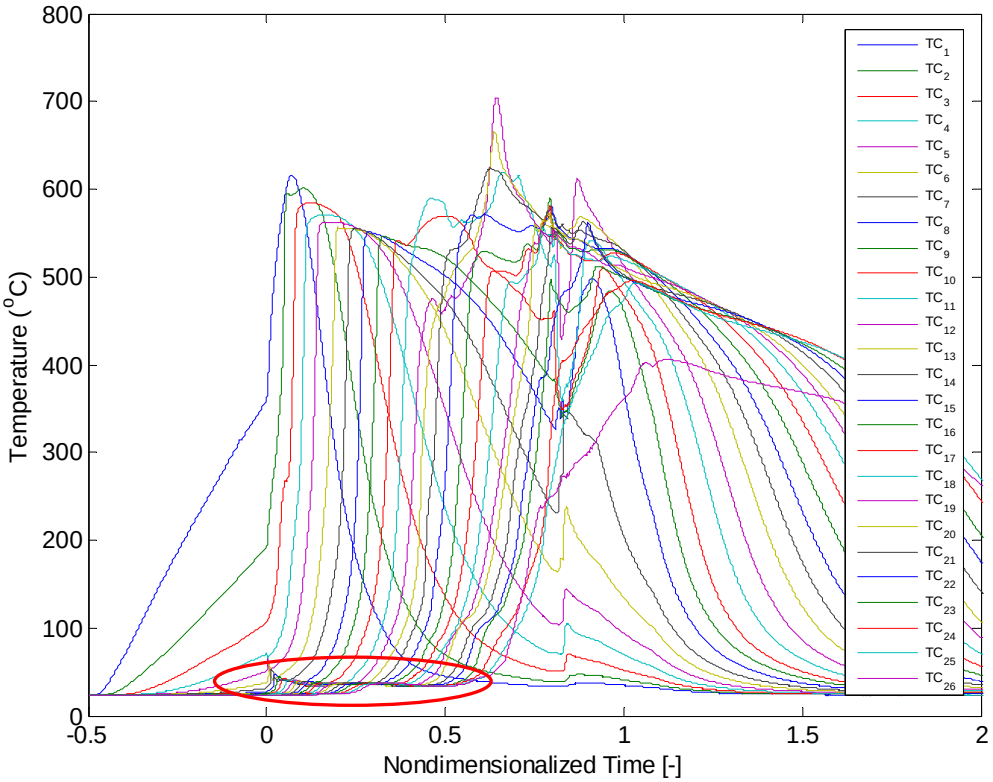

Figure 4.6: Temperature history for 90 cm column with air flux of 2.50 cm/s as a function of nondimensionalized time (time zero represents the start of forced air injection). The thermocouples are located at 3.5 cm intervals, with TC1 located 1 cm above the base of the contaminated zone. The red circle highlights the effects of the latent heat of condensation for this column test.

The temperature rise to 40°C occurs approximately 75 min (or 30 cm) ahead of the arrival of the smouldering front. It is expected that the temperature of the plateaus would be different between tests in this study and Baud et al. (2015) since the effective latent heats of condensation are likely dependent on fuel type, condensable compounds, and experimental conditions. Nevertheless, this provides additional evidence of the propagation of a condensation front ahead of the smouldering front until the condensation zone disappears.

Further evidence of this recondensation behaviour can be observed in Test 7, which consists of a 30 cm contaminated zone with an overlying 30 cm clean sand cap. The forced air flux in this case is 2.50 cm/s. As shown in Figure 4.7, there are two distinct peaks in contaminant mass loss rate.

During the first peak in mass loss rate, occurring between a NDT of 0 and 1.7, there is a simultaneous peak in CO and CO_2 indicating that combustion is occurring. Therefore this first peak in mass loss rate is due to smouldering destruction of the contaminant. Note that, in this case, when the smouldering front reached the end of the contaminated zone (black dashed line), no sharp rise in emissions occurred unlike for all experiments with no clean sand cap (see Figure 4.4). This is because the clean sand cap provided the condensation zone.

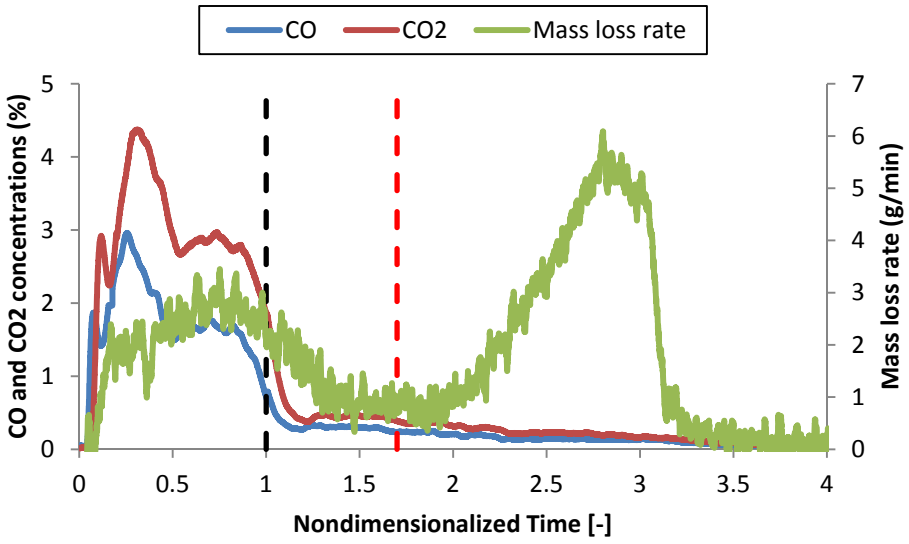

Figure 4.7: Graph showing CO and CO_2 emissions in comparison with rate of mass loss of contaminant as a function of nondimensionalized time. The experimental setup consists of a 30 cm contaminated zone (canola oil and VI improver) and an overlying 30 cm clean sand pack with a forced air flux of 2.50 cm/s. The dashed black line represents the time at which the leading edge of the smouldering front reaches the end of the contaminated zone while the dashed red line represents the time at which the top of the clean sand reaches 50°C.

Figure 4.7 reveals that, in contrast, a second peak in mass loss rate occurs during a time when minimal combustion gases are being produced and only after the clean sand pack begins to increase in temperature (red dashed line). The clean sand pack heats up, despite the lack of combustion, due to conduction and convection of energy accumulated in the column. This experiment demonstrates that the time associated with the emission of condensable compounds depends upon the thickness and temperature of a clean sand pack above the smouldering region. The magnitude of the mass loss rate of this second peak, approximately one-fifth of that observed in the cases with no clean sand cap at the same forced air flux (Figure 4.4), suggests further that the magnitude of the emissions rate will depend on the size of the clean sand cap, probably in combination with other factors that affects its temperature (e.g., amount of energy accumulated, air flux, etc).

4.3.2 Categorization of Emissions

A closed system test (Test 8) was conducted to collect and identify condensable compounds in the emissions stream. This test was similar to Test 2 except a shorter contaminant pack height (20 cm) was employed. A schematic of the system is shown in Appendix C. A total of 253 g of condensable products was captured in the water bubbler. A separatory funnel was used to determine that, of the condensed mass, 19% was water and 81% was an oil. It is therefore likely that the majority of the mass released during the final mass loss peak is a result of recondensation of volatile compounds and aerosols, as opposed to water vapour formed as a combustion product. Due to challenges in sealing all leaks within the closed system, it is possible that some condensable products escaped. Therefore, this test cannot be used for mass balance purposes, but is indicative of the relative fraction between water vapour and organic-phase condensable products.

In order to better understand the composition of the oil fraction collected in Test 8, elemental analysis was conducted on both the initial fuel and the oil condensate (Table 4.2). It is expected that the elemental (C:H:O:N:S) ratios between the initial fuel and the condensate would be similar if the condensate was formed primarily due to volatilization and aerosolization processes. On the contrary, if the condensate was composed primarily from incomplete combustion products, it is expected that this elemental ratio would be altered due to preferential transformation of some elements to incondensable products (e.g., CO and CO_2) during combustion which would not be collected in the condensate. As shown in Table 4.2, while the carbon content of the condensate was slightly lower, the elemental composition is largely unchanged from the initial fuel. This suggests that the

origin of the oil fraction of the condensate is primarily due to volatilization and aerosol formation of the virgin fuel, as opposed to products formed during pyrolysis or oxidation.

Table 4.2 Elemental Analysis of Initial Fuel versus Condensate

	Initial Fuel (% mass)	Condensate (% mass)
Carbon (C)	80.6	77.4
Hydrogen (H)	11.5	12.3
Oxygen (O)	8.2	10.4
Nitrogen (N)	0	0
Sulfur (S)	0	0

4.3.3 Comparison with Other Contaminants

In order to ensure that the detailed investigation conducted with the surrogate fuel was applicable to real contaminant systems, column tests were conducted with crude oil sludge (Test 11) and coal tar (Test 12).

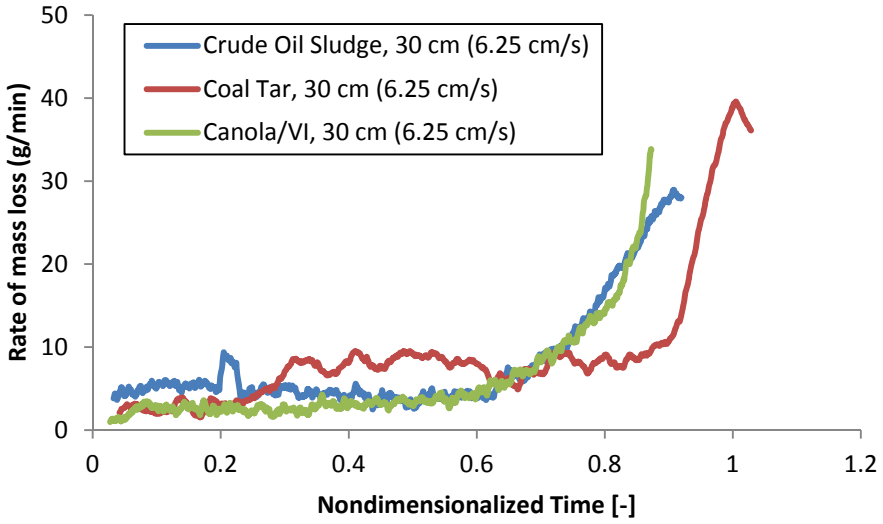

Figure 4.8: Rate of mass loss of crude oil sludge and coal tar as a function of nondimensionalized time in comparison with canola oil and VI surrogate fuel.

As shown in Figure 4.8, the same characteristic mass loss rate behaviour is observed for real contaminants, where there is a lower baseline mass loss rate followed by a distinct

increase as the reaction approaches the end of the column. This baseline mass loss rate may vary depending on the contaminant, with coal tar displaying a higher rate. Coal tar had a pseudo-steady mass loss rate of 7 g/min, which is 1.4 to 2.0 times the mass loss rate of crude oil sludge and canola oil/VI improver, respectively. Moreover, its mass loss rate did not begin to peak until a nondimensionalized time of approximately 0.9 (as compared to 0.6 to 0.7 for the other two fuels).

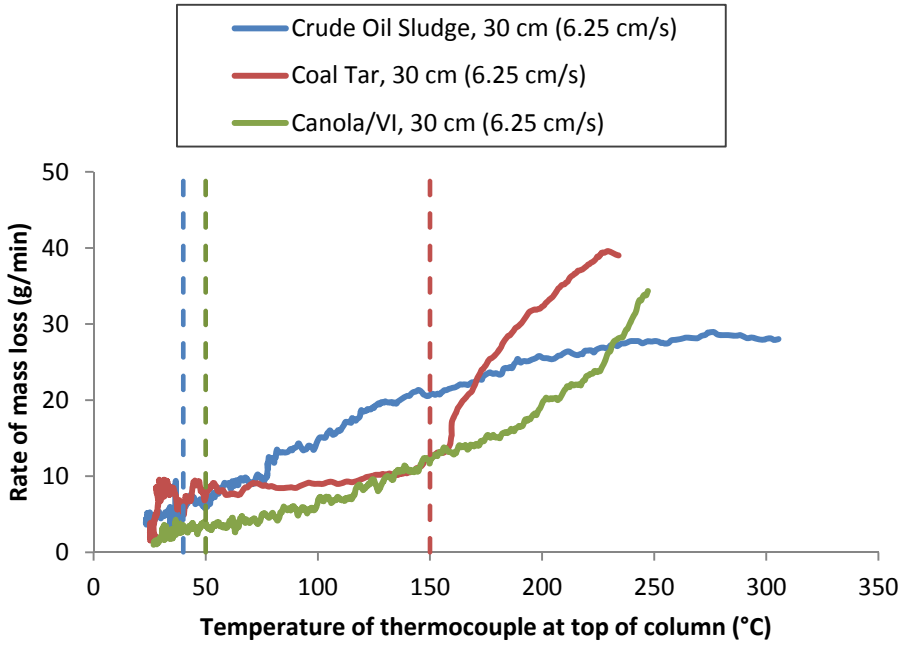

Figure 4.9: Mass loss rate as a function of the temperature just below the interface between the contaminated sand pack and the air within the column for Tests 3, 11 and 12 (30 cm columns, canola oil/VI, crude oil sludge and coal tar, 6.25 cm/s forced air flux). Approximate critical temperatures for the respective fuels are represented by the vertical dashed lines.

As shown in Figure 4.9, the mass loss rate of coal tar does not begin to increase appreciably above baseline rates until the temperature at the top of the column reaches approximately 150°C. This critical temperature is significantly higher than the 50°C critical temperature defined for canola oil/VI improver in Figure 4.5 (the mass loss rate of

canola oil/VI from Figure 4.5 for comparable experimental conditions – same column height and forced air flux – is also shown on Figure 4.9). The mass loss behaviour of crude oil sludge differs further, with a slightly higher initial mass loss rate than the canola oil/VI surrogate fuel, but with a lower critical temperature than the other two fuels (approximately 40°C on Figure 4.9). This difference in critical temperature and resulting effects on mass loss behaviour between coal tar and the other two fuels (canola oil/VI and crude oil sludge) is attributed to the presence of less volatile fractions in coal tar, therefore favouring a higher fraction destroyed by smouldering in situ.

4.3.4 Effect of Moisture Content

Tests 9-11 were conducted using crude oil sludge to explore the effect of moisture content on the emissions. Moisture content, by adding a heat sink to the system, is known to reduce the peak temperature and rate of smouldering (Pironi et al., 2011; Yerman et al., 2015). Since, as shown, the amount and distribution of heat in the system affects condensable emissions, plus the peak temperature affects the pyrolysis and oxidation combustion reactions (Schult et al., 1996), moisture content is hypothesized to have an influence on emissions.

A comparison of the rate of mass loss as a function of nondimensionalized time for experimental conditions with/without added moisture content is shown in Figure 4.10. In the case where there is no moisture content and no clean sand cap is present, the same characteristic mass loss behaviour that was described previously for the canola oil/VI surrogate fuel was observed: mass loss rate accelerates when the condensation zone disappears. In the case where there is a clean sand cap but no moisture content, there is a much smaller increase in mass loss rate as the reaction progresses through the

contaminated zone. As the top of the clean sand cap increases in temperature, there is a second, smaller peak in mass loss rate. The results of this test display the same qualitative behaviour as Test 7 for surrogate fuel smouldering with a clean sand cap. The quantitative differences in mass loss rate and relative proportion of the peaks can be attributed to different fuel composition and air flux.

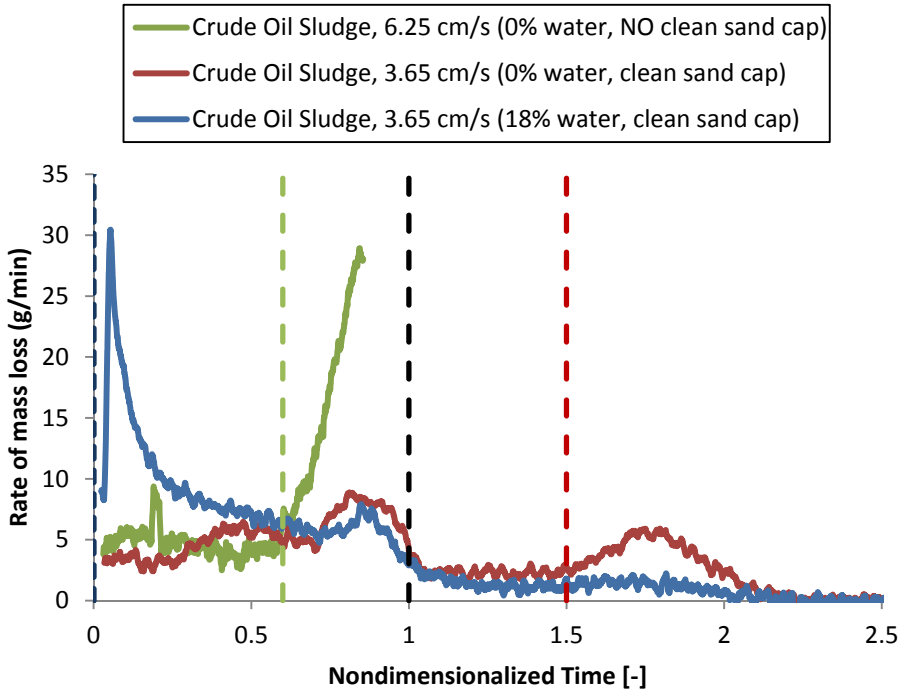

Figure 4.10: Comparison of rate of mass loss as a function of nondimensionalized time for crude oil sludge with/without a clean sand cap and with/without added water content (expressed as % saturation of pore space). The black dotted line represents the time at which the leading edge of the smouldering front reaches the end of the contaminated zone in all experiments. The coloured dotted lines represent the time at which the top of the column (either clean or contaminated sand) reaches 50°C for the respective experiments (i.e., condensation zone disappears); note that the blue dashed line is coincident with the vertical axis.

In the case where water is added to the sand and crude oil sludge mixture, the mass loss behaviour changes further. First, there is a strong initial peak in mass loss rate when the air is turned on. This likely represents the release of steam generated during the

preheating period. This is unique in these experiments as this is the only test where water was mixed with the fuel. However, a similar initial spike in mass loss has been observed with wet fuels such as biosolids (Rashwan, 2015). After this, a somewhat steady mass loss rate is approached as the reaction propagates up the column, but it is approximately 1.5 to 2 times larger than observed in the other two experiments. There is again a slight increase in mass loss rate as the reaction approaches the end of the contaminated zone, but when water is present there is no second peak in mass loss rate as the top of the clean sand increases in temperature. As indicated in the figure, due to transport of the steam from the onset of air flow, the top of the column in this case reaches 50°C from the beginning of the experiment. The propagation of a boiling front ahead of the smouldering front ensures that this threshold temperature is exceeded at the top of the column throughout the entire test, essentially eliminating any condensation zone from this test with water in the pore space.

The differing behaviour with the presence of water may be due to several reasons. First, water could change the dynamics of the reaction and preheating zones such that it shortens the heating front, enhancing combustion and reducing the formation of aerosols and volatile fractions. Second, steam may simply help to carry condensable products through the clean sand since elevated temperatures (approximately 50°C) are observed throughout the column from the time air is initiated. This would minimize the amount of condensation throughout the experiment and eliminate the distinct peak mass loss rate near the end of the experiment. Based on the mass loss data in Figure 4.10, there is no clear distinction between regions representing mass destroyed via combustion versus mass released as condensable emissions. Therefore, further investigation of operational

parameters is required to understand the conditions under which combustion is enhanced and the volatilization of condensable products is minimized.

4.3.5 Fraction of Mass Destroyed

The mass loss rate plots, shown in Figures 4.4 (canola oil and VI improver, no clean cap), 4.7 (canola oil and VI improver, clean cap), 4.8 (crude oil sludge and coal tar, no clean cap) and 4.10 (crude oil sludge, with and without clean cap) provide the ability to (i) calculate the total mass balance on the system by taking the integral over time, and (ii) estimate the fraction of mass removed via destruction versus removed as condensable emissions. For the 30 cm and 90 cm experiments, the total mass of fuel was approximately 545 g and 1640 g, respectively. Comparing these values to the total mass accounted for by the integration of the curves in Figures 4.4, 4.7, 4.8 and 4.10 finds an excellent mass balance within ± 4%. The exception is mass balance errors up to 25% in the column tests (No. 5, 6 and 11) that were stopped early for safety precautions and thus data is missing at late time.

For all column tests with no clean cap present, the fraction of mass destroyed via combustion is calculated as the integral of the mass loss rate while the condensation zone was present plus an estimate of the mass lost to combustion occurring after the condensation zone was eliminated; the latter was estimated by assuming that the average mass loss rate from combustion observed at the time the condensation zone disappeared continued until the end of the test (e.g., the data shown in Figure 4.4 from NDT 0.6 to 0.7 continued until NDT 1.0). The fraction removed via condensable emissions is calculated as the integral of the mass loss rate after the condensation zone was eliminated minus the amount estimated to have been combusted during this period. For Experiments 5, 6 and

11, the mass not accounted for due to stopping the experiment early was added to the fraction removed via condensable emissions. Due to the excellent mass balance in all other column experiments, this extrapolation of mass loss behaviour is a reasonable assumption. These calculations for Experiments 1 to 6 (conducted using the canola oil and VI improver surrogate fuel) reveal that on average 40% of the mass was destroyed via combustion and 60% was emitted as condensable products.

For Tests 7 and 9, where there was a clean sand cap, the fraction of mass destroyed is calculated as the integral of the first peak in mass loss rate where there is evidence of combustion and the clean sand cap serves as the condensation zone. The fraction removed via condensable emissions is calculated as the integral of the second peak in mass loss rate where combustion gases are no longer detected and the clean sand cap is at elevated temperatures. For the canola oil and VI improver surrogate fuel (Test 7), the integral of the mass loss rate curve provided a 95% mass balance, of which an estimated 41% of the mass was destroyed via combustion.

A comparison of the relative proportion of the total fuel that is estimated to be destroyed during quasi-steady combustion (i.e., baseline mass loss for experiments with no clean cap, or mass lost during the first peak in mass loss rate for experiments with a clean cap) as a function of forced air flux for all experiments is shown in Figure 4.11. Test 10 (crude oil sludge with 18% water saturation) is not included in this plot because it is not possible to separate mass lost due to combustion from volatilization without further investigation of the effect of water content. Test 8 is also omitted as mass data could not be collected using the closed system experimental apparatus.

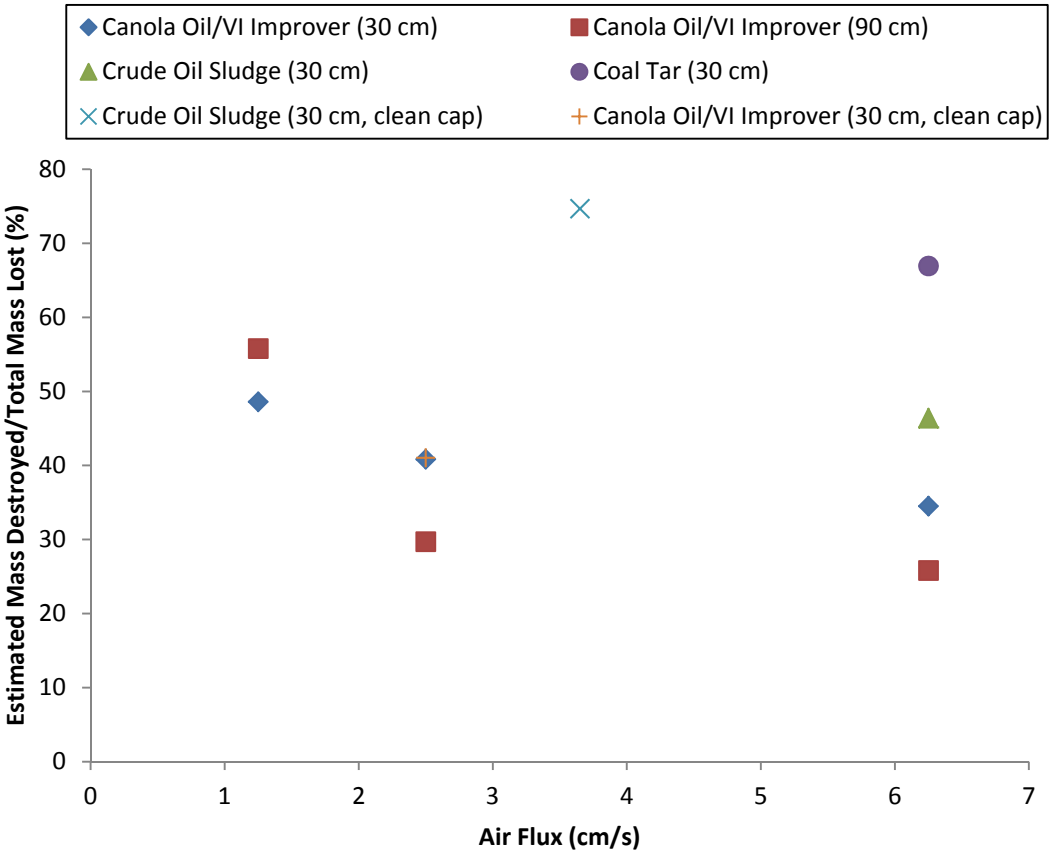

Figure 4.11: Comparison of estimated mass destroyed expressed as a percentage of total mass lost as a function of injection air flux for Tests 1-7, 9, 11 and 12.

Figure 4.11 suggests that there is a qualitative and quantitative difference between the emissions of real contaminants considered for smouldering destruction, coal tar and crude oil sludge, and the surrogate fuel used in this work, canola oil/VI improver. It is possible that the nature of the emissions between these fuels is considerably different. It is hypothesized that the bulk of the non-combustion (i.e., condensable) emissions from the surrogate fuel are aerosols while a larger fraction of those emissions from the real contaminants are volatile organic compounds. There are numerous lines of evidence for this hypothesis. First, the thermogravimetric (TGA) and differential thermogravimetric (DTG) data for the different fuel types, shown in Figure 4.12, suggests that the VI

improver and canola oil contain virtually no volatile compounds; this is shown by the fact that their initial mass loss occurs at well over 200ºC and 300ºC, respectively, and this mass loss coincides with pyrolysis and oxidation reactions. However, the figure shows that both coal tar and crude oil sludge exhibit significant mass loss, up to 50%, below 300ºC where pyrolysis reactions begin. This mass loss at relatively low (relative to smouldering) temperatures is attributed to volatilization of low molecular weight compounds, which is expected in sludge and coal tar which are complex mixtures of hundreds of hydrocarbons of varying carbon chain length (Haeseler et al., 1999; Hughey et al., 2002).

The second line of evidence is the fact that aerosol droplet formation is well known to be highly dependent on air velocity and properties of the fuel including viscosity, density, and interfacial tension (Esteban et al., 2012). Vegetable oils are known to be aerosolized and their propensity for this decreases (due to larger drop formation, and reduced number of drops formed) as viscosity is increased (Smolinski et al, 1996). Viscosity is a function of molecular weight and molecular composition and the complex and heavy hydrocarbons crude oil and coal tar typically have viscosities that are orders of magnitude larger than that of vegetable oils (see Figure 3.3). Therefore, it is expected that they are much less susceptible to the formation of aerosols than vegetable oils. It is noted that viscosity decreases dramatically with increasing temperature (Figure 3.3, Esteban et al., 2012) up to 120ºC; nevertheless, while the heavy hydrocarbons may experience some aerosolization at elevated temperature, it is still expected to be much less prevalent than for vegetable oil due to their liquid properties (larger molecular weight and therefore higher viscosity, higher density, and higher surface tension).

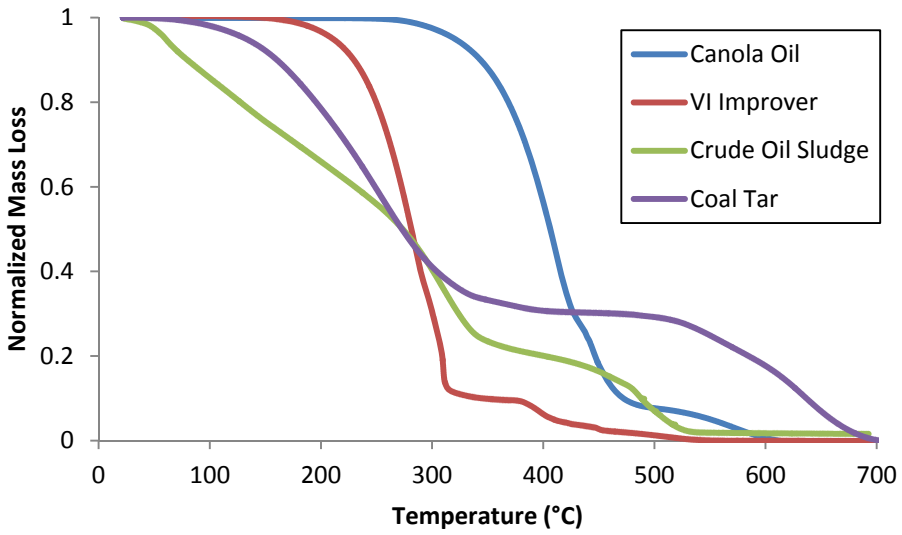

(a)

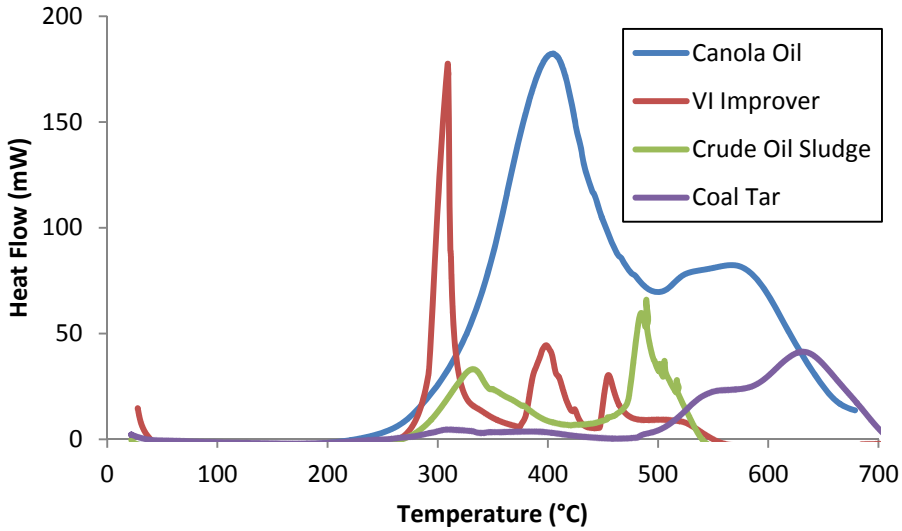

(b)

Figure 4.12: (a) Thermogravimetric analysis (TGA) data showing normalized mass loss as a function of temperature for canola oil, VI improver, crude oil sludge and coal tar, and (b) differential thermogravimetric (DTG) data showing heat flow as a function of temperature for the fuels investigated.

It can be seen that all factors explored, including: contaminant type, forced air flux, contaminated zone height, presence or absence of a clean sand cap, and water saturation (not included in plot), may affect the relative proportion of mass lost during quasi-steady

combustion (i.e., in presence of condensation zone) in comparison to end effects (i.e., loss of condensation zone). Based on Figure 4.11, it is hypothesized that the percentage of mass lost during quasi-steady combustion may increase with lower injection air flow rates, heavier and higher viscosity fuels (e.g., coal tar), lower proportions of volatile compounds in complex mixtures, and potentially the presence of a clean sand cap and moisture content. Conclusive evidence of these predictions and full optimization of smouldering systems would, however, require a detailed investigation into emissions composition for these scenarios.

4.4 Summary

In summary, a detailed investigation of laboratory column experiments with varying contaminant types and moisture content, air flow rate, and presence or absence of a clean sand cap provided insight into the transport and fate of aerosols and condensable compounds in emissions. It was found that there is typically a lower baseline mass loss rate which occurs while these condensable compounds (moisture, aerosols, volatile compounds, some pyrolysis and incomplete combustion products) are retained within the column system through a continuous cycle of generation and recondensation. In this sense, a batch smouldering reactor is behaving much like a chemical distillation column. This recondensation cycle will continue until there is no longer a cool upper region (i.e., condensation zone) in the column to temporarily collect and retain these compounds.

The condensation zone becomes progressively smaller as the smouldering reaction moves upwards in the column. At a critical point, the position of the leading edge of the smouldering front is close enough to the top of the column that all sand above is affected

by the transfer of heat from the reaction zone and rises to a critical temperature. At this time, these compounds may be released from the column and the rate of release is approximately linearly related to the temperature at the top of the column. The critical temperature at which this increase in the rate of release of condensable products occurs is fuel dependent, with heavier fuels such as coal tar exhibiting a higher critical temperature (e.g., critical temperature for coal tar is approximately 150°C as compared to 50°C for the canola oil/VI surrogate fuel). The mass emitted is composed partly of water vapour formed during combustion processes, or from steam generated ahead of the smouldering front if a wet fuel or wet porous medium is used, and includes lighter hydrocarbons and aerosols.

It is thought that the relative proportion of combustion to volatilization may be partly a function of fuel type. Lighter compounds in complex hydrocarbons are clearly susceptible to volatilization in the heated zone ahead of the front. Low viscosity oils, like vegetable oil, are more susceptible to forming aerosols at elevated temperatures. Heavy hydrocarbons like coal tar, appear to be least susceptible to either of these processes and therefore favour destruction over gaseous mass transport.

It is also expected that the relative proportion of mass combusted to emitted as gaseous compounds may be affected through manipulation of operational parameters such as moisture content and forced air flux. Further investigation into this optimization should permit enhanced contaminant destruction and reduce the strain on emissions treatment systems during larger scale operations.

4.5 References

Baud, G., Salvador, S., Debenest, G., & Thovert, J. F. (2015). New granular model medium to investigate smoldering fronts propagation-experiments. *Energy & Fuels*, *29*(10), 6780-6792.

Davis, E. L. (1997). *How heat can enhance in-situ soil and aquifer remediation: Important chemical properties and guidance on choosing the appropriate technique*. EPA 540-S-97-502. Washington, DC: U.S. Environmental Protection Agency.

Demirbas, A. (2010). Fuels from Biomass, *Biorefineries* (pp. 33-73). London: Springer-Verlag.

Drysdale, D. (2011). Spontaneous Ignition within Solids and Smouldering Combustion, *An Introduction to Fire Dynamics* (pp. 317-348). UK: John Wiley & Sons, Ltd.

Esteban, B., Riba, J., Baquero, G., Rius, A., & Puig, R. (2012). Temperature dependence of density and viscosity of vegetable oils. *Biomass and Bioenergy*, *42*, 164-171.

Guillen, M. D., Dominguez, A., Iglesias, M. J., & Blanco, C. G. (1996). Analysis of coal tar pitch: Relations between thermal behaviour and composition. *Fuel*, *75*(9), 1101-1107.

Haeseler, F., Blanchet, D., Druelle, V., Werner, P., & Vandecasteele, J. (1999). Analytical characterization of contaminated soils from former manufactured gas plants. *Environmental Science & Technology, 33*(6), 825-830.

Hughey, C. A., Rodgers, R. P., & Marshall, A. G. (2002). Resolution of 11 000 compositionally distinct components in a single electrospray ionization fourier transform ion cyclotron resonance mass spectrum of crude oil. *Analytical Chemistry, 74*(16), 4145-4149.

Kaslusky, S. F., & Udell, K. S. (2005). Co-injection of air and steam for the prevention of the downward migration of DNAPLs during steam enhanced extraction: An experimental evaluation of optimum injection ratio predictions. *Journal of Contaminant Hydrology*, *77*(4), 325-347.

Ohlemiller, T., & Shaub, W. (1988). *Products of wood smolder and their relation to wood-burning stoves.* NBSIR 88-3767. Washington, DC: U.S. Department of Energy.

Pironi, P., Switzer, C., Gerhard, J. I., Rein, G., & Torero, J. L. (2011). Self-sustaining smoldering combustion for NAPL remediation: Laboratory evaluation of process sensitivity to key parameters. *Environmental Science & Technology, 45*(7), 2980-2986.

Pironi, P., Switzer, C., Rein, G., Fuentes, A., Gerhard, J. I., & Torero, J. L. (2009). Small-scale forward smouldering experiments for remediation of coal tar in inert media. *Proceedings of the Combustion Institute, 32*, 1957-1964.

Rashwan, T. L. (2015). *Self-Sustaining Smouldering Combustion as a Novel Disposal Destruction Method for Waste Water Biosolids.* (M.E.Sc), The University of Western Ontario, London, ON.

Salman, M., Gerhard, J. I., Major, D. W., Pironi, P., & Hadden, R. (2015). Remediation of trichloroethylene-contaminated soils by star technology using vegetable oil smoldering. *Journal of Hazardous Materials*, *285*, 346-355.

Scholes, G. C., Gerhard, J. I., Grant, G. P., Major, D. W., Vidumsky, J. E., Switzer, C., & Torero, J. L. (2015). Smoldering remediation of coal tar contaminated soil: Pilot field tests of STAR. *Environmental Science & Technology*, Article ASAP.

Schult, D. A., Matkowsky, B. J., Volpert, V. A., & FernandezPello, A. C. (1996). Forced forward smolder combustion. *Combustion and Flame, 104*(1-2), 1-26.

Siegmann, K., & Sattler, K. (1996). Aerosol from hot cooking oil, a possible health hazard. *Journal of Aerosol Science, 27*(1), S493-S494.

Smolinski, J. M., Gulari, E., & Manke, C.W. (1996). Atomization of dilute polyisobutylene/mineral oil solutions. *Fluid Mechanics and Transport Phenomena, 42*(5), 1201-1212.

Switzer, C., Pironi, P., Gerhard, J. I., Rein, G., & Torero, J. L. (2009). Self-sustaining smoldering combustion: A novel remediation process for non-aqueous-phase liquids in porous media. *Environmental Science & Technology, 43*(15), 5871-5877.

Switzer, C., Pironi, P., Gerhard, J. I., Rein, G., & Torero, J. L. (2014). Volumetric scale-up of smouldering remediation of contaminated materials. *Journal of Hazardous Materials, 268*, 51-60.

Torero, J. L., & Fernandezpello, A. C. (1995). Natural-convection smolder of polyurethane foam, upward propagation. *Fire Safety Journal, 24*(1), 35-52.

Triplett Kingston, J. L., Johnson, P. C., Kueper, B. H., & Mumford, K. G. (2014). In situ thermal treatment of chlorinated solvent source zones. In Kueper, B. H., Stroo, H.F., Vogel, C. M., & Ward, C. H. (Eds.), *Chlorinated Solvent Source Zone Remediation* (pp. 509-558). New York: Springer.

Yerman, L., Hadden, R. M., Carrascal, J., Fabris, I., Cormier, D., Torero, J. L., Gerhard, J. I., Krajcovic, M., Pironi, P., & Cheng, Y. L. (2015). Smouldering combustion as a treatment technology for faeces: Exploring the parameter space. *Fuel*, *147*, 108-116.

5 CONCLUSIONS AND RECOMMENDATIONS

5.1 Conclusions

This thesis focused on the investigation of dynamic processes that occur during the propagation of a smouldering front through a porous matrix partially saturated with liquid fuel (contaminant). A suite of laboratory scale column experiments with a range of contaminated and clean sand zone heights, contaminant types, air flux and moisture content were conducted to understand the influence of the processes of fuel mobility and the transport of condensable products on smouldering metrics. These experiments were quantified in terms of temperature distributions in both time and space, mass loss rate, propagation velocities of both the leading and trailing edge of the smouldering front, and combustion gas (CO and CO_2) emissions. Numerical modelling and a simple analytical model were also developed to better understand liquid fuel mobility and provide a tool to be able to predict the potential for downward fuel mobilization given fuel and soil properties, fuel saturation and air flux.

Results of the laboratory and numerical investigation on fuel mobility suggest that:

- Under the correct conditions, fuel mobilization can occur and has the potential to influence smouldering behaviour.
- Three conditions must exist simultaneously for downward fuel migration to occur:
    - The forced air flux must be sufficiently low to induce a downward fuel hydraulic gradient within the column.

    - The viscosity of the liquid fuel within the preheating zone must be sufficiently low to permit the rate of mobilization to be relevant to the time scales of smouldering.
    - The height of the preheating zone ahead of the smouldering front must be large enough to provide a volume of low viscosity fuel that will noticeably influence smouldering metrics.
- These three conditions are more likely to exist in taller systems operated at low air flow rates.
- Given these conditions, downward fuel mobilization can result in three key impacts on smouldering metrics:
    - A slowing in the advance of the trailing edge of the smouldering front as downward mobilization provides additional fuel to sustain combustion.
    - An increase in the thickness of the smouldering front due to the constant rate of propagation of the leading edge of the smouldering front while the trailing edge is stalled.
    - Quasi-superadiabatic conditions leading to elevated peak temperatures as there is an accumulation of fuel and energy at a given location due to migration.

Results of the laboratory testing program on the transport of heat and condensable combustion products suggest that:

- The processes of volatilization, aerosolization, condensation and deposition occurring due to the distribution of heat within a smouldering system can influence emissions and mass loss rate over time.

- A lower baseline mass loss rate occurs while there is a cool upper region in the column to retain condensable products (moisture, aerosols, volatile compounds, and pyrolysis or incomplete combustion products). This baseline mass loss rate represents the mass estimated to be destroyed during quasi-steady combustion.
- A continuous cycle of generation and recondensation will occur until the top of the column reaches a critical elevated temperature such that these compounds can no longer recondense.
- At this critical point, the rate of release of condensable compounds is approximately linearly related to the temperature at the top of the column. As the leading edge of the smouldering front approaches the top of the column, the release of these compounds therefore results in a peak in mass loss rate.
- The composition of the mass emitted is partly water vapour either formed as a by-product of combustion or generated as steam if the fuel or porous medium has initial water content, and also includes volatilized lighter hydrocarbon fractions and aerosols.
- It is expected that the relative proportion of combustion to volatilization is partly a function of the fuel type, with heavier hydrocarbons being less susceptible to volatilization and aerosol formation and therefore favouring mass destruction over gaseous mass transport.
- It is anticipated that the relative proportion of combustion to volatilization may also be affected by the manipulation of operational parameters such as injection air flux and moisture content.

In summary, transient processes such as liquid fuel mobility and the transport of condensable products within a smouldering column may have considerable effects on smouldering metrics, most notably peak temperatures, emissions and mass loss rates. In order to observe and understand these processes, it is necessary to analyze smouldering data in both space and time. The scale of the experiment is also critical as the column must have a sufficient height for these dynamic processes to become apparent.

While liquid fuel mobilization and the transport of condensable products do not impact the overall degree of remediation due to the robust nature of the smouldering reaction, the effects of these processes on smouldering metrics are important for the design of full scale remediation systems, both in-situ and ex-situ. The potential for quasi-superadiabatic conditions, or elevated peak temperatures, due to fuel mobilization is significant for the selection of construction materials in ex-situ treatment systems. The transport of condensable products and the rate and total amount of gaseous emissions is essential for the design of emissions treatment systems in in-situ and ex-situ applications. Furthermore, the potential to manipulate operational parameters, such as air flux and moisture content, to control the relative significance of these processes may be used to optimize the efficiency of large scale systems.

5.2 Recommendations

Through this work it was demonstrated that complex transient processes may occur during smouldering remediation, which are relevant to the design of full-scale remediation systems. In the context of this work, these processes were studied in controlled laboratory columns with a forward propagating smouldering front in an

upward configuration. While select experiments were also conducted with field contaminants, including coal tar and crude oil sludge, the majority of the experiments were conducted with a surrogate fuel which behaved similarly to hazardous contaminants.

Recommendations for further research and development are provided below:

- A study of liquid fuel mobility and the transport of condensable products in a horizontal configuration would be beneficial for developing a better understanding of these processes for in-situ applications.
- Other fuels should be tested to develop a correlation between fuel properties (e.g., molecular weight) and the relative proportion of mass destruction versus volatilization and subsequent gaseous mass transport.
- Optimization of operational parameters (e.g., air flux) should be developed for a range of fuel types and grain size distributions to develop a guideline for conditions that will enhance the relative proportion of contaminant destruction.
- The effect of moisture content on the smouldering front and relative fraction of condensable products should be further investigated to assess if this parameter may be beneficial for large scale operations.

APPENDIX A –NAPL MIGRATION AT AMBIENT TEMPERATURES

The average time for the remediation of a laboratory column via smouldering combustion, including preheating and completion of combustion, is approximately 3 hours for a 30 cm contaminated zone and 7 hours for a 90 cm contaminated zone, with some variation depending on contaminant type, concentration and airflow rate. To assess the potential for NAPL mobilization at room temperature conditions, a column was packed to a height of 50 cm with the same NAPL and sand mixture as used for the combustion tests and was left at ambient conditions for 20 hours. During packing of the column, subsamples were taken 12.5 cm intervals, weighed and placed in a muffle furnace at 550°C for 8 hours and then re-weighed to determine the NAPL concentration. After 20 hours, the column was then incrementally excavated, with samples taken at 5 cm intervals for the determination of final NAPL concentration.

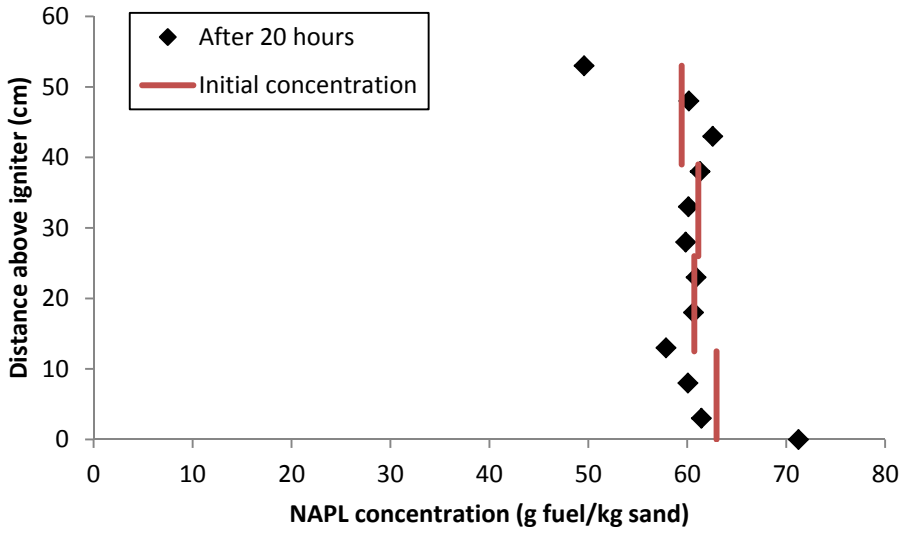

Figure A-1: Migration of canola oil and viscosity index improver after 20 hours at ambient conditions.

A comparison of before and after concentrations (Figure A-1) showed that there was not significant migration occurring at ambient conditions within the column over a timescale relevant to smouldering for the contaminant type and concentration used in the combustion experiments. Minor migration effects were seen in the bottom and top 5 cm of the column, but the remainder of the contaminant pack concentration profile remained unchanged. The elevated temperature regions in the preheating zone above the smouldering front is therefore particularly important for investigating fuel migration.

APPENDIX B – REPEAT 90 CM COLUMN, 2.5 CM/S

A repeat column experiment was conducted for the 90 cm contaminated zone height with an injected forced air flux of 2.5 cm/s. This test was conducted to ensure that the NAPL mobilization and subsequent increase in smouldering peak temperatures occurring when the smouldering front was approximately half way up the column was not an isolated incident.

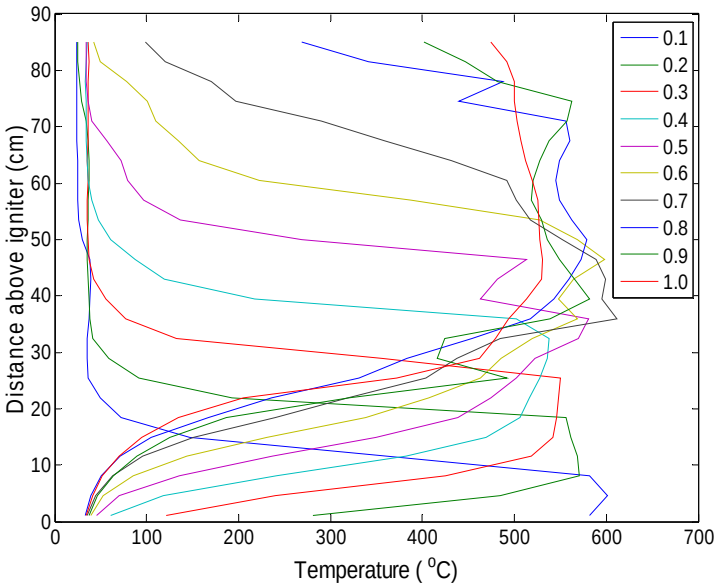

Figure B-1: Temperature profile for repeat 90 cm column with forced air flux of 2.5 cm/s, showing similar effects of a regime change beginning at a nondimensionalized time of 0.5.

As shown in Figure B-1, while the exact location of the regime change varies slightly due to experimental variability, the effect of migration and subsequent regime change is an event linked to the experimental conditions and not solely an outlying result.

APPENDIX C – SCHEMATIC OF CLOSED SYSTEM

A schematic diagram of the closed system apparatus used in Chapter 4, Test No. 8 is shown below in Figure C-1. The configuration was identical to all other column experiments, with the exception that a sealed conical top was placed on top of the column. This forced all emissions to be directed through a water bubbler with the intent of capturing condensable products. Any non-condensable products were released into the fume hood after passing through the water bubbler similar to open column tests.

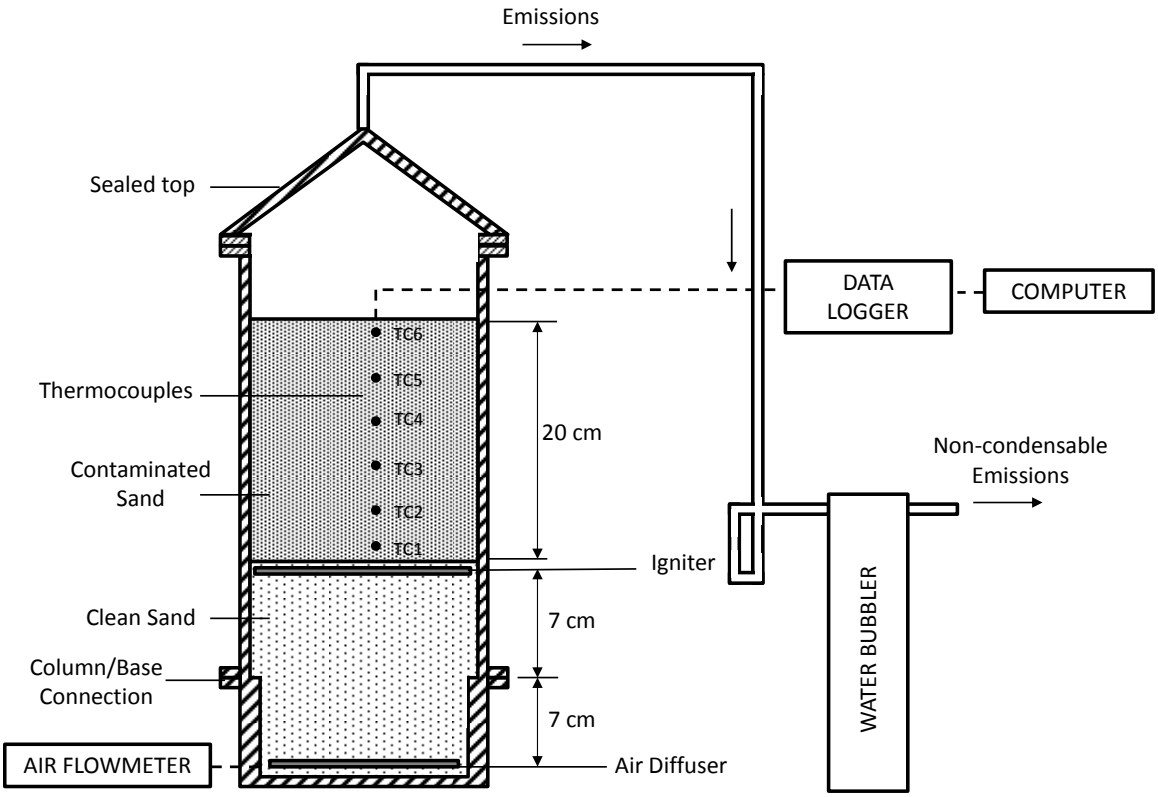

Figure C-1: Schematic diagram of closed system test (Chapter 4, Test No. 8).

APPENDIX D – SUPPLEMENTARY GRAPHS

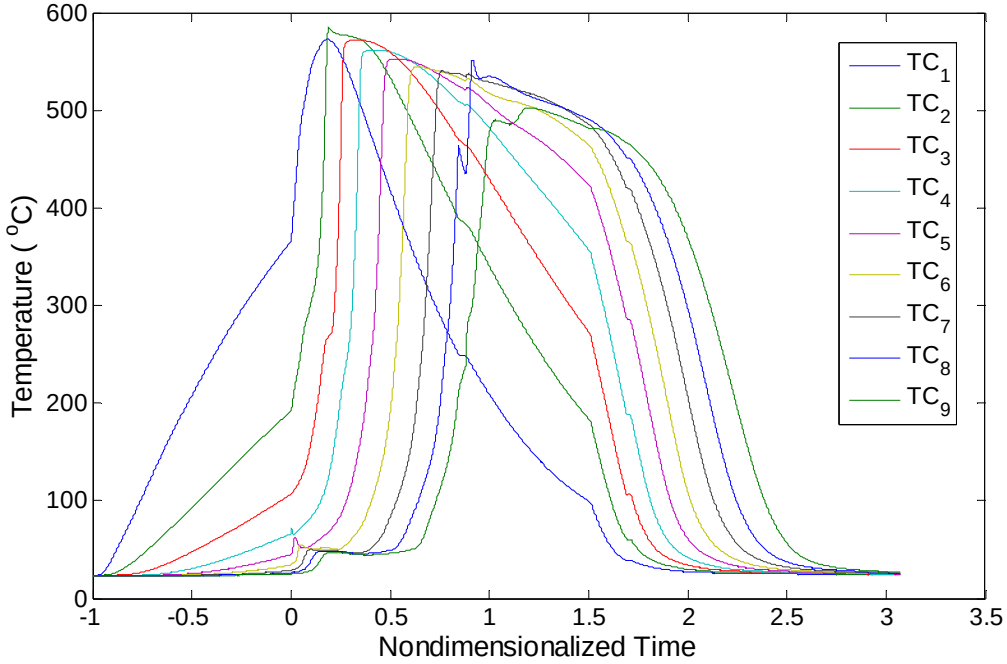

Figure D-1: Temperature history for 30 cm column with forced air flux of 1.25 cm/s

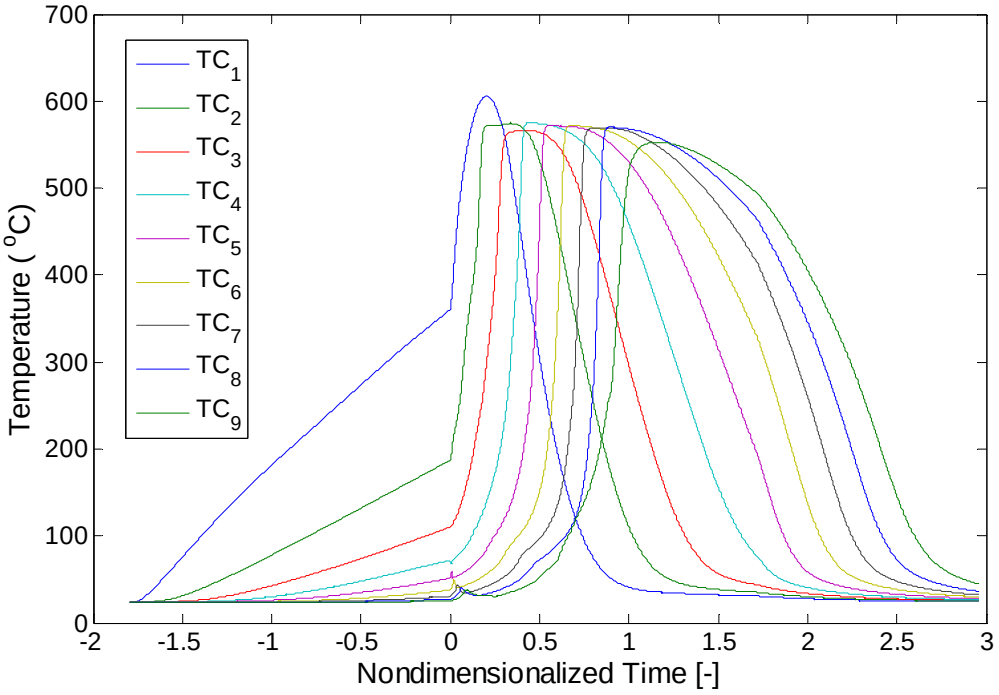

Figure D-2: Temperature history for 30 cm column with forced air flux of 6.25 cm/s

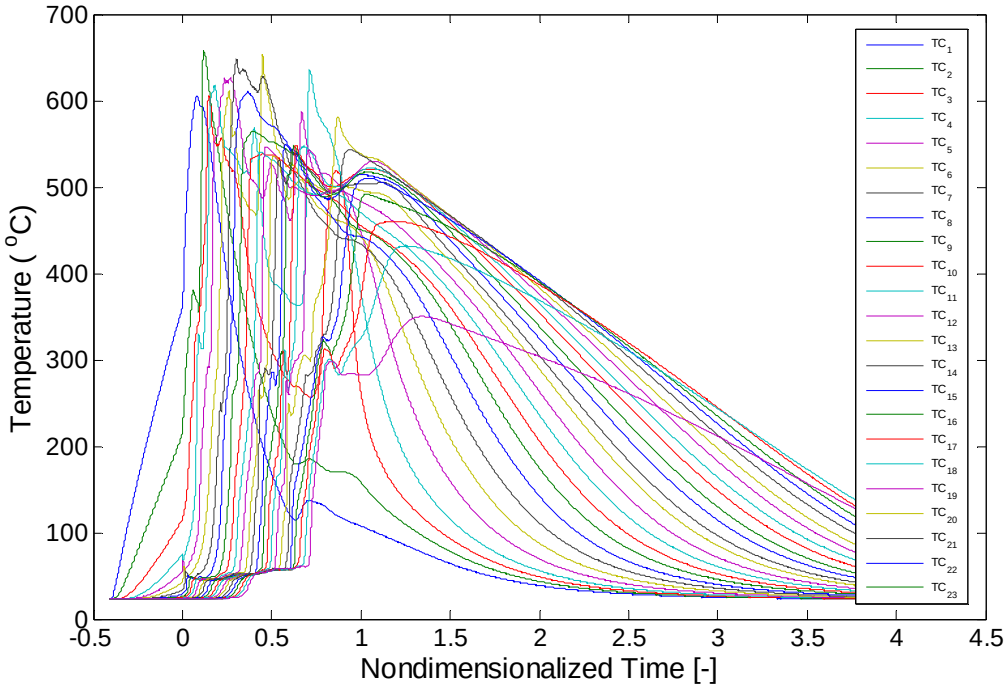

Figure D-3: Temperature history for 90 cm column with forced air flux of 1.25 cm/s

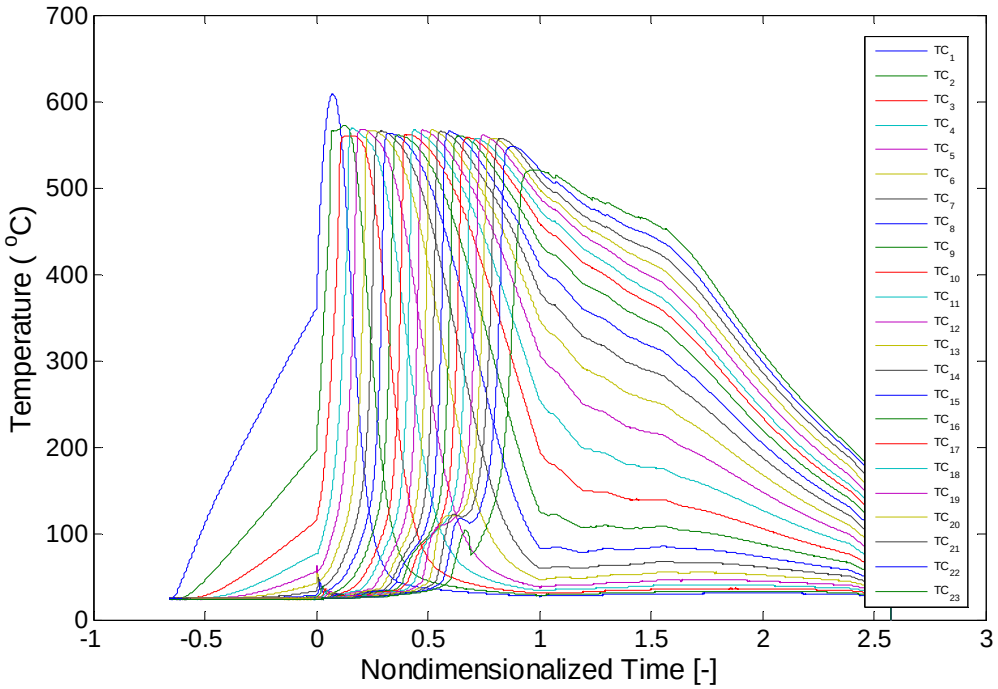

Figure D-4: Temperature history for 90 cm column with forced air flux of 6.25 cm/s

CURRICULUM VITAE

Name:	Laura Kinsman
Post-secondary Education and Degrees:	The University of Western Ontario London, Ontario, Canada 2006-2012 B.E.Sc. The University of Western Ontario London, Ontario, Canada 2006-2012 B.Sc.
Honours and Awards:	Province of Ontario Graduate Scholarship 2013-2014 L.G. Soderman Award in Civil Engineering 2013 NSERC Michael Smith Foreign Study Supplement 2013 NSERC Canada Graduate Scholarship 2012-2013
Related Work Experience:	Staff Engineer Savron Solutions 2014-Present Teaching Assistant The University of Western Ontario 2012-2014